

## METAL ABUNDANCES, RADIAL VELOCITIES AND OTHER PHYSICAL CHARACTERISTICS FOR THE RR LYRAE STARS IN THE *KEPLER* FIELD \*

JAMES M. NEMEC<sup>1,2</sup> JUDITH G. COHEN<sup>3</sup>, VINCENZO RIPEPI<sup>4</sup>, ALIZ DEREKAS<sup>5,6</sup>,  
PAWEŁ MOSKALIK<sup>7</sup>, BRANIMIR SESAR<sup>3</sup>, MERIEME CHADID<sup>8</sup> & HANS BRUNTT<sup>9</sup>

*Accepted 2013 June 28 for publication in the Astrophysical Journal*

### ABSTRACT

Spectroscopic iron-to-hydrogen ratios, radial velocities, atmospheric parameters, and new photometric analyses are presented for 41 RR Lyrae stars (and one probable high-amplitude  $\delta$  Sct star) located in the field-of-view of the *Kepler* space telescope. Thirty-seven of the RR Lyrae stars are fundamental-mode pulsators (*i.e.*, RRab stars) of which 16 exhibit the Blazhko effect. Four of the stars are multiperiodic RRc pulsators oscillating primarily in the first-overtone mode. Spectroscopic [Fe/H] values for the 34 stars for which we were able to derive estimates range from  $-2.54 \pm 0.13$  (NR Lyr) to  $-0.05 \pm 0.13$  dex (V784 Cyg), and for the 19 *Kepler*-field non-Blazhko stars studied by Nemeč *et al.* (2011) the abundances agree well with their photometric [Fe/H] values. Four non-Blazhko RR Lyrae stars that they identified as metal-rich (KIC 6100702, V2470 Cyg, V782 Cyg and V784 Cyg) are confirmed as such, and four additional stars (V839 Cyg, KIC 5520878, KIC 8832417, KIC 3868420) are also shown here to be metal-rich. Five of the non-Blazhko RRab stars are found to be more metal-rich than [Fe/H]  $\sim -0.9$  dex while all of the 16 Blazhko stars are more metal-poor than this value. New  $P-\phi_{31}^s$ -[Fe/H] relationships are derived based on  $\sim 970$  days of quasi-continuous high-precision Q0-Q11 long- and short-cadence *Kepler* photometry. With the exception of some Blazhko stars, the spectroscopic and photometric [Fe/H] values are in good agreement. Several stars with unique photometric characteristics are identified, including a Blazhko variable with the smallest known amplitude and frequency modulations (V838 Cyg).

*Subject headings:* variable stars: RR Lyrae stars, fundamental parameters — stars: abundances — telescopes: *Kepler*, Keck, CFHT

### 1. INTRODUCTION

A knowledge of the chemical compositions and kinematics of individual RR Lyrae stars is important for studying problems concerning stellar and galactic evolution and for understanding the evolution of stellar populations in our Galaxy and other nearby galaxies.

\* Based in part on observations made at the W.M. Keck Observatory, which is operated as a scientific partnership among the California Institute of Technology, the University of California and the National Aeronautics and Space Administration. The Keck Observatory was made possible by the generous financial support of the W.M. Keck Foundation. Also, based in part on observations obtained at the Canada-France-Hawaii Telescope (CFHT) which is operated by the National Research Council of Canada, the Institut National Des Sciences de l'Univers of the Centre National de la Recherche Scientifique of France, and the University of Hawaii.

<sup>1</sup> Department of Physics & Astronomy, Camosun College, Victoria, British Columbia, V8P 5J2, Canada, *nemec@camosun.ca*

<sup>2</sup> International Statistics & Research Corp., Brentwood Bay, BC, V8M 1R3, Canada, *jmn@isr.bc.ca*

<sup>3</sup> Department of Physics and Astronomy, Caltech, USA, *jl@astro.caltech.edu*, *bsesar@astro.caltech.edu*

<sup>4</sup> INAF-Osservatorio Astronomico di Capodimonte, Salita Moiariello 16, I-80131, Napoli, Italy, *ripepi@na.astro.it*

<sup>5</sup> Konkoly Observatory, Research Centre for Astronomy and Earth Sciences, Hungarian Academy of Sciences, H-1121 Budapest, Hungary, *derekas@konkoly.hu*

<sup>6</sup> Sydney Institute for Astronomy, School of Physics, University of Sydney, NSW 2006, Australia

<sup>7</sup> Copernicus Astronomical Centre, ul.Bartycka 18, 00-716, Warsaw, Poland *pam@camk.edu.pl*

<sup>8</sup> Observatoire de la Côte d'Azur, Univ.Nice, Sophia-Antipolis, UMR 6525, Parc Valrose, 06108, Nice Cedex 02, France, *chadid@marseille.fr*

<sup>9</sup> Department of Physics & Astronomy, Aarhus Univ., DK-8000 Aarhus C, Denmark *bruntt@phys.au.dk*

With iron-to-hydrogen abundances, [Fe/H], ranging from smaller than  $-2.5$  dex to larger than  $0.0$  dex, RR Lyrae stars help to define the halo and old-disk stellar populations. They are ubiquitous, having been found in most globular clusters (see Clement *et al.* 2001), throughout the halo of our Galaxy (Le Borgne *et al.* 2012), in the Galactic bulge (Udalski *et al.* 1997; Alcock *et al.* 1998; Moskalik & Poretti 2003; Collinge *et al.* 2006; Kunder & Chaboyer 2008, 2009; Soszynski *et al.* 2011; Pietrukowicz *et al.* 2012), and in a growing number of nearby galaxies. Of particular interest are the large numbers found in the Large Magellanic Cloud (Alcock *et al.* 1998, 2000; Gratton *et al.* 2004; Nemeč, Walker & Jeon 2009; Soszynski *et al.* 2009), in the Small Magellanic Cloud (Soszynski *et al.* 2010), and in nearby dwarf spheroidal galaxies (see Garofalo *et al.* 2013, and references therein).

RR Lyrae stars are particularly valuable for stellar evolution studies because they are in an advanced (post-RGB) evolutionary stage and therefore serve to improve our understanding of mass loss, convection, rotation and magnetic fields. One of their primary uses has been for distance estimation using an absolute magnitude, metallicity relation (see Sandage 1981). The linear form of this relation for field and cluster RR Lyr stars is usually written as  $M_V(RR) = \alpha[\text{Fe}/\text{H}] + \beta$ , where  $\beta \sim 0.6$  and  $\alpha$  ranges from  $\sim 0.18$ - $0.30$ ; however, there is strong evidence that the  $M_V$ -[Fe/H] relationship is nonlinear over the range [Fe/H]  $\sim -2.5$  to  $\sim 0$  dex (Cassisi *et al.* 1999; Caputo *et al.* 2000; Rey *et al.* 2000; Bono *et al.* 2007). In either case it now seems clear that the more metal-

rich RR Lyr stars have lower luminosities than their more metal-poor counterparts, at least for those stars near the zero-age horizontal branch (ZAHB) that are not evolved away from the ZAHB.

Another astrophysical problem of great interest is the unsolved Blazhko effect (see Kovács 2009, Buchler & Kolláth 2011). Whatever the eventual explanation, the correct model will undoubtedly be subject to observational constraints such as are currently being provided by the Konkoly and Vienna Blazhko star surveys, and the high-precision, long-timeline photometry from the MOST, CoRoT and *Kepler* space telescopes, as well as from ground-based follow-up surveys. These surveys suggest that a significant fraction of all RR Lyr stars, maybe as many as half, exhibit Blazhko characteristics; according to the Konkoly survey the fraction is at least 40% (Jurcsik *et al.* 2009c; Szeidl *et al.* 2012). For RR Lyr stars in the LMC the Blazhko effect is seen to be more frequent for stars with  $[\text{Fe}/\text{H}] < -1.4$  dex than for more metal rich RR Lyrae stars (Smolec 2005). To test for a similar trend in our Galaxy, and for the derivation of distances and evolutionary states, requires accurate photometry and metal abundances.

In the 115 deg<sup>2</sup> field of view of NASA’s *Kepler* space telescope  $\sim 45$  RR Lyrae stars have been identified among stars down to 17.5 mag. Although this number is small compared with the sample sizes for the MACHO (Alcock *et al.* 2003, 2004), OGLE (Soszynski *et al.* 2009, 2010), SDSS (Sesar *et al.* 2010), ASAS and other modern large surveys, *Kepler* photometry provides the most precise and extensive set of photometry ever assembled for RR Lyr stars.

An early discovery made possible with *Kepler* data was the phenomenon of ‘period doubling’, which manifests itself as alternating high and low amplitude pulsations (Szábo *et al.* 2010; Kolenberg *et al.* 2010; Buchler & Kolláth 2011). The effect most probably is associated with the 9:2 resonance of the fundamental and overtone modes that destabilizes the fundamental-mode full amplitude pulsation (see Kolláth, Molnár & Szabó 2011). Such period doubling usually is not detectable from the ground because day-night bias prevents observations of successive pulsation cycles. Period doubling is well-known in RV Tau and W Vir stars, and from models has been predicted in classical Cepheids (Moskalik & Buchler 1991) and in BL Her stars (Buchler & Moskalik 1992), the latter having been seen recently by Smolec *et al.* (2012).

The RR Lyrae stars in the *Kepler* field have been identified and studied previously by Kolenberg *et al.* (2010, 2011; hereafter K10, K11), Benkő *et al.* (2010, hereafter B10), Nemec *et al.* (2011, hereafter N11) and Guggenberger *et al.* (2012, hereafter G12). K10 published the first results based on early-release (Q0,Q1) *Kepler* data, and carried out a detailed analysis of the Blazhko stars RR Lyrae and V783 Cyg. B10 presented a detailed analysis of 29 *Kepler*-field RR Lyrae stars based on the long cadence photometry from the first 138 days (Q0-Q2) of the *Kepler* observations, and found that almost half of the stars (14/29) show amplitude modulations. K11 studied RR Lyrae itself in great detail using Q1-Q2 long cadence data. The N11 study consisted of an extensive Fourier decomposition analysis (using Q0-Q5 *Kepler* photometry) of 19 non-Blazhko *Kepler*-field RRab stars. And most recently, G12 studied in detail the most ex-

treme Blazhko star, V445 Lyr. The RRc stars, all of which are multiperiodic, are being studied in detail by Moskalik *et al.* (2012).

The primary goal of the present investigation was to derive spectroscopic  $[\text{Fe}/\text{H}]_{\text{spec}}$  abundances (and the corresponding atmospheric parameters) for the *Kepler*-field RR Lyrae stars. Prior to the current investigation only photometric  $[\text{Fe}/\text{H}]_{\text{phot}}$  values were known for the 19 non-Blazhko stars studied by N11; and neither spectroscopic nor photometric abundances had been measured for the RRc and Blazhko stars (a notable exception being RR Lyrae itself).

The reliability of the N11 photometric metallicities, especially for the four non-Blazhko stars identified as probable metal-rich old-disk stars, was of particular interest. Thus, a secondary goal was to confirm the *Kepler*-based  $[\text{Fe}/\text{H}]_{\text{phot}}$  values for the non-Blazhko stars, and to use the longer time frame of the Q0-Q11 *Kepler* photometry (approaching 1000 days of quasi-continuous measurements) and the improved *Kepler* pipeline to derive  $[\text{Fe}/\text{H}]_{\text{phot}}$  abundances for the Blazhko and RRc stars.

With  $[\text{Fe}/\text{H}]_{\text{spec}}$  and  $[\text{Fe}/\text{H}]_{\text{phot}}$  measurements in hand, a comparison of the metal abundances was possible. The good agreement found between the spectroscopic and photometric abundances suggests that high-precision photometry alone can be used to derive iron-to-hydrogen ratios, thereby providing a reliable means for the derivation of metallicities for stars too faint for high-dispersion spectroscopy.

In §2 the program stars are identified, and in §3 the *Kepler* photometry is described and used to derive photometric characteristics for the stars. In §4 the CFHT and Keck high-dispersion spectra are described, from which radial velocities (*RVs*), spectroscopic metallicities, and correlations of the resulting atmospheric parameters are derived and discussed. The *Kepler* photometry and the new spectroscopic results are used in §5 to better establish the relationship between metal abundance and light curve morphology, in particular the RRab and RRc  $P$ - $\phi_{31}$ - $[\text{Fe}/\text{H}]$  relations. Our results are summarized in §6.

## 2. PROGRAM STARS

The *Kepler*-field RR Lyrae stars studied here can be sorted into four distinct categories: (a) non-Blazhko RRab stars; (b) Blazhko RRab stars; (c) RRc stars; and (d) RRc/HADS? star. **Table 1** contains some basic photometric characteristics for the stars. The first three columns contain the common star name (GCVS or other), the star number in the *Kepler* Input Catalog (KIC, see Brown *et al.* 2011), and the mean *Kp* magnitude given in the KIC. Columns 4-5 contain our best estimate of the pulsation period,  $P_{\text{puls}}$ , and a recent time of maximum light,  $t_0$  (Barycentric Julian Date). Columns 6-8 contain the total amplitude,  $A_{\text{tot}}$ , the Fourier  $A_1$  amplitude coefficient, and the Fourier  $\phi_{31}^s$  phase parameter (defined as  $\phi_3^s - 3\phi_1^s$ , where the superscript ‘s’ indicates Fourier decomposition with a sine series), all derived from the *Kp* photometry (see §3). Column 9 contains the photometric metallicity,  $[\text{Fe}/\text{H}]_{\text{phot}}$ , derived in §5 using new bivariate linear regression analyses computed with the *Kepler* photometry (§3) and the new spectroscopic metallicities (§4).

In Table 1 the number of non-Blazhko stars is two greater than the 19 stars studied by N11: KIC 9658012,

TABLE 1  
SOME BASIC PHOTOMETRIC CHARACTERISTICS FOR THE *Kepler*-FIELD RR LYRAE STARS

Star	KIC	$\langle Kp \rangle$ [mag]	$P_{\text{puls}}$ [day]	$t_0$ (BJD) 2400000+	$A_{\text{tot}}$ [mag]	$A_1$ [mag]	$\phi_{31}^s$ [rad]	[Fe/H] <sub>phot</sub>
(1)	(2)	(3)	(4)	(5)	(6)	(7)	(8)	(9)
(a) 21 Non-Blazhko RRab-type stars								
NR Lyr	3733346	12.684	0.6820264	54964.7403	0.767	0.266	5.120	$-2.51 \pm 0.06$
V715 Cyg	3866709	16.265	0.47070609	54964.6037	0.988	0.338	4.901	$-1.18 \pm 0.04$
V782 Cyg	5299596	15.392	0.5236377	54964.5059	0.523	0.190	5.808	$-0.30 \pm 0.04$
V784 Cyg	6070714	15.37	0.5340941	54964.8067	0.634	0.234	6.084	$-0.14 \pm 0.07$
KIC 6100702	6100702	13.458	0.4881457	54953.8399	0.575	0.209	5.747	$-0.21 \pm 0.04$
NQ Lyr	6763132	13.075	0.5877887	54954.0702	0.811	0.280	5.096	$-1.81 \pm 0.03$
FN Lyr	6936115	12.876	0.52739847	54953.2656	1.081	0.380	4.818	$-1.90 \pm 0.04$
KIC 7021124	7021124	13.550	0.6224925	54965.6471	0.831	0.283	5.060	$-2.18 \pm 0.04$
KIC 7030715	7030715	13.452	0.68361247	54953.8427	0.647	0.231	5.616	$-1.28 \pm 0.05$
V349 Lyr	7176080	17.433	0.5070740	54964.9588	0.988	0.346	4.850	$-1.63 \pm 0.04$
V368 Lyr	7742534	16.002	0.4564851	54964.7860	1.133	0.405	4.772	$-1.29 \pm 0.05$
V1510 Cyg	7988343	14.494	0.5811436	54964.6700	0.980	0.345	5.075	$-1.80 \pm 0.03$
V346 Lyr	8344381	16.421	0.5768288	54964.9231	0.964	0.330	5.052	$-1.82 \pm 0.03$
V350 Lyr	9508655	15.696	0.5942369	54964.7820	0.973	0.340	5.119	$-1.81 \pm 0.03$
V894 Cyg	9591503	13.293	0.5713866	54953.5624	1.105	0.377	5.067	$-1.74 \pm 0.03$
KIC 9658012	9658012	16.001	0.533206	55779.9450	0.924	0.312	5.144	$-1.28 \pm 0.02$
KIC 9717032	9717032	17.194	0.5569092	55779.8956	0.844	0.293	5.183	$-1.38 \pm 0.02$
V2470 Cyg	9947026	13.300	0.5485905	54953.7832	0.599	0.220	5.737	$-0.47 \pm 0.03$
V1107 Cyg	10136240	15.648	0.5657781	54964.7551	0.818	0.280	5.196	$-1.42 \pm 0.02$
V839 Cyg	10136603	14.066	0.4337747	55778.7060	0.793	0.273	5.600	$-0.06 \pm 0.05$
AW Dra	11802860	13.053	0.6872160	54954.2160	0.892	0.307	5.558	$-1.42 \pm 0.05$
(b) 16 Blazhko RRab-type stars								
V2178 Cyg	3864443	15.593	0.4869538	54976.3672	0.749	0.305	4.895	$-1.35 \pm 0.03$
V808 Cyg	4484128	15.363	0.5478642	54970.2834	0.879	0.298	5.254	$-1.18 \pm 0.03$
V783 Cyg	5559631	14.643	0.62070001	54975.5439	0.799	0.271	5.517	$-1.15 \pm 0.03$
V354 Lyr	6183128	16.260	0.561691	55245.1590	0.815	0.303	5.191	$-1.40 \pm 0.02$
V445 Lyr	6186029	17.401	0.5131158	55160.5957	0.591	0.255	5.198	$-1.02 \pm 0.03$
RR Lyrae	7198959	7.862	0.566788	55278.2263	0.717	0.255	5.307	$-1.21 \pm 0.03$
KIC 7257008	7257008	16.542	0.51177516	55758.5859	0.818	0.290	5.191	$-1.02 \pm 0.03$
V355 Lyr	7505345	14.080	0.4737027	55124.7072	0.955	0.373	4.928	$-1.16 \pm 0.04$
V450 Lyr	7671081	16.653	0.5046123	54996.3226	0.850	0.335	4.976	$-1.35 \pm 0.03$
V353 Lyr	9001926	16.914	0.5568016	55082.6820	0.834	0.293	5.123	$-1.50 \pm 0.02$
V366 Lyr	9578833	16.537	0.5270283	55326.1915	0.856	0.308	5.167	$-1.18 \pm 0.02$
V360 Lyr	9697825	16.001	0.5575765	54988.9332	0.647	0.257	5.065	$-1.63 \pm 0.02$
KIC 9973633	9973633	16.999	0.51075	55780.3655	0.848	0.293	4.122	$-1.17 \pm 0.03$
V838 Cyg	10789273	13.770	0.48027971	55807.9302	1.100	0.390	4.857	$-1.36 \pm 0.04$
KIC 11125706	11125706	11.367	0.6132200	54981.0658	0.471	0.180	5.824	$-0.61 \pm 0.05$
V1104 Cyg	12155928	15.033	0.43638507	55120.8363	1.103	0.394	4.861	$-0.93 \pm 0.05$
(c) 4 RRc-type stars								
KIC 4064484	4064484	14.641	0.33700953	55552.1567	0.377	0.193	0.494	$-1.59 \pm 0.02$
KIC 5520878	5520878	14.214	0.26917082	55800.0883	0.325	0.164	0.908	$-0.36 \pm 0.06$
KIC 8832417	8832417	13.051	0.2485492	54964.6391	0.281	0.141	0.727	$-0.20 \pm 0.07$
KIC 9453114	9453114	13.419	0.3660236	55740.6420	0.414	0.209	0.865	$-1.70 \pm 0.02$
(d) High-amplitude Delta Scuti (HADS) star?								
KIC 3868420	3868420	10.110	0.2082275	54960.5192	0.171	0.083	4.109	...

NOTE. — The columns contain: (1) star name (GCVS or other); (2) number in the Kepler Input Catalog (KIC); (3) mean *Kepler* magnitude (given in the KIC catalog); (4) pulsation period, with the number of digits giving a measure of the accuracy of the value; (5) time of maximum light (BJD – 2400000); (6) total amplitude ( $Kp$  system) - for the Blazhko and RRc variables the mean values are given; (7) Fourier  $A_1$  coefficient ( $Kp$  system); (8) average value of the Fourier  $\phi_{31}^s(Kp)$  parameter; (9) photometric metal abundance,  $[\text{Fe}/\text{H}]_{\text{phot}}$ , on the high dispersion spectroscopy scale (c9), and derived using the nonlinear regression analyses discussed in §5; the uncertainties are standard errors of the regression fit.

KIC 9717032 and V839 Cyg (KIC 10136603) are new additions, while V838 Cyg (KIC 10789273) has been moved to the Blazhko list. KIC 9658012 and KIC 9717032 were discovered during the course of the BOKS survey (Feldmeier *et al.* 2011); both stars were observed with *Kepler* for the first time in Q10, and neither star shows any evidence for amplitude modulations. A  $g$ -band light curve for KIC 9717032 is shown in Fig.17 of the Feldmeier paper. V839 Cyg is new and was discovered as a by-product of the ASAS-North survey (Pigulski *et al.* 2013, in preparation).

The Blazhko variables listed in Table 1 include three

stars in addition to those in the B10 list: KIC 7257008 and KIC 9973633 (also discovered by Pigulski *et al.* 2013, in preparation) which show amplitude modulations in the Q10 and Q11 *Kepler* data; and V838 Cyg which was previously thought to be a non-Blazhko variable but now appears to be the lowest-amplitude Blazhko star yet discovered (see below). Wils *et al.* (2006) listed NR Lyr (KIC 3733346) as a Blazhko star with an uncertain modulation period of 27 days; however, our analysis of the Q1-Q13 long cadence data (51883 data points) and the Q11.1 short cadence data (45512 data points) showed no evidence for amplitude modulations, thus supporting the

B10 and N11 conclusion that NR Lyr is a non-Blazhko RRab variable. The faint star V349 Lyr (KIC 7176080) is in the B10 Blazhko list, but was classified by N11 as a probable non-Blazhko star; our analysis of the Q1-Q13 long cadence data (51877 data points) and the Q9 short cadence data (51878 data points) again shows no evidence for amplitude modulations.

To date only four *bona fide* c-type RR Lyrae (RRc) stars have been identified in the *Kepler* field. Two were observed at CFHT and two at Keck: the two shorter period stars are metal rich, and the two longer period stars are metal poor (see §4 – 5 below). All four stars have been found to be multiperiodic and are being studied in detail by Moskalik *et al.* (2012; 2013, in preparation). Owing to the challenges of distinguishing RRc stars from high-amplitude  $\delta$  Sct (HADS) stars and some close eclipsing binaries, all of which have similar light curves, the RRc section of Table 1 probably is more incomplete than the RRab sections. KIC 10063343 ( $Kp=13.16$ ) has a pulsation period appropriate for an RRc star,  $P_{\text{puls}} = 0.332764$  d, but the variable light curve and Fourier parameters raise serious doubts that it is an RR Lyrae star. Other candidate RRc stars are being sought by Kinemuchi *et al.* (2013, in preparation).

The relatively bright star KIC 3868420 ( $Kp=10.11$ ) is of particular interest. The early *Kepler* photometry suggested that it might be an RRc star, and as such a single spectrum was taken at CFHT. Analysis of this spectrum revealed it to be a hot, high surface gravity star with spectroscopic  $[\text{Fe}/\text{H}] = -0.32 \pm 0.13$  dex; however, with a dominant period of only 0.208 day, a light curve that is more symmetric and more sharply peaked than the light curves of the RRc stars, and a relatively small  $RV$ , it more probably is a HADS star.

Three additional RRab stars recently have been identified in the *Kepler* field, in the directions of KIC 3448777, KIC 4917786 and KIC 7295372. All have  $P_{\text{puls}} \sim 0.5$  d, low amplitudes resulting from ‘crowding’ by brighter nearby stars<sup>11</sup>, and unknown metal abundances. These newly discovered RR Lyr stars continue to be observed by *Kepler*.

### 3. KEPLER PHOTOMETRY

An unprecedented amount of high-precision *Kepler* photometry is currently available for deriving the photometric characteristics (including photometric metal abundances) for the majority of the stars in Table 1. Most of the program RR Lyr stars have been observed every quarter since the first *Kepler* flux measurements were made in May 2009. Up to and including Q11 a typical RRab star with a pulsation period of 0.5 day had over 3.5 years of quasi-continuous high-precision photometric data. Long cadence observations (LC, *i.e.*, 29.4 minute flux integrations) over this 3.5-year interval amount to  $\sim 350,000$  data points spread over 2500 pulsation cycles, with  $\sim 24$  brightness measurements per cycle. For most of the stars the CFHT and Keck spectra had simultaneously-acquired *Kepler* photometry. The CFHT spectroscopic observations were made during the sixth and seventh quarters (Q6,Q7) of the *Kepler* observations, and the Keck spectra were acquired during the

<sup>11</sup> The ‘crowding’ here is determined by the  $3.98$  arcsec pixel<sup>-1</sup> image scale of the CCD chips on the *Kepler* telescope.

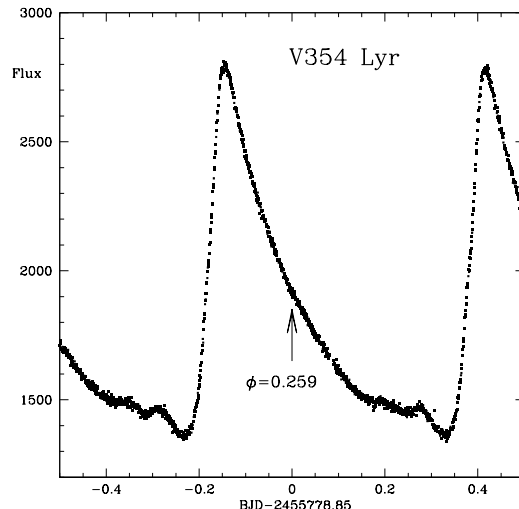


FIG. 1.— A typical *Kepler* light curve, in this case for V354 Lyr (KIC 6183128), a Blazhko RRab star with  $P_{\text{puls}} = 0.561691 \pm 0.000001$  d and  $P_{\text{BL}} = 723 \pm 12$  days. The data plotted are a one-day segment of short cadence flux measurements made simultaneously with three Keck-I 10-m spectra. The abscissa is time (Barycentric Julian Date), starting 0.5 day before and ending 0.5 day after the mid time of the spectra; and the ordinate is the *Kepler* raw flux (counts per second). The pulsation phase at the mid-time of the spectroscopic observations is indicated by a labelled arrow.

first month of the tenth quarter (Q10.1).

Five of the RR Lyr stars in Table 1 were not observed with *Kepler* prior to the start of Q10: KIC 7257008, KIC 9658012, KIC 9717032, KIC 9973633 and V839 Cyg. Fortunately, the Keck observations for the last four stars were made in August 2011, which occurs in Q10.1 of the *Kepler* observations. KIC 7257008 ( $Kp=16.54$ ), KIC 7021124 ( $Kp=13.55$ ) and V349 Lyr ( $Kp=17.43$ ) have yet to be observed spectroscopically.

In addition to the LC data most of the program stars also have been observed at short cadence (SC, *i.e.*, a flux measurement every 1 minute) for at least one or two quarters. The available SC data for these stars usually amounts to almost half a million observation points per star. RR Lyrae itself has been observed at SC every quarter since Q5, the total number of data points being just under  $9 \times 10^5$ .

A typical RRab star with SC data has  $\sim 720$  brightness measurements per pulsation cycle, which is sufficient for defining extremely-well the shape of the light curve (as illustrated in **Fig. 1**), and for detecting and defining from precise Fourier parameters the smallest amplitude and frequency modulations.

The task of processing the *Kepler* raw flux data has been discussed by Koch *et al.* (2010), Jenkins *et al.* (2010) and Gilliland *et al.* (2010). Of particular concern was the detrending of data within quarters, the ‘stitching together’ of the data from the different quarters, and the merging of long and short cadence observations. The reduction methods (transforming the raw flux counts to  $Kp$  magnitudes) that were used here were similar to those described in N11. To achieve the highest levels of photometric precision multiple detrending passes were found to be necessary to reduce the residuals about the non-Blazhko light curves to  $\sim 0.2$  mmag.

TABLE 2  
AMPLITUDE AND PERIOD (PHASE) MODULATIONS OF 16 BLAZHKO STARS IN THE *Kepler* FIELD

Star (1)	$\Delta A_{\text{tot}}$ [mag] (2)	$\Delta P_{\text{puls}}$ [day] (3)	$\Delta A_1$ [mag] (4)	$\Delta \phi_1$ [rad] (5)	$\Delta \phi_{31}^s$ [rad] (6)
V445 Lyr	0.80 (0.20-1.00)	0.013 (0.509-0.522)	0.380 (0.018-0.398)	3.12 (1.48-4.60)	6.28 (0.00-6.28)
V2178 Cyg	0.84 (0.30-1.14)	0.0014 (0.4859-73)	0.279 (0.162-0.441)	1.09 (3.91-5.00)	3.55 (3.41-6.96)
V450 Lyr	0.56 (0.57-1.13)	0.0007 (0.5042-49)	0.240 (0.207-0.447)	0.44 (4.74-5.18)	1.12 (4.53-5.65)
KIC 7257008	0.68 (0.44-1.12)	0.0030 (0.5105-35)	0.211 (0.179-0.390)	0.60 (3.00-3.60)	1.05 (4.77-5.82)
V354 Lyr	0.60 (0.49-1.09)	0.0003 (0.5616-19)	>0.20 (<0.19-0.39)	1.26 (2.51-3.77)	0.70 (4.85-5.55)
V360 Lyr	0.21 (0.54-0.75)	0.0010 (0.5570-80)	0.162 (0.176-0.338)	0.37 (0.99-1.36)	0.82 (4.78-5.60)
V808 Cyg	0.35 (0.71-1.06)	0.0020 (0.5467-87)	0.130 (0.237-0.367)	0.67 (0.28-0.95)	0.64 (4.96-5.60)
RR Lyrae	0.23 (0.59-0.82)	0.0024 (0.5657-81)	0.127 (0.186-0.313)	0.65 (4.77-5.42)	1.21 (4.85-6.06)
V366 Lyr	0.18 (0.77-0.95)	0.0003 (0.5269-72)	0.127 (0.248-0.375)	0.14 (1.21-1.35)	0.98 (4.75-5.73)
KIC 9973633	0.39 (0.61-1.00)	0.0009 (0.5105-14)	0.119 (0.225-0.344)	0.22 (4.00-4.22)	0.78 (4.80-5.58)
V355 Lyr	0.15 (0.87-1.02)	0.0008 (0.4733-41)	0.110 (0.313-0.423)	0.15 (1.05-1.20)	0.62 (4.67-5.29)
V353 Lyr	0.24 (0.71-0.95)	0.0004 (0.5566-70)	0.082 (0.250-0.332)	0.16 (0.59-0.75)	0.24 (5.01-5.25)
V1104 Cyg	0.17 (1.03-1.20)	0.0003 (0.4363-66)	0.062 (0.365-0.427)	0.070 (0.165-0.235)	0.16 (4.78-4.94)
V783 Cyg	0.08 (0.76-0.84)	0.0005 (0.6204-09)	0.033 (0.253-0.286)	0.08 (1.82-1.90)	0.14 (5.44-5.58)
KIC 11125706	0.03 (0.45-0.48)	0.0004 (0.6128-32)	0.008 (0.176-0.184)	0.031 (5.452-5.483)	0.112 (5.772-5.884)
V838 Cyg	0.02 (1.09-1.11)	0.0002 (0.4801-03)	0.0016 (0.3871-87)	0.0010 (3.3577-87)	0.003 (4.855-4.858)

NOTE. — The columns contain: (1) star name; (2) range of total amplitude (*Kp*-system), with minimum and maximum values in parentheses; (3) range of the pulsation period (min and max in parentheses); (4) range of the Fourier  $A_1$  amplitude coefficient (min and max in parentheses) – note that  $\Delta A_1$  here is the  $A_1$  range, which is not the same as the  $\Delta A_1$  defined by B10; (5) range of the first Fourier phase coefficient,  $\phi_1$  (min and max in parentheses); (6) range of the Fourier phase-difference parameter  $\phi_{31}^s$  (min and max in parentheses).

### 3.1. Pulsation Periods, Amplitudes and Phases

Pulsation periods,  $P_{\text{puls}}$ , times of maximum light,  $t_0$ , and total amplitudes on the *Kepler* photometric system,  $A_{\text{tot}}$ , are given for the program RR Lyrae stars in columns 4-6 of Table 1. All values are newly derived based on analyses of the available *Kepler* Q0-Q11 long and short cadence data, which in most cases comprises almost 1000 days of quasi-continuous high-precision photometry.

The  $P_{\text{puls}}$  are mean values of the dominant oscillation frequencies, ignoring the secondary periods that are present in some non-Blazhko stars (V350 Lyr, KIC 7021124) and in all the Blazhko stars, ignoring changing periods, and averaging over many modulation cycles for the Blazhko stars. The periods were computed with the ‘Period04’ package of Lenz & Breger (2005) using the Monte Carlo mode for error estimation, Stellingwerf’s (1978) ‘PDM2’ program<sup>12</sup>, updated to deal with rich data sets, and the period-finding program of Kolaczowski (see Moskalik & Kolaczowski 2009).

The accuracy of the pulsation periods reported in Table 1 is  $\sim$  few units in the last decimal place given, with the periods for the Blazhko and RRc stars tending to be less accurate than those for the non-Blazhko stars. The uncertainties depend on several factors: the particular data set (or subset) that was analyzed, the search method, the constancy of the primary pulsation period, and whether or not amplitude or frequency modulations are present. In general the periods agree well with those given by B10 for 15 non-Blazhko and 14 Blazhko stars, and with the more precise values derived by N11 for 19 non-Blazhko stars. Since the new periods were computed with longer time baselines than these earlier studies, and are based on both long and short cadence data, they are the best available values yet reported for these stars. In general, the accuracy of the  $P_{\text{puls}}$  values is more than sufficient for estimating the phases at which the spectroscopic observations were made.

The  $A_{\text{tot}}$  in Table 1 are the trough-to-peak *Kp* amplitudes. For the non-Blazhko stars they are time invariant values obtained by inspection of the complete light curve and by averaging  $A_{\text{tot}}$  calculated from individual light curves for successive time segments (see Fig.2). For the Blazhko variables and the four RRc stars, all of which are multiperiodic and show amplitude variations,  $A_{\text{tot}}$  is the time-averaged value. According to the transformation given in equation 2 of N11 the  $A_{\text{tot}}(Kp)$  are  $\sim$  0.14 mag smaller than the  $A_{\text{tot}}(V)$ , where  $V$  is for the Johnson *UBV* system.

The zero points  $t_0$  were estimated from the mean light curves and correspond to times of zero-slope at maximum light. For the non-Blazhko stars they were usually chosen to approximately coincide with the time of the first *Kepler* observations (*i.e.*, just after BJD 2454953), and for the Blazhko variables the  $t_0$  generally coincide with a time of maximum light occurring during a period of maximum amplitude. Thus,  $t_0$  serves as the zero point for both the pulsation phase,  $\phi_{\text{puls}}$ , defined to be the fractional part of  $(t - t_0)/P_{\text{puls}}$ , and for the Blazhko phase,  $\phi_{\text{BL}}$ , defined to be the fractional part of  $(t - t_0)/P_{\text{BL}}$ .

### 3.2. Blazhko Period and Amplitude Modulations

The most noticeable signature of the Blazhko effect is variation in the light curve shape, in particular amplitude modulations, over time scales ranging from several days to several years. The amplitude that is usually considered is the total amplitude (*i.e.*, from trough to peak) through the *V* or *B* filter, but may also be one of the Fourier amplitude coefficients. In the absence of *BV* photometry for most of the *Kepler*-field RR Lyr stars we focus in this paper on the  $A_{\text{tot}}$  and  $A_1$  amplitudes derived from the *Kp* photometry. The  $A_1$  values are from Fourier decompositions of the *Kp* data performed using the following sine-series sum:

$$m(t) = A_0 + \sum_{k=1}^N A_k \sin(k2\pi t/P + \phi_k), \quad (1)$$

<sup>12</sup> PDM2 is freely available at <http://www.stellingwerf.com>.

where  $m(t)$  is the apparent  $Kp$  magnitude as a function of time,  $A_0$  is the mean  $Kp$  magnitude (assumed to be the value given in the KIC catalog),  $N$  is the adopted number of terms in the Fourier series, the  $A_k$  and  $\phi_k$  are the Fourier amplitudes and phases, and  $P$  is the pulsation period.

Blazhko stars are also known to exhibit period (frequency, or phase) modulations, although usually these are less noticeable than the amplitude modulations. Frequency modulations were detected previously in the *Kepler*-field Blazhko stars studied by B10, in RR Lyrae by K10 and K11, and in V445 Lyr by G12. The 16 *Kepler*-field Blazhko stars studied here all exhibit both amplitude and frequency modulations.

While the detection of amplitude and frequency modulations is usually straightforward, the physical mechanism responsible remains unknown, and Blazhko stars are almost as enigmatic now (see Kovács 2009) as when they were discovered over 100 years ago (Blazhko 1907). The problem in recent years has taken on new significance with the discovery that almost half of all RRab stars are Blazhko variables (Jurcsik *et al.* 2009c), and that possibly all RRC stars are multiperiodic (Moskalik *et al.* 2012). These discoveries raise the question whether all RR Lyrae stars might be amplitude and frequency modulators.

The measured amplitude and frequency modulations for the Blazhko RRab stars in our sample are summarized in **Table 2**, where the stars have been ordered from largest to smallest amplitude modulations,  $\Delta A_1$  (*i.e.*, from the most extreme Blazhko variability to the least variability). All the quantities are newly-derived from both the long and short cadence Q0-Q11 photometry, and the uncertainties are at the level of the precisions given. Columns 2-6 contain, respectively, the measured ranges (minimum to maximum values) for: the total amplitude in the  $Kp$ -passband,  $\Delta A_{\text{tot}}$ ; the pulsation period,  $\Delta P_{\text{puls}}$ ; the Fourier amplitude coefficient,  $\Delta A_1$ ; the first Fourier phase coefficient,  $\Delta \phi_1$ ; and the Fourier phase-difference parameter  $\Delta \phi_{31}^s$ , where  $\phi_{31}^s = \phi_3 - 3\phi_1$  (adjusted to the value closest to the mean value of 5.8) and the superscript ‘s’ indicates that a sine (rather than a cosine) series was used for the Fourier decomposition (see equation 1).

The amplitude modulations,  $\Delta A_{\text{tot}}$ , range from as large as  $\sim 0.82$  mag (V445 Lyr, V2178 Cyg) to as small as  $\sim 0.02$  mag (V838 Cyg, KIC 11125706), corresponding to 2-80% of  $A_{\text{tot}}$  (max). The stars with the largest amplitude variations tend also to exhibit the largest period variations. The average period range  $\Delta P_{\text{puls}}$  is 0.0010 d. Plots of  $\Delta A_{\text{tot}}$  versus period, and  $\Delta \phi_{31}^s$  versus period, show an approximately normal distribution with the largest modulations occurring for those stars with pulsation periods around 0.53 d. In the period- $\Delta \phi_{31}^s$  diagram the extreme Blazhko stars V445 Lyr and V2178 Cyg (see Fig. 3) are clearly outliers with  $\Delta \phi_{31}^s$  values considerably larger than for all the other Blazhko stars. Estimates of  $\Delta P_{\text{puls}}$  and  $\Delta A_1$  of RR Lyrae by K11, and V445 Lyr by G12, agree well with the values reported in Table 2.

### 3.2.1. V838 Cyg and KIC 11125706

When the amplitude modulations of Blazhko stars are very small careful analysis is required to ensure that the fluctuations are not artificial, perhaps caused by

the data reduction methods. Such borderline Blazhko stars among the *Kepler*-field RR Lyr stars include KIC 11125706, V838 Cyg and V349 Lyr (discussed by N11). Previously, KIC 11125706 was found by B10 to have “the lowest amplitude modulation ever detected in an RR Lyrae star”, even smaller than the small amplitude modulations seen in RR Gem (Jurcsik *et al.* 2005) and in SS Cnc (Jurcsik *et al.* 2006); and V838 Cyg was classified as non-Blazhko by both B10 and N11. We confirm the low amplitude modulations of KIC 11125706, but also find that V838 Cyg exhibits amplitude and frequency modulations and that these are even smaller than those of KIC 11125706 ( $\Delta A_1 = 0.0016$  mag vs. 0.008 mag, and  $\Delta P_{\text{puls}} = 0.0002$  d vs. 0.0004 d). The two stars are considerably different in that V838 Cyg has a much higher amplitude and shorter period than KIC 11125706 ( $A_{\text{tot}} = 1.10$  mag vs. 0.47 mag;  $P_{\text{puls}} = 0.48$  d vs. 0.61 d; see Fig. 4 below).

**Fig. 2** shows for V838 Cyg (left) and KIC 11125706 (right) four Fourier variables plotted as time series. The plotted variables are (from bottom to top): the amplitude  $A_1$  and the phase  $\phi_1$ , both from the first term in the Fourier sine series; the ratio  $R_{21}$  of the second and first Fourier amplitudes; and the Fourier phase difference parameter,  $\phi_{31}^s$ . The four variables were obtained by dividing the long cadence data from Q1 to Q11 into time segments, each segment corresponding to three pulsation periods (*cf.* Fig. 5 of N11 where the *Kepler* stars NQ Lyr and V783 Cyg are plotted). Approximately 40000 data points were analyzed for each star, and 15 terms were used for the Fourier decompositions.

For both stars the mid-times and Blazhko phases of the respective CFHT spectra are indicated (labelled red vertical lines), as are the adopted  $t_0$  zero points (labelled blue vertical lines). For KIC 11125706 the large gaps at  $t=253-323$  and at  $t=600-688$  are because no observations were made in the second two months of Q4 and in Q8. For the same star the blue open squares result from analysis of the 126955 short cadence photometric measurements made in Q7 – agreement of the short and long cadence results is excellent<sup>13</sup>.

The modulation periods are obvious and seen to be close to 55 d for V838 Cyg, and 40 d for KIC 11125706 – these are the basic Blazhko periods. In addition to the amplitude modulations seen in the  $A_1$  and  $R_{21}$  panels, the variation of  $\phi_1$  is indicative of frequency modulation. That the time-series plots for  $\phi_1$  and  $\phi_{31}^s$  (which measures the pulse shape) are mirror images of each other is not uncommon (but not always the case, as is seen for V2178 Cyg in Fig. 3 below).

On relatively short time scales, such as the  $\sim 90$  day baseline of the available SC:Q10 data for V838 Cyg (not plotted), the modulations look sinusoidal; however, closer inspection shows that they are not. That the  $A_1$  waves are compressed around time  $t = 200$  and 550 but are wider around  $t = 400$  and 750 proves that the modulation period for V838 Cyg is varying. Thus the amplitude and frequency modulations are complex. A “Period04” frequency analysis of the long cadence data iden-

<sup>13</sup> Such agreement is not always the case owing to different normalizations used during the detrending procedure, but the differences appear always to be small (less than 1% for each variable) and do not affect our main results.

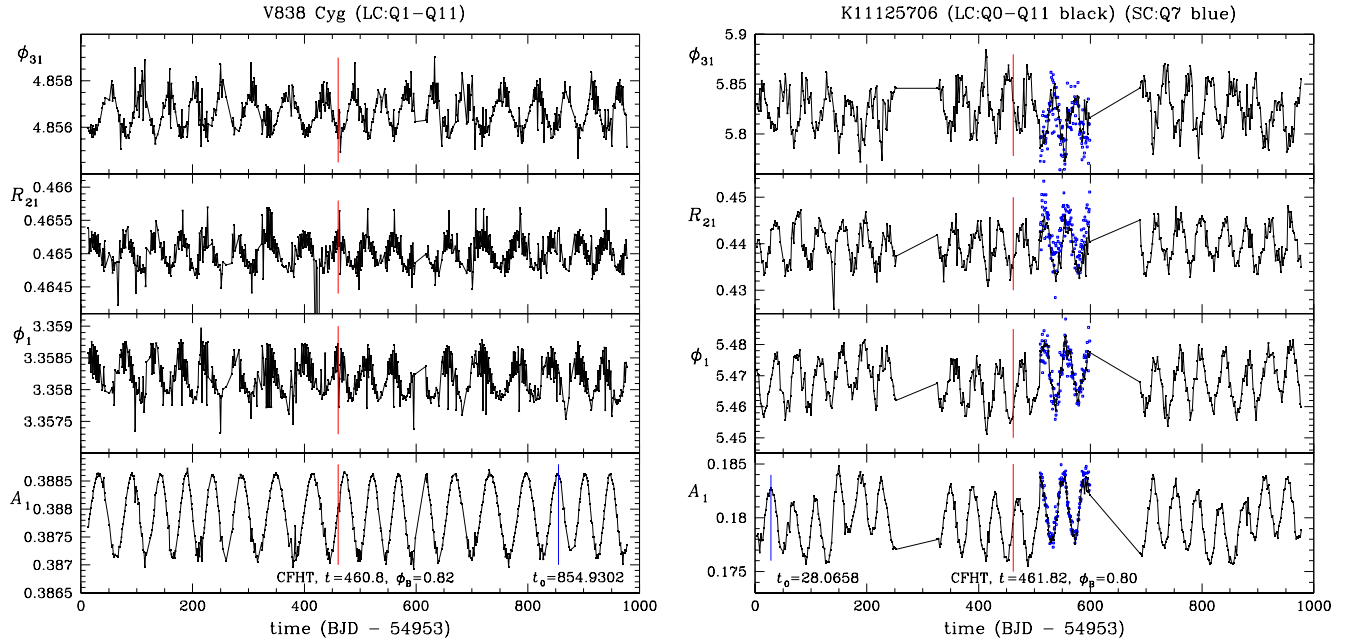


FIG. 2.— Amplitude and frequency modulations for V838 Cyg (left) and KIC 11125706 (right), as seen in time series graphs for four Fourier parameters. The results from analyses of both the long cadence *Kepler* photometry (black connected points) and the short cadence *Kepler* photometry (blue open squares) are plotted. Vertical lines (labelled) are drawn at the mid-times of the CFHT spectroscopic observations (red) and at the adopted  $t_0$  zero points (blue). A color version of this figure is given in the on-line version of the paper.

tified multiple Blazhko periods of 54, 64 and 47 days, the first being the most significant. Finally, the cycle-to-cycle amplitude variations seen in the bottom right panel suggest that additional amplitude modulations may be present for KIC 11125705.

Many other *Kepler*-field Blazhko stars in addition to V838 Cyg and KIC 11125706 have been found to exhibit interesting and complex modulation behaviours. In the next subsection two quite different Blazhko variables (V1104 Cyg and V2178 Cyg) are used to illustrate the time- and frequency-domain methods that were used for deriving the Blazhko periods and Blazhko types.

### 3.2.2. Blazhko Periods and Types from Power Spectra

Blazhko periods can also be inferred from power spectra. In fact, the Blazhko classification scheme of Alcock *et al.* (2000, 2003) is based solely on characteristic power-spectra patterns. When the Fourier transform of prewhitened photometry shows a single major feature at  $f_1$ , offset from the fundamental pulsation frequency  $f_0$ , the Blazhko type is said to be ‘RR0-BL1’. In this case the Blazhko frequency is  $f_{BL} = |f_1 - f_0|$ , and  $P_{BL} = 1/f_{BL}$ . When the Fourier transform of the prewhitened data shows two major features, symmetric about the fundamental frequency, the type is said to be ‘RR0-BL2’. For such stars  $P_{BL}$  is equal to the reciprocal of the mean frequency shift (assuming that the two features are equidistant from  $f_0$ ). For other types found in the MACHO surveys see Table 1 of Alcock *et al.* (2003).

**Fig. 3** illustrates the time- and frequency-domain methods used here. V1104 Cyg (left panels) is a typical Blazhko star having relatively-low amplitude modulation (although much larger than that of KIC 11125706 and V838 Cyg) and a  $P_{BL} \sim 53$  d (18 cycles in  $\sim 950$  d); and V2178 Cyg (right panels) exhibits extreme amplitude modulation (similar to but not as extreme as V445 Lyr)

with  $P_{BL} \sim 235$  d (four cycles in  $\sim 940$  d). The top panel for each cluster shows the folded light curves phased with the mean pulsation period (Table 1), where amplitude variations and phase shifting (indicative of the frequency modulation) are clearly seen. The middle panels show portions of the power spectra for frequencies near the primary pulsational frequency before (upper graph) and after prewhitening with the primary frequency and its harmonics (lower graph). And the bottom multipanels are time series plots similar to those shown in Fig. 2.

The V1104 Cyg light curve (top left panel of Fig. 3) is derived from the Q9 short cadence photometry (138540 data points), and the power spectra and time series plots are based on the Q1-Q11 long cadence photometry (43341 points). A nonlinear least squares fit to the long cadence data gave an estimated primary frequency of  $f_0 = 2.29155411(\pm 5)c/d$  (radial fundamental mode), corresponding to pulsation period  $P = 0.43638507(\pm 5)d$ . The secondary frequencies are symmetric about  $f_0$  and occur at  $f_0 - f_{BL} = 2.2723$  c/d and  $f_0 + f_{BL} = 2.3108$  c/d, from which we derive the Blazhko frequency,  $f_{BL} = 0.01925$  c/d and  $P_{BL} = 51.995 \pm 0.005$  d, and classify the star as type RR0-BL2. In the time series plots the variations of all four Fourier parameters are seen to be nearly sinusoidal, with an estimated mean Blazhko period of 52.003 d. The agreement with the  $P_{BL}$  derived from the Fourier transform is excellent, and we adopt the mean of the two values,  $51.999 \pm 0.005$  days. The flatness of the  $\phi_1$  graph lends supports to the derived  $P_{puls}$ . An upwards sloping line would have resulted if the assumed period had been longer; in this sense the  $\phi_1$  panels are analogous to O-C diagrams. Finally, the  $A_1$  panel shows amplitude maxima around  $t = 200, 550$  and  $900$  days, corresponding to an additional period around 1 year; it is quite possible that this is an artifact of the pre-processing procedure.

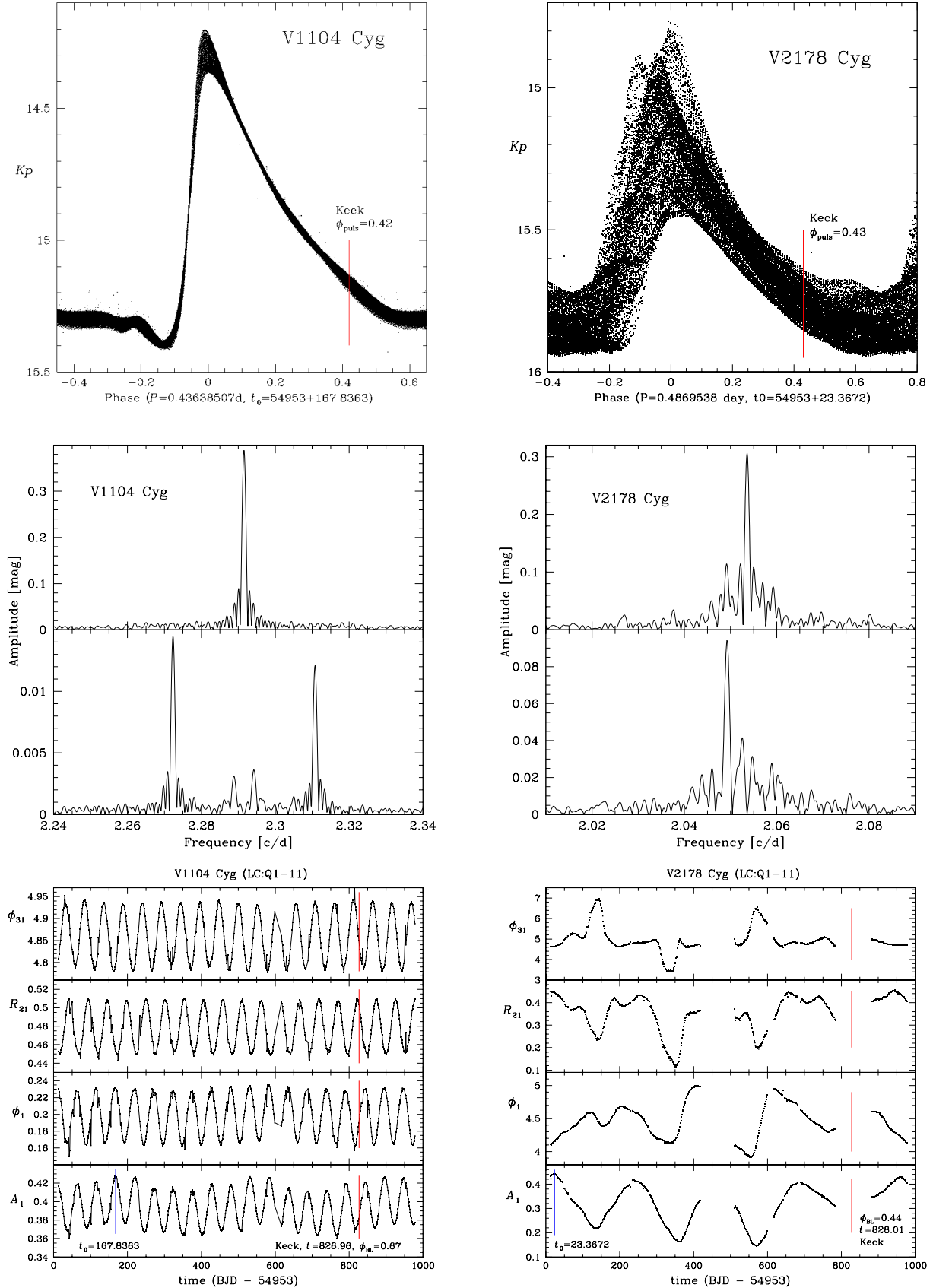


FIG. 3.— **(Top)** Phased light curves for V1104 Cyg (KIC 12155928, left) and V2178 Cyg (KIC 3864443, right) - the mean pulsation phases of the Keck spectroscopic observations are indicated by a vertical line and labelled; **(Middle)** Power spectra, where the upper panel shows the Fourier transform in the vicinity of the primary frequency, and the lower panel shows the Fourier transform after prewhitening with the primary frequency and its harmonics. V1104 Cyg is characterized by a symmetric triplet (RR0-BL2) and V2178 Cyg by an possible asymmetric doublet (RR0-BL1?). **(Bottom)** Time-series graphs for four Fourier parameters - the vertical lines indicate the assumed times of maximum amplitude and light,  $t_0$ , and the mean times,  $t$ , and Blazhko phases,  $\phi_{\text{BL}}$ , at which the Keck observations were made. A color version of this figure is given in the on-line version of the paper.

The V2178 Cyg light curve (top right panel of Fig. 3) is derived from the long cadence photometry from Q1-Q11 (34994 data points). The primary frequency,  $f_0 = 2.053586 \pm 0.000004$  c/d, corresponds to  $P_{\text{puls}} = 0.486954 \pm 0.000004$  d. After prewhitening with this frequency and its harmonics, a single strong sidepeak is seen (mag $\sim$ 0.09), accompanied by several weaker sidepeaks (mag $\sim$ 0.02-0.04). Thus we have what appears to be an asymmetric doublet pattern, and a classification of RR0-BL1. However, this star, and to a lesser extent V354 Lyr which has an uncertain Blazhko type owing to its long  $P_{\text{BL}}$ , are the only such possible RR0-BL1 types in our sample and it is possible that both are BL2 stars with very asymmetric sidelobes. Such borderline classifications are quite common: Alcock *et al.* (2003) found that “160 out of the 400 BL1 stars [in the MACHO LMC sample] could be classified as BL2”. In any case, the Blazhko period that follows from the frequency difference,  $f_0 - f_{\text{BL}} = 0.00433$  c/d, is  $P_{\text{BL}} = 234 \pm 10$  days. The time-series plots are unusual and in general the variations are seen to be considerably more complex than for V1104 Cyg (the gaps in the time-series plots near  $t \sim 450$  and 800 are due to no observations having been made in Q6 and in Q10). The alternating up-down bumps seen in the  $\phi_{31}^s$  panel is, to our knowledge, unique among Blazhko stars.

Diagrams similar to those plotted in Figs. 2 and 3 were constructed for all the program stars. While each of the stars seems to be of considerable interest in its own right, many of the findings are only indirectly pertinent to the subject of the metal abundances. Where the diagrams are most relevant is in the adopted mean  $\phi_{31}^s$  values that go into the photometric [Fe/H] analysis (see §5), in the pulsation phases that are related to the effective temperatures (and are used to calculate  $\gamma$ -velocities), and in the Blazhko phases that affect luminosities and effective temperatures needed for deriving spectroscopic [Fe/H] values. Detailed discussions of our findings concerning modulation characteristics of the individual Blazhko stars will be presented elsewhere.

**Table 3** gives the estimated Blazhko periods and types of the 16 Kepler-field Blazhko stars. The  $P_{\text{BL}}$  estimates were derived by fitting sine functions to time series plots of the amplitudes (see bottom panels of Figs. 2 and 3), and from power spectra of the raw and prewhitened photometry, with both methods producing nearly identical estimates. The final  $P_{\text{BL}}$  values range from  $27.667 \pm 0.001$  days (V783 Cyg) to  $723 \pm 12$  days (V354 Lyr), with an average  $\langle P_{\text{BL}} \rangle = 111$  days. It is somewhat surprising that none of the stars have Blazhko periods shorter than 27 days, the median  $P_{\text{BL}}$  for the 14 Blazhko stars discovered in the Konkoly Blazhko Survey (see Table 2 of Jurcsik *et al.* 2009c). None of the stars has  $P_{\text{BL}}$  as long as the four OGLE-III Galactic Bulge stars which have  $P_{\text{BL}}$  up to  $\sim 3000$  days (see Fig. 5 of Soszynski *et al.* 2011 for light curves). V353 Lyr seems to exhibit doubly-periodic modulation with periods of  $71.64 \pm 0.06$  d and  $132.6 \pm 0.7$  d.

For those stars with  $P_{\text{BL}} < 100$  d and in common with B10 our estimates of  $P_{\text{BL}}$  agree well with the values given in their Table 2. The estimated uncertainties from our analyses are considerably smaller (by factors  $\sim 10$ -100 times) owing to the much longer time baseline and the inclusion of the short cadence photometry. The longer baseline also allowed us to derive Blazhko periods for

TABLE 3  
BLAZHKO PERIODS, PHASES AND TYPES

Star (1)	$P_{\text{BL}}$ [days] (2)	$t_0(\text{BL})$ (3)	$\phi_{\text{BL}}$ (4)	Type (5)
V2178 Cyg	$234 \pm 10$	23.3672	0.44	BL1?
V808 Cyg	$92.14 \pm 0.01$	17.2834	0.82	BL2
V783 Cyg	$27.667 \pm 0.001$	22.5439	0.93	BL2
V354 Lyr	$723 \pm 12$	292.1590	0.74	unc.
V445 Lyr	$54 \pm 1$	207.5957	0.32	BL2
RR Lyrae	$39.20 \pm 0.10$	325.2263	0.77	BL2
KIC 7257008	$39.56 \pm 0.08$	805.5859	-	BL2
V355 Lyr	$31.05 \pm 0.04$	171.7072	0.64	BL2
V450 Lyr	$123.7 \pm 1.6$	43.3226	0.34	BL2
V353 Lyr	[71.6, 132.6]	129.6820	0.74	BL2x2
V366 Lyr	$62.84 \pm 0.03$	373.1915	0.24	BL2
V360 Lyr	$52.07 \pm 0.02$	35.9332	0.17	BL2
KIC 9973633	$73.0 \pm 0.6$	827.3655	0.99	BL2
V838 Cyg	[54.64, 47]	854.9302	0.82	BL2x3
KIC 11125706	$40.23 \pm 0.03$	28.0658	0.76	BL2
V1104 Cyg	$51.999 \pm 0.005$	167.8363	0.67	BL2

NOTE. — The columns contain: (1) star name; (2) Blazhko period (=period of amplitude modulation); (3) time of maximum amplitude (=BJD–2454953); (4) Blazhko phase at the mid-time of our spectroscopic observations; (5) RR0 Blazhko type, as defined by Alcock *et al.* (2000, 2003); the type for V354 Lyr is uncertain owing to its long  $P_{\text{BL}}$ .

those stars with amplitude modulations that are occurring on time scales longer than 100 days. For example, we derived the following estimates of  $P_{\text{BL}}$  for V2178 Cyg, V808 Cyg, V354 Lyr, V450 Lyr:  $234 \pm 10$ ,  $92.14 \pm 0.01$ ,  $723 \pm 12$  and  $123.7 \pm 1.6$  days, respectively. Table 3 also includes the first estimates of  $P_{\text{BL}}$  for three stars not in the B10 list: KIC 7257008, KIC 9973633 and V838 Cyg.

### 3.2.3. Blazhko Phases

The Blazhko phase at which the spectra were taken,  $\phi_{\text{BL}}$ , and the adopted time of zero phase for the Blazhko cycles,  $t_0(\text{BL})$ , assumed to be when the pulsation amplitude was largest, are also given in Table 3. The  $t_0(\text{BL})$  are identical to the values given in Table 1, but are more conveniently expressed to correspond with the time-series graphs (see Figs. 2-3). For a given star the Blazhko phases were necessarily random.

If the  $P_{\text{BL}}$  and  $A_{\text{tot}}$  were time invariant then any time of maximum amplitude could have been chosen as the zero-point for the Blazhko variations. However, this is not the case (see Table 2) since many of the Blazhko stars also have multiple Blazhko frequencies and complex power spectra. For such stars the  $\phi_{\text{BL}}$  depend on many factors, and in these cases local maxima before and after the times of the observed spectra were identified and these were used to compute the Blazhko phase.

The time series plots shown in Figs. 2-3 serve to illustrate the  $\phi_{\text{BL}}$  determinations. Four spectra of V838 Cyg were taken at CFHT, between BJD–54953=460.79 and 460.82, with a mid-time of 460.80. The times of maximum amplitude immediately preceding and following 461 are at 415 and 472, respectively. Thus  $\phi_{\text{BL}} = 0.82$  for V838 Cyg. V1104 Cyg and V2178 Cyg were both observed at Keck, with mid-times of the observations at 826.96 and 828.01, respectively. Since the times of maximum amplitude immediately before and after 826.96 d occur at 791.1 and 844.8 the  $\phi_{\text{BL}}$  for V1104 Cyg is 0.67. A similar calculation made for V2178 Cyg gave  $\phi_{\text{BL}} = 0.44$ .

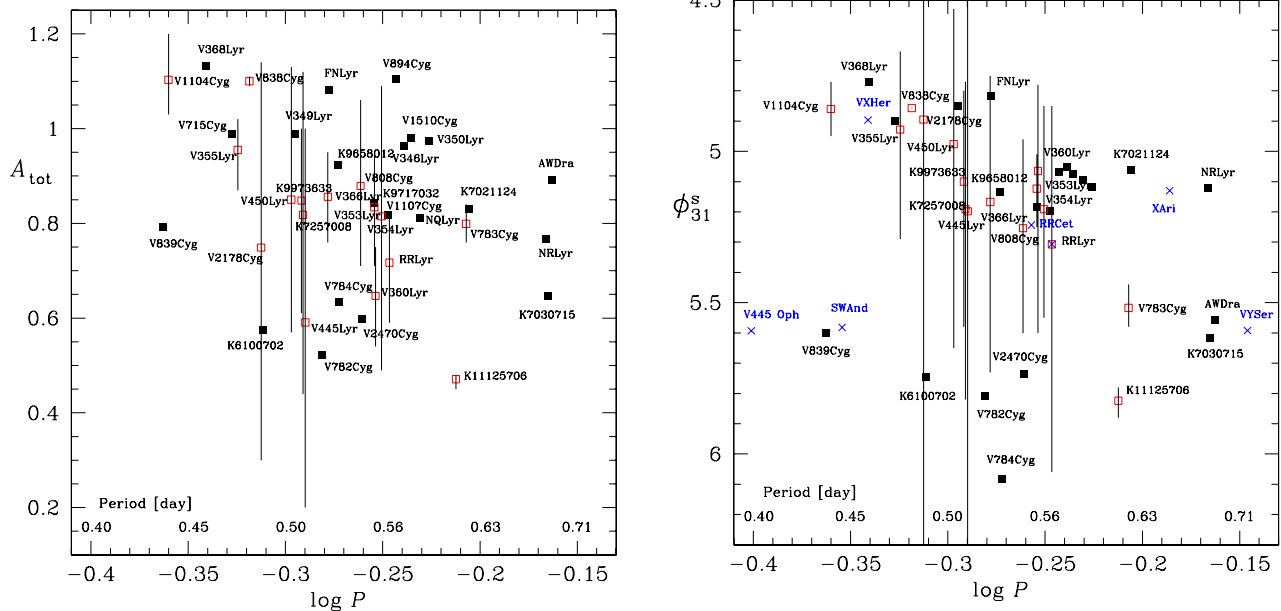


FIG. 4.— Period-amplitude diagram (left) and period- $\phi_{31}^s$  diagram (right) for the non-Blazhko (black squares) and Blazhko (red open squares) RRab stars in the *Kepler* field. Also represented in the right panel are several Keck spectroscopic standard stars (blue crosses). The periods are pulsation periods, the  $A_{\text{tot}}$  are on the  $Kp$ -system, and the Fourier phase parameters  $\phi_{31}^s$  are from sine-series Fourier decomposition of the *Kepler* photometry. The  $\phi_{31}^s$  axis has been reversed to emphasize the similarity of the two diagrams. For the Blazhko stars the vertical lines indicate the measured ranges in their  $A_{\text{tot}}$  and  $\phi_{31}^s$  values (see Table 2), and the (red open) boxes are plotted at the mean  $\phi_{31}^s$  values. A color version of this figure is given in the on-line version of the paper.

### 3.3. Period-Amplitude and Period- $\phi_{31}^s$ Diagrams

The early studies by Oosterhoff (1939, 1944), Arp (1955) and Preston (1959) established that in the period-amplitude diagram for RR Lyrae stars there is a separation by metal abundance, with metal-poor RRab stars tending to have longer pulsation periods at a given amplitude than metal-rich RRab stars. This effect has been used to better understand the Oosterhoff dichotomy and to derive metallicities for RR Lyrae stars found in different environments, such as in globular clusters (Sandage 1981, 1990, 2004; Cacciari *et al.* 2005), in different fields of our Galaxy, and in other galaxies. The effect is now known to be due to the lower metal abundance stars having greater luminosities and therefore longer periods (see Sandage 2010; Bono *et al.* 2007), a result which is consistent with the recent Warsaw convective pulsation hydro-models (see Fig.14 of N11).

In the 1980's Simon and his collaborators introduced Fourier decomposition techniques for describing the shapes of RR Lyr light curves, and established useful correlations between various Fourier parameters and  $[\text{Fe}/\text{H}]$ , mass, luminosity, and other physical parameters (Simon & Lee 1981; Simon & Teays 1982; Simon 1985, 1988; Simon & Clement 1993). Since the mid-1990's Kovács and Jurcsik and their collaborators (Kovács & Zsoldos 1995; Jurcsik & Kovács 1996, hereafter JK96; Kovács & Jurcsik 1996; Kovács & Walker 2001; Kovács 2005) have expanded upon these Fourier ideas and have produced useful empirical equations that describe the relationships between RRab light curve parameters and physical characteristics. In particular, JK96 derived a  $P$ - $\phi_{31}^s$ - $[\text{Fe}/\text{H}]$  relation (their equation 3) which is often used to estimate the metallicities of RRab stars. More recently, Morgan *et al.* (2007, hereafter M07) derived analogous equations for RRc stars.

In **Fig. 4** the  $\log P$ - $A_{\text{tot}}$  and  $\log P$ - $\phi_{31}^s$  diagrams are plotted for the *Kepler*-field RRab stars. The pulsation periods,  $A_{\text{tot}}(Kp)$  and  $\phi_{31}^s(Kp)$  are the new values given in Table 1, and the diagrams include both non-Blazhko (black squares) and Blazhko stars (red open squares). By reversing the direction of the  $\phi_{31}^s$  axis one observes directly the similarity of the two diagrams (see Sandage 2004) and that those stars with the largest amplitudes tend to have the most asymmetric light curves, *i.e.*, the smallest  $\phi_{31}^s$  values. In both diagrams all but a few of the most crowded points have been labelled with the star names. For the two most extreme Blazhko stars, V445 Lyr and V2178 Cyg, the  $\phi_{31}^s$  ranges exceed the range of the plotted y-axis. The RRc stars in the *Kepler* field are off-scale to the left of both graphs, with small amplitudes, large  $\phi_{31}^s$  values, and periods shorter than 0.4 d.

Several trends are apparent in Fig. 4, the most obvious being the similarity of the two diagrams. There is also an apparent separation of the stars into two groups, discriminated better by  $P_{\text{puls}}$  and  $\phi_{31}^s$  than by  $P_{\text{puls}}$  and  $A_{\text{tot}}$ . Most of the stars are observed to have  $A_{\text{tot}} > 0.8$  mag and  $\phi_{31}^s < 5.4$  radians. According to the metallicity correlations mentioned above these are metal-poor stars with  $[\text{Fe}/\text{H}] < -1.0$  dex. The other group, those shorter-period stars with lower amplitudes and higher  $\phi_{31}^s$  values, are expected to be more metal-rich, with  $[\text{Fe}/\text{H}] > -1.0$  dex. For a fixed metallicity as the pulsation period increases the stars tend to have smaller amplitudes and more sinusoidal light curves (*i.e.*, smaller  $\phi_{31}^s$  values).

When all the stars in a given sample are suspected of having the same or similar metallicities (e.g., in globular clusters with narrow red giant branches), or when there exist independent spectroscopic metal abundances for the sample stars, then diagonal lines can be fit to

the observational data (e.g., Sandage 2004, Cacciari *et al.* 2005, N11). Such diagonal trends are evident in the Fig. 4  $\log P-\phi_{31}^s$  diagram, especially when the spectroscopic standard stars (blue crosses) are included in the diagram. This diagram also suggests that the new non-Blazhko star V839 Cyg, and the low-amplitude-modulation star KIC 11125706 (Fig. 2) are metal rich. Indeed, we show below that V839 Cyg is metal-rich, with  $[\text{Fe}/\text{H}] = -0.05 \pm 0.14$  dex; however, the CFHT spectra of KIC 11125706, with  $[\text{Fe}/\text{H}] = -1.09 \pm 0.08$  dex (see Table 7), indicate that it probably belongs to the metal-poor group.

The Blazhko stars require special consideration. They are represented in Fig. 4 by their mean pulsation periods and their mean  $A_{\text{tot}}$  or  $\phi_{31}^s$  values (red open squares), with vertical lines spanning the measured ranges of  $A_{\text{tot}}$  and  $\phi_{31}^s$ . If metal abundances are derived by substituting the mean  $\phi_{31}^s$  values given in Table 1 into the JK96  $P-\phi_{31}^s-[\text{Fe}/\text{H}]$  relation, then the resulting photometric  $[\text{Fe}/\text{H}]$  values suggest that almost all of the Blazhko variables are metal-poor; indeed, this is supported by the spectroscopic metallicities (next section), and runs contrary to the suggestion by Moskalik & Poretti (2003) that the incidence of Blazhko variables increases with  $[\text{Fe}/\text{H}]$ . Also, since the Blazhko stars appear to have, at a given period, lower mean  $A_{\text{tot}}$  values and higher mean  $\phi_{31}^s$  values than the non-Blazhko stars, it appears that the *Kepler* Blazhko stars must be more metal-rich, on average, than the non-Blazhko stars. The validity of these conclusions depends on the applicability of the JK96 formula, and on the appropriateness of the assumed  $\phi_{31}^s$  values, the latter being particularly true for the most extreme Blazhko stars (V445 Lyr, V2178 Cyg) where the  $\phi_{31}^s$  show large modulations. These topics will be discussed further in §5.

#### 4. CFHT AND KECK SPECTROSCOPY

High-resolution spectroscopic observations were made of the *Kepler*-field RR Lyrae stars using the Canada-France-Hawaii 3.6-m telescope (CFHT) and the Keck-I 10-m telescope (W.M. Keck Observatory), both located on Mauna Kea, Hawai'i. A total of 123 spectra were taken of 42 stars and in most cases the derived spectroscopic metal abundances are the first available estimates.

Since a primary goal of this study was derivation of  $[\text{Fe}/\text{H}]_{\text{spec}}$  values, spectra were taken at pulsation phases between  $\sim 0.2$  and  $\sim 0.5$ , at the changeover from outflow to infall. Away from these phases the spectra are increasingly affected by velocity-gradients in the atmosphere and shock waves that broaden the spectral lines (see Preston 2009, 2011; K11; For *et al.* 2011). The pulsation phases for the mid-times of the individual spectra are given in Tables 4-5 below and were derived using the updated pulsation periods and  $t_0$  values that were calculated using Q0-Q11 photometry. Nearly 80% of the spectra were acquired at phases between 0.25 and 0.55 (see upper panel of Fig. 5). The overall median and mean  $\phi_{\text{puls}}$  are 0.35 and 0.38, respectively, with  $\sigma = 0.13$ ; the mean  $\phi_{\text{puls}}$  for the 54 Keck spectra is larger than that for the 68 CFHT spectra (0.48 vs. 0.30).

##### 4.1. CFHT 3.6-m ESPaDOnS Spectra

The CFHT spectra were acquired from July-December 2010 using the ESPaDOnS prism cross-dispersed échelle

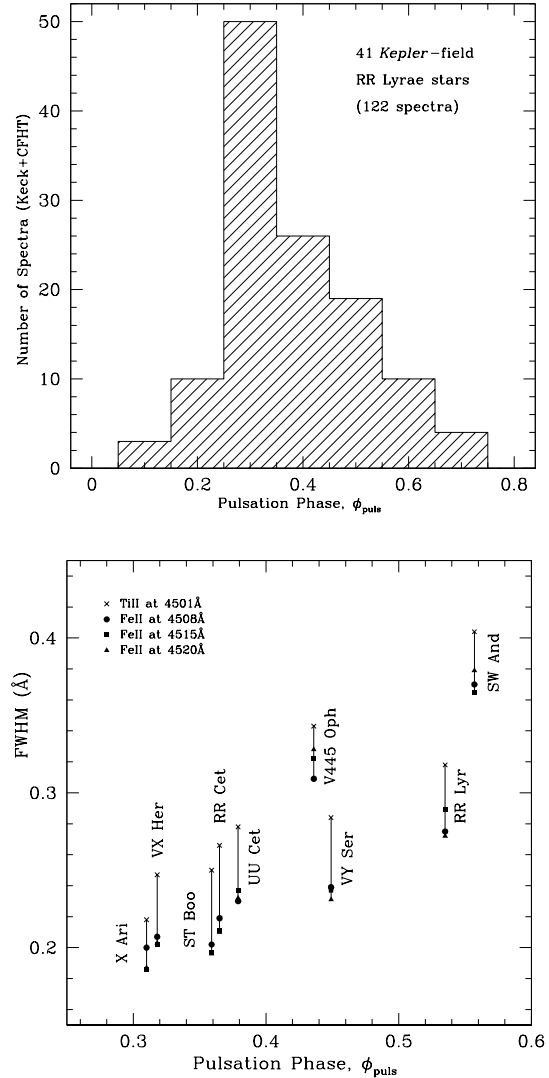


FIG. 5.— (Top) Histogram of the observed pulsation phases for the 41 *Kepler*-field RR Lyrae stars, based on the 122 spectra taken with the CFHT 3.6-m and Keck-I 10-m telescopes. (Bottom) Full-width half minimum (FWHM) values for four spectral lines near 450 nm, as a function of the pulsation phase. The points plotted are for the bright RR Lyrae standard stars observed with Keck, and the FWHM values were measured using the IRAF ‘splot’ routine. The narrowest lines are seen to occur at phases between 0.3 and 0.4, and for a given phase the three Fe II lines (at 450.8, 451.5 and 452.0 nm) are narrower than the Ti II line (at 450.1 nm).

spectrograph in the ‘star+sky’ non-polarimetric mode. Two optical fibers fed the star and sky images from the Cassegrain focus to the Coudé focus, then onto a Bowen-Walraven image slicer at the entrance of the spectrograph. The resolving power was  $R = \lambda/\Delta\lambda \sim 65000$ , which corresponds to a spectral resolution of  $\Delta\lambda \sim 0.008$  nm at  $\lambda = 517$  nm (Mg triplet). The spectra are spread over 40 grating orders (on an EEV1 CCD chip), with wavelength coverage from 370 to 1048 nm, an average reciprocal dispersion of 0.00318 nm/pixel, and  $\sim 3$  pixels per resolution element.

Eighteen of the brightest RR Lyrae stars in the *Kepler* field were observed at CFHT (Service Observing). The total observing time amounted to 20 hours. The observations were made under photometric skies for all but

TABLE 4  
 CFHT ESPADONS SPECTRA OF *Kepler* RR LYRAE STARS

Star	Spectrum	$t_{\text{exp}}$	Observation	S/N	FWHM	AM	HJD (mid)	$\phi_{\text{puls}}$	$RV$ (fxcor)
(1)	No. (2)	[s] (3)	date (UT) (4)	(5)	[mÅ] (6)	(7)	2400000+ (8)	(9)	[km/s] (10)
KIC 6100702	1218711	900	2010-07-30	23	308 (10)	1.13	55407.9264	0.227	-54.16 (20)
	1218712	900	2010-07-30	22	269 (08)	1.17	55407.9406	0.256	-52.38 (17)
	1218713	900	2010-07-30	21	283 (06)	1.20	55407.9515	0.279	-50.54 (17)
	1218714	900	2010-07-30	20	249 (20)	1.24	55407.9625	0.301	-47.85 (17)
AW Dra	1218715	900	2010-07-30	32	226 (23)	1.34	55407.9754	0.287	-197.85 (18)
	1218716	900	2010-07-30	31	210 (16)	1.34	55407.9863	0.302	-196.25 (21)
	1218717	900	2010-07-30	32	200 (03)	1.44	55407.9973	0.318	-194.65 (21)
	1218718	900	2010-07-30	31	198 (08)	1.51	55408.0082	0.334	-193.70 (22)
FN Lyr	1218719	900	2010-07-30	32	226 (21)	1.49	55408.0204	0.265	-261.20 (23)
	1218720	900	2010-07-30	33	203 (03)	1.57	55408.0313	0.286	-258.57 (21)
	1218721	900	2010-07-30	32	236 (12)	1.68	55408.0423	0.307	-256.85 (23)
	1218722	900	2010-07-30	29	217 (18)	1.81	55408.0533	0.328	-254.67 (16)
V894 Cyg	1219066	900	2010-08-01	27	178 (18)	1.63	55409.7372	0.354	-234.14 (21)
	1219067	900	2010-08-01	29	214 (28)	1.54	55409.7482	0.383	-232.47 (18)
	1219068	900	2010-08-01	29	189 (18)	1.47	55409.7591	0.402	-230.38 (18)
	1219069	900	2010-08-01	29	196 (11)	1.40	55409.7702	0.422	-228.90 (21)
NQ Lyr	1219070	900	2010-08-01	27	198 (09)	1.23	55409.7836	0.301	-72.45 (18)
	1219071	900	2010-08-01	27	183 (34)	1.19	55409.7945	0.320	-70.47 (15)
	1219072	900	2010-08-01	27	185 (12)	1.16	55409.8054	0.339	-68.43 (22)
	1219073	900	2010-08-01	26	152 (12)	1.14	55409.8164	0.357	-66.97 (13)
NR Lyr	1219477	900	2010-08-02	35	222 (28)	1.24	55410.9703	0.274	-124.30 (26)
	1219478	900	2010-08-02	35	147 (24)	1.29	55410.9813	0.290	-123.20 (19)
	1219479	900	2010-08-02	36	129 (05)	1.34	55410.9922	0.306	-121.82 (15)
	1219480	900	2010-08-02	35	094 (04)	1.41	55411.0032	0.322	-119.42 (28)
V355 Lyr	1219876	1200	2010-08-05	17	309 (05)	1.37	55413.7353	0.144	-240.73 (16)
	1219877	1200	2010-08-05	16	161 (34)	1.29	55413.7497	0.175	-238.03 (34)
	1219878	1200	2010-08-05	15	195 (50)	1.24	55413.7641	0.205	-233.78 (17)
	1219879	1200	2010-08-05	16	219 (13)	1.19	55413.7785	0.236	-231.82 (11)
V838 Cyg	1219880	900	2010-08-05	14	173 (34)	1.23	55413.7924	0.328	-209.05 (21)
	1219881	900	2010-08-05	14	231 (47)	1.21	55413.8033	0.351	-206.91 (25)
	1219882	900	2010-08-05	13	140 (60)	1.18	55413.8143	0.374	-205.73 (26)
	1219883	900	2010-08-05	13	166 (06)	1.17	55413.8252	0.396	-202.29 (19)
V2470 Cyg	1220136	900	2010-08-06	23	250 (13)	1.37	55414.7545	0.289	-57.06 (18)
	1220137	900	2010-08-06	23	225 (17)	1.32	55414.7654	0.309	-55.16 (22)
	1220138	900	2010-08-06	23	255 (07)	1.28	55414.7764	0.329	-53.38 (22)
	1220139	900	2010-08-06	23	257 (16)	1.24	55414.7874	0.349	-51.59 (25)
KIC 11125706	1220140	900	2010-08-06	57	228 (04)	1.19	55414.8033	0.308	-69.42 (20)
	1220141	900	2010-08-06	59	229 (07)	1.17	55414.8142	0.326	-68.08 (22)
	1220142	900	2010-08-06	59	223 (05)	1.16	55414.8251	0.343	-66.58 (22)
	1220143	900	2010-08-06	61	236 (03)	1.15	55414.8361	0.361	-65.19 (22)
KIC 3868420 <sup>†</sup>	1220147	600	2010-08-06	96	359 (09)	1.06	55414.9016	0.173	-27.63 (16)
KIC 9453114 (RRc)	1220148	900	2010-08-06	29	283 (13)	1.16	55414.9120	0.241	-152.09 (20)
	1220149	900	2010-08-06	30	320 (60)	1.19	55414.9230	0.271	-153.53 (22)
	1220150	900	2010-08-06	30	375 (42)	1.22	55414.9339	0.301	-152.31 (19)
	1220151	900	2010-08-06	29	267 (42)	1.25	55414.9449	0.331	-151.70 (15)
V1104 Cyg	1259187	1200	2010-11-16	19	316 (57)	1.33	55516.6860	0.117	-325.49 (63)
	1259188	1200	2010-11-16	20	294 (13)	1.39	55516.7004	0.150	-320.87 (69)
	1259189	1200	2010-11-16	19	287 (49)	1.46	55516.7148	0.184	-318.40 (24)
	1259190	1200	2010-11-16	15	380 (10)	1.55	55516.7293	0.217	-313.73 (38)
V1510 Cyg	1259908	1200	2010-11-18	20	250 (50)	1.19	55518.6891	0.316	-350.35 (40)
	1259909	1200	2010-11-18	20	220 (40)	1.24	55518.7035	0.341	-348.22 (18)
	1259910	1200	2010-11-18	19	250 (50)	1.29	55518.7179	0.366	-345.90 (53)
	1259911	1200	2010-11-18	19	-	1.36	55518.7323	0.391	-343.55 (20)
V783 Cyg	1261460	1200	2010-11-25	17	200 (60)	1.24	55525.6867	0.324	-197.26 (27)
	1261461	1200	2010-11-25	16	250 (100)	1.30	55525.7011	0.347	-195.38 (22)
	1261462	1200	2010-11-25	16	250 (70)	1.38	55525.7156	0.370	-193.16 (22)
	1261463	1200	2010-11-25	17	250 (100)	1.48	55525.7300	0.394	-190.49 (36)
KIC 8832417 (RRc)	1262172	900	2010-11-27	30	243 (74)	1.59	55527.7291	0.223	-28.52 (15)
	1262173	900	2010-11-27	29	293 (09)	1.69	55527.7400	0.267	-27.07 (16)
	1262174	900	2010-11-27	28	324 (33)	1.82	55527.7509	0.311	-25.86 (17)
	1262175	900	2010-11-27	27	351 (28)	1.96	55527.7619	0.355	-25.41 (51)
V808 Cyg	1265907	1200	2010-12-15	9	-	1.71	55545.6950	0.256	-
	1265908	1200	2010-12-15	8	-	1.89	55545.7094	0.283	-
	1265909	1200	2010-12-15	8	-	2.14	55545.7238	0.309	-
	1265910	1200	2010-12-15	7	-	2.47	55545.7382	0.335	-
KIC 7030715	1266124	900	2010-12-16	23	330 (140)	1.89	55546.6890	0.238	-373 (8)
	1266125	900	2010-12-16	26	222 (34)	2.06	55546.6999	0.254	-365.41 (17)
	1266126	900	2010-12-16	23	208 (02)	2.27	55546.7109	0.270	-364.41 (48)
	1266127	900	2010-12-16	14	-	2.53	55546.7218	0.286	-361.98 (62)

NOTE. — The columns contain: (1) star name (upper) and metal abundance (lower, from Table 7); (2) ESPaDOnS spectrum number; (3) exposure time [s]; (4) Observation date (UT); (5) Signal-to-noise ratio per CCD pixel, at  $\lambda \sim 570$  nm and computed by *Upena* at CFHT; (6) Average FWHM (full-width at half-minimum) value for the three Fe II lines at 4508, 4515 and 4520 Å, where the uncertainty (given in parentheses) is approximated by the standard deviation of the mean (*e.g.*, 10 mÅ for spectrum number 1218711); (7) airmass at start of observation; (8) heliocentric Julian date at mid-exposure; (9) pulsation phase at mid-exposure time; (10) heliocentric radial velocity, calculated using the IRAF ‘fxcor’ routine.

<sup>†</sup>KIC 3868420 is either a rare short-period multiperiodic RRc (RRc?) star, or a possible high-amplitude  $\delta$  Scuti (HADS) star; in either case our VWA and SME analyses indicate that it is metal rich.

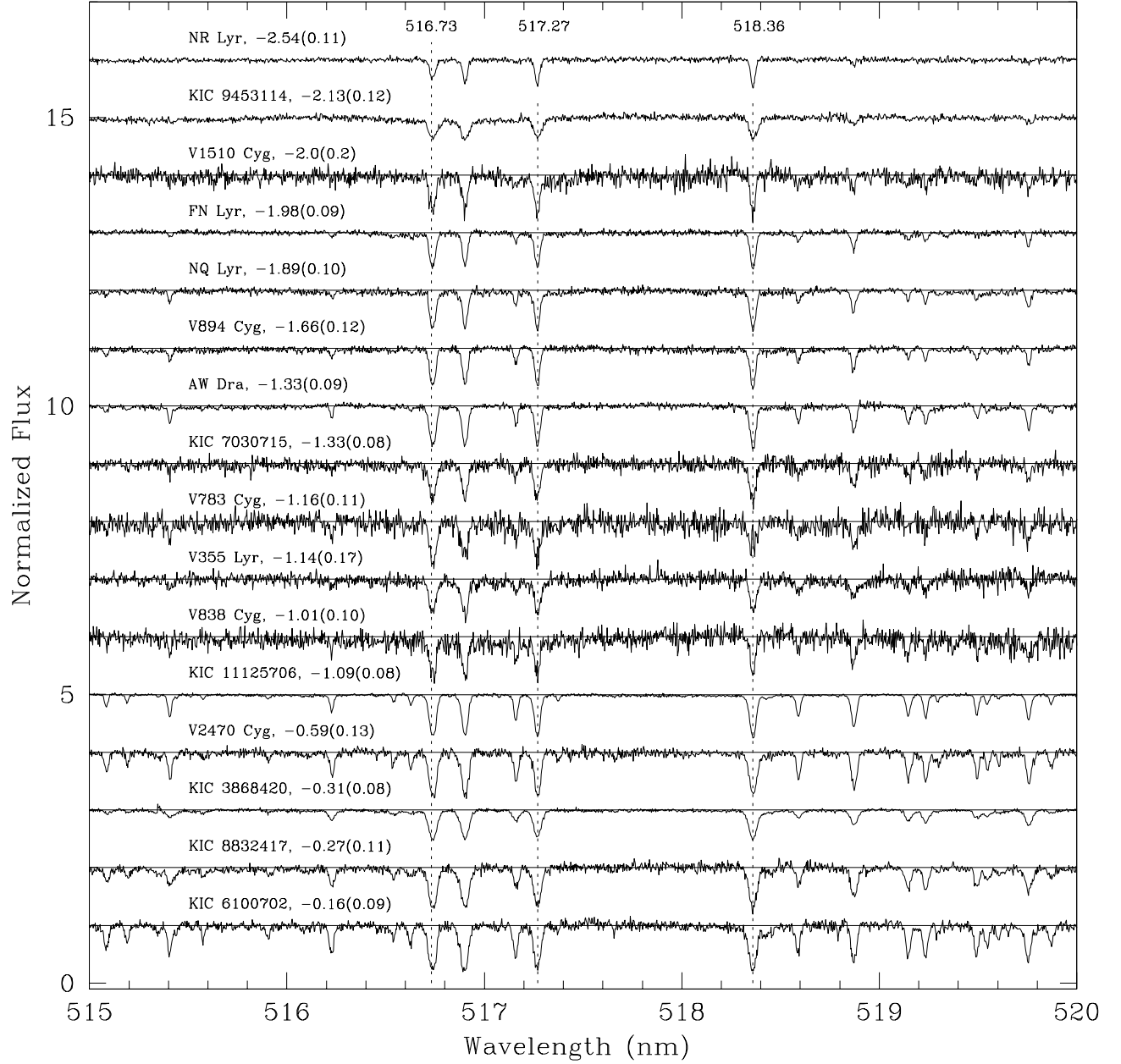


FIG. 6.— Mosaic showing the 517 nm Mg I triplet region of the CFHT spectra for the 16 stars for which metallicities could be derived. The rest wavelengths of the Mg I triplet lines are given at the top of the graph. The enhanced line strengths of the most metal-rich stars (bottom) clearly distinguish them from the more metal-poor stars (top). The probable HADS star, KIC 3868420, is third from the bottom.

three of the stars (V355 Lyr, V838 Cyg, KIC 7030715), and at various hour angles and airmasses. The seeing was rarely better than 1 arcsec. Multiple spectra were taken for most stars, usually with exposure times of  $4 \times 900$  s; for the faintest observed stars ( $14.5 < Kp < 15.0$ ) the exposure times were increased to  $4 \times 1200$  s.

The ‘Upena’ software, which uses ‘Libre-ESpRIT’<sup>14</sup>, was used to pre-process the CFHT spectra – *i.e.*, perform bias subtraction and flat fielding, subtract the sky and scattered light, identify the echelle orders and perform optimal image extraction, make the wavelength calibrations (using spectra of a Th-Ar lamp), calculate the signal-to-noise ratios (S/N per pixel), and make the necessary heliocentric corrections for the Earth’s motion. The individual spectra were normalized and the overlapping échelle orders merged using the VWA ‘rainbow’ widget (Bruntt *et al.* 2010a,b). For those stars with multiple observations the normalized spectra were co-added to increase the signal-to-noise ratios. Details of the individual spectra are given in **Table 4**. The S/N per pixel values (column 5) were measured at 570 nm<sup>15</sup> and range from 7-96, with typical values  $\sim 20$ -30. The full-width at half-minimum (FWHM) values (column 6) were measured using the Fe II lines at 450.8, 451.5 and 452.0 nm, and range from  $\sim 100$ -400 mÅ<sup>16</sup>.

Co-added spectra for the 16 CFHT stars for which metallicities could be derived are plotted in **Fig. 6**, where the wavelength range  $515 < \lambda < 520$  nm contains the green Mg I triplet lines. The spectra have been corrected for Doppler shifts, and, to illustrate the effect of increasing metallicity, are ordered by [Fe/H]. The spectra of V1104 Cyg ( $Kp=15.03$ ) and V808 Cyg ( $Kp=15.36$ ) were of insufficient quality to permit the derivation of metal abundances (but were sufficient for deriving *RVs* for V1104 Cyg) and are not shown; both stars were re-observed with the Keck telescope.

#### 4.2. Keck-I 10-m HIRES Spectra

The faintest *Kepler*-field RR Lyrae stars were observed on the nights of 2011 August 4/5, 5/6 and 6/7 with the HIRES echelle spectrograph (Vogt *et al.* 1994) mounted on the Keck-I 10-m telescope (see Cohen *et al.* 2005a,b; 2009) – see **Table 5** for details. The spectrograph was used in the HIRES-r configuration and thus optimized for long wavelength observations (QE > 60% between 400 and 900 nm). A slit of width 1.15 arcsec and length 7 arcsec (C5 decker, no filters) was used, resulting in resolving power  $R \sim 36,000$  ( $\Delta\lambda \sim 0.014$  nm at 517 nm) over the range 389-836 nm. The average reciprocal dispersion is 0.00230 nm/pixel (140 nm spread over 60882 pixels) and the number of pixels per resolution element is  $\sim 6$ . The spectra were spread over a mosaic of three

MIT/Lincoln Labs 2048 $\times$ 4096 CCD chips<sup>17</sup>. The  $\lambda$ -scale was calibrated using Th-Ar lamp exposures taken at the beginning and end of each night; measurements of the widths of typical emission lines suggest an instrumental FWHM of  $5.6 \pm 0.3$  pixels, corresponding to  $129 \pm 7$  mÅ. To reduce phase-smearing and potential cosmic ray problems exposure times for the program stars were never longer than 1200 sec, and usually multiple exposures were taken and co-added. The Mauna Kea Echelle Extraction (MAKEE<sup>18</sup>) reduction package was used to pre-process the data.

In addition to the program stars we observed nine bright RR Lyr standard stars studied by Layden (1994, hereafter L94) and Clementini *et al.* (1995, hereafter C95), and three red giant stars in the very metal-poor globular cluster M92 (mean [Fe/H] =  $-2.33$  dex, with little within-cluster variation - Cohen 2011). All of the RR Lyr standard stars are RRab pulsators and include RR Lyrae itself ( $Kp = 7.862$ ), which happens to be located in the *Kepler* field and has been the subject of several recent detailed investigations (K10, K11, Benedict *et al.* 2011). The M92 stars served primarily as *RV* standards and the bright RR Lyr stars as metallicity standards. The most metal poor and metal rich standard stars are X Ari and SW And, respectively, for which [Fe/H] =  $-2.74 \pm 0.09$  dex and  $+0.20 \pm 0.08$  dex (see Table 7), and the corresponding *Kepler*-field RR Lyr stars are NR Lyr and V784 Cyg, for which [Fe/H] =  $-2.54 \pm 0.11$  dex and  $-0.05 \pm 0.10$  dex. Although X Ari and NR Lyr are very metal poor, and have metallicities similar to those of the most metal-poor RR Lyr stars known in the Large and Small Magellanic Clouds (see Haschke *et al.* 2012), they are not the most metal poor stars known in our Galaxy (see Schörk *et al.* 2009).

Sample Keck spectra are plotted in **Fig. 7**, for the same wavelength range (515-520 nm) as Fig. 6. The three panels, each of which includes the high S/N spectrum of RR Lyrae, show program stars more metal-poor than RR Lyrae (Fig. 7a), program stars more metal-rich than RR Lyrae (Fig. 7b), and Keck RR Lyr standard stars (Fig. 7c). The high-resolution, S/N  $\sim 1000$ , solar spectrum supplied with VWA (Fig. 7c) was acquired with the KPNO Fourier Transform Spectrometer (Kurucz *et al.* 1984; Hinkle *et al.* 2000).

Typical FWHM values were measured for individual and co-added Keck spectra using the same three Fe II spectral lines that were used for the CFHT spectra. The measured FWHM values for the individual spectra (see Table 5) and for the co-added spectra (see Table 7) range from 150 to 470 mÅ, which is similar to the range for the CFHT spectra. As expected the measured FWHM values tend to be largest for phases away from maximum

<sup>14</sup> The original ‘ESpRIT’ program is described by Donati *et al.* (1997); ‘Libre-ESpRIT’ is the current release used at CFHT and documented at <http://www.cfht.hawaii.edu/Instruments/Spectroscopy/Espadons/Espadons.esprit.html>.

<sup>15</sup> The S/N ratio is largest in the interval 550-580 nm, but does not vary by more than  $\sim 20\%$  over the interval 500-900 nm. Since one resolution element is approximately 1.4 pixels, or 2.6 km/s, the S/N per resolution element are  $\sim 1.2$  times larger.

<sup>16</sup> The measured FWHM values are related to the true (or instrument-corrected) values according to  $\text{FWHM}_{\text{true}} = (\text{FWHM}_{\text{meas}}^2 - \text{FWHM}_{\text{instr}}^2)^{1/2}$ , where for the ESPaDOnS spectra the  $\text{FWHM}_{\text{instr}}$  was measured to be  $\sim 2.0$  pixels, or 64 mÅ.

<sup>17</sup> The blue chip (CCD1) covers the range 389 nm to 529 nm (24 spectral orders) and includes H $\beta$ , H $\gamma$ , H $\delta$  and the H and K lines. The green chip (CCD2) covers the range 538-689 nm (15 orders) and includes H $\alpha$  – for the last few orders there are small gaps in the spectrum. And the red chip (CCD3) covers the range 698-836 nm (9 orders), with between-order gaps ranging from 2-5 nm, the largest gaps occurring at the longest wavelengths (e.g., at 734-736 nm, 749-752 nm, 799-803 nm, and 817-822 nm). The largest gaps in the spectral coverage occur between the chips (9.5 nm between CCD1 and CCD2, and 9 nm between CCD2 and CCD3).

<sup>18</sup> MAKEE was written by T.A. Barlow specifically for the reduction of HIRES spectra, and is publicly available at <http://spider.ipac.caltech.edu/staff/tab/makee/>.

TABLE 5  
 KECK-I 10-M HIRES SPECTRA OF PROGRAM AND STANDARD STARS

Star	Spec. No.	$t_{\text{exp}}$ [s]	S/N	FWHM [mÅ]	AM	HJD (mid) 2400000+	$\phi_{\text{puls}}$	$RV$ (fxcor) [km/s]
(1)	(2)	(3)	(4)	(5)	(6)	(7)	(8)	(9)
(a) 22 <i>Kepler</i> -field RR Lyrae program stars (excluding RR Lyrae)								
V839 Cyg	5951	1200	51	379 (01)	1.40	55778.7493	0.100	-97.48 (14)
	5952	1200	50	368 (02)	1.30	55778.7639	0.133	-93.78 (14)
V360 Lyr	5953	1200	17	348 (11)	1.24	55778.7786	0.495	-170.80 (26)
	5954	1200	18	353 (04)	1.20	55778.7931	0.521	-168.85 (14)
	5955	1200	19	343 (15)	1.16	55778.8076	0.547	-167.95 (17)
V354 Lyr	5957	1200	20	272 (05)	1.08	55778.8347	0.354	-207.67 (14)
	5958	1200	19	327 (11)	1.08	55778.8492	0.380	-205.35 (14)
	5959	1200	18	282 (05)	1.08	55778.8637	0.405	-202.95 (17)
V368 Lyr	5960	1200	15	161 (08)	1.09	55778.8786	0.401	-267.41 (14)
	5961	1200	11	195 (11)	1.11	55778.8931	0.432	-264.59 (22)
	5962	1200	12	201 (13)	1.18	55778.9076	0.464	-261.43 (99)
V353 Lyr	5963	1200	9	199 (18)	1.18	55778.9220	0.415	-199.42 (53)
	5964	1200	8	145 (17)	1.22	55778.9366	0.443	-196.91 (21)
	5965	1200	7	204 (51)	1.27	55778.9510	0.467	-194.38 (29)
	5966	1200	7	-	1.33	55778.9656	0.493	-192.30 (17)
	6000	1200	13	192 (07)	1.39	55779.9752	0.307	-210.26 (11)
	6001	1200	12	219 (35)	1.48	55779.9897	0.332	-207.77 (11)
V782 Cyg	5967	1200	22	277 (19)	1.19	55778.9814	0.418	-60.97 (15)
	5968	1200	22	287 (06)	1.24	55778.9962	0.446	-58.88 (14)
V784 Cyg	5969	1200	19	306 (13)	1.31	55779.0128	0.462	-10.31 (17)
	5970	1200	19	304 (09)	1.39	55779.0273	0.489	-8.81 (16)
V1107 Cyg	5983	1200	15	215 (20)	1.46	55779.7425	0.475	-117.07 (12)
	5984	800	14	221 (27)	1.38	55779.7549	0.497	-115.08 (23)
KIC 9973633	5985	1200	8	-	1.47	55779.7679	0.576	-206.84 (48)
	5986	1200	8	-	1.38	55779.7837	0.606	-203.70 (23)
	5987	1200	8	-	1.31	55779.7982	0.635	-202.93 (35)
	5988	1200	9	-	1.26	55779.8127	0.664	-205.54 (32)
KIC 4064484	5990	800	37	288 (11)	1.10	55779.8324	0.586	-290.79 (12)
KIC 9658012	5991	1200	21	369 (31)	1.15	55779.8457	0.499	-312.52 (10)
	5992	1200	20	403 (29)	1.13	55779.8602	0.527	-310.41 (09)
	5993	1200	21	423 (09)	1.12	55779.8748	0.554	-309.32 (11)
V445 Lyr	5996	1200	14	319 (24)	1.13	55779.9167	0.285	-392.79 (24)
	5997	1200	14	237 (25)	1.17	55779.9312	0.314	-390.40 (17)
	5998	1200	14	245 (21)	1.21	55779.9457	0.342	-388.18 (11)
V1104 Cyg	5999	1000	37	174 (03)	1.31	55779.9599	0.420	-293.96 (10)
KIC 5520878	6002	1000	45	319 (02)	1.47	55780.0041	0.459	-0.70 (29)
KIC 9717032	6003	1200	13	303 (19)	1.46	55780.0179	0.321	-457.11 (21)
	6004	1200	14	281 (31)	1.57	55780.0324	0.347	-454.63 (11)
V450 Lyr	6017	900	11	273 (42)	1.37	55780.7406	0.546	-269.48 (19)
	6018	1200	13	240 (07)	1.32	55780.7535	0.571	-267.65 (10)
	6019	1200	16	254 (10)	1.25	55780.7703	0.606	-265.84 (10)
V366 Lyr	6022	1200	15	301 (01)	1.13	55780.8367	0.658	-68.51 (16)
	6023	1200	16	357 (05)	1.12	55780.8512	0.685	-68.47 (18)
	6024	1200	16	350 (28)	1.12	55780.8657	0.712	-67.61 (18)
V346 Lyr	6027	1200	10	293 (08)	1.18	55780.9138	0.619	-272.88 (14)
V808 Cyg	6028	1200	19	473 (16)	1.10	55780.9338	0.630	+32.40 (15)
	6029	600	4	-	1.12	55780.9449	0.649	+31.83 (33)
V350 Lyr	6032	1200	22	283 (25)	1.44	55780.9775	0.523	-91.41 (14)
	6033	1200	23	324 (17)	1.54	55780.9920	0.547	-89.56 (15)
V2178 Cyg	6034	1200	26	212 (13)	1.36	55781.0085	0.241	-116.89 (20)
	6035	1200	26	213 (09)	1.46	55781.0230	0.270	-115.04 (16)
V715 Cyg	6036	1200	15	238 (17)	1.57	55781.0387	0.494	-78.36 (18)
	6037	1200	15	229 (09)	1.73	55781.0532	0.525	-75.87 (20)
(b) Nine bright RR Lyrae stars (including RR Lyrae)								
ST Boo	5950	600	160	198 (02)	1.04	55778.7289	0.359	1.23 (10)
V445 Oph	5956	600	125	315 (05)	1.24	55778.8211	0.436	-11.96 (13)
RR Lyr	5971	200	324	276 (06)	1.68	55779.0361	0.535	-56.48 (06)
SW And	5972	300	184	367 (06)	1.04	55779.0416	0.557	-4.32 (07)
X Ari	5973	300	168	188 (05)	1.63	55779.0441	0.310	-42.01 (13)
VX Her	5982	200	109	202 (02)	1.01	55779.7287	0.318	-381.72 (20)
VY Ser	5989	300	135	232 (03)	1.40	55779.8218	0.449	-137.41 (10)
UU Cet	6006	300	74	226 (03)	1.25	55780.0649	0.379	-112.28 (12)
RR Cet	6042	300	226	212 (03)	1.06	55781.1104	0.365	-77.06 (09)
(c) Three red giants in the globular cluster M92								
M92-XII-34	5994	1200	77	178 (02)	1.28	55779.8894	-	-113.86 (26)
	5995	800	59	173 (03)	1.35	55779.9017	-	-114.23 (26)
M92-IV-79	6025	1200	70	158 (04)	1.27	55780.8828	-	-120.74 (13)
	6026	1200	59	156 (05)	1.33	55780.8975	-	-120.92 (13)
M92-IV-10	6030	1200	41	171 (06)	1.78	55780.9545	-	-120.31 (19)
	6031	500	39	182 (12)	1.98	55780.9650	-	-120.04 (19)

NOTE. — The columns contain: (1) star name; (2) spectrum number; (3) exposure time; (4) SNR per CCD pixel, at  $\lambda \sim 517$  nm (CCD1, 23rd order) and computed using MAKEE – for SNR per resolution element multiply the given values by 2.5; (5) Measured mean FWHM values for the three Fe II lines at 4508, 4515 and 4520 Å, where the uncertainty is approximated by the standard deviation of the mean (e.g., 1mÅ for spectrum 5951); (6) airmass (1.4 corresponds to a zenith angle of  $45^\circ$ ); (7) heliocentric JD at mid-exposure; (8) puls.phase at mid-exposure; (9) heliocentric RV derived using 'fxcor' - the uncertainties are in units of 0.01 km/s.

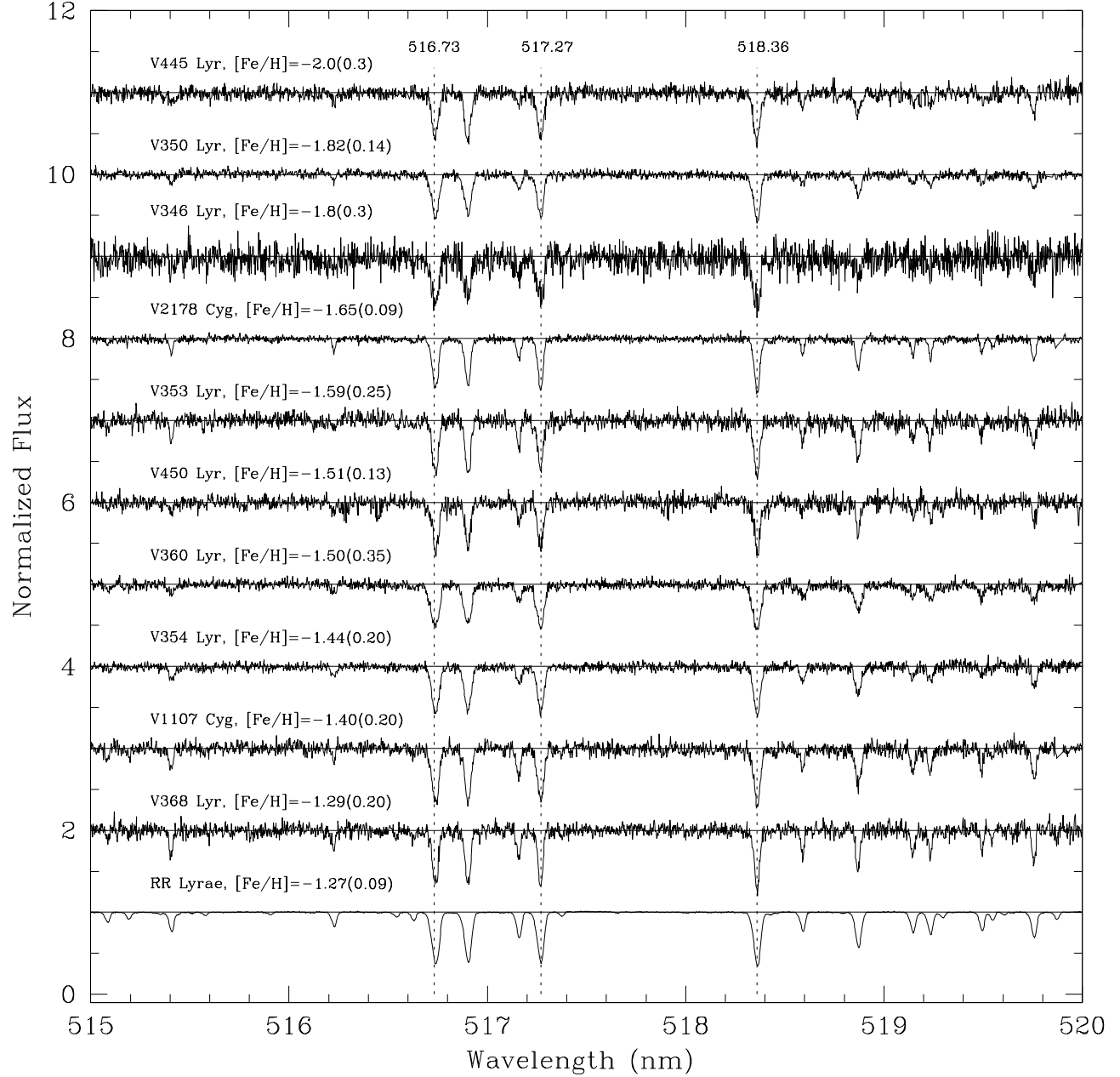


FIG. 7A.— Mosaic showing the 517nm Mg I triplet region of the Keck spectra for ten *Kepler*-field RRab stars more metal poor than RR Lyrae itself. (Note: this region is a small fraction of the available  $\lambda=389\text{-}838$  nm range of the HIRES spectra). The rest wavelengths of the three Mg I lines are given at the top of the graph. As in Fig.6 the stars have been ordered according to increasing metal abundance. The Keck spectrum of RR Lyrae ( $S/N\sim 250$ ) is plotted at the bottom of this mosaic.

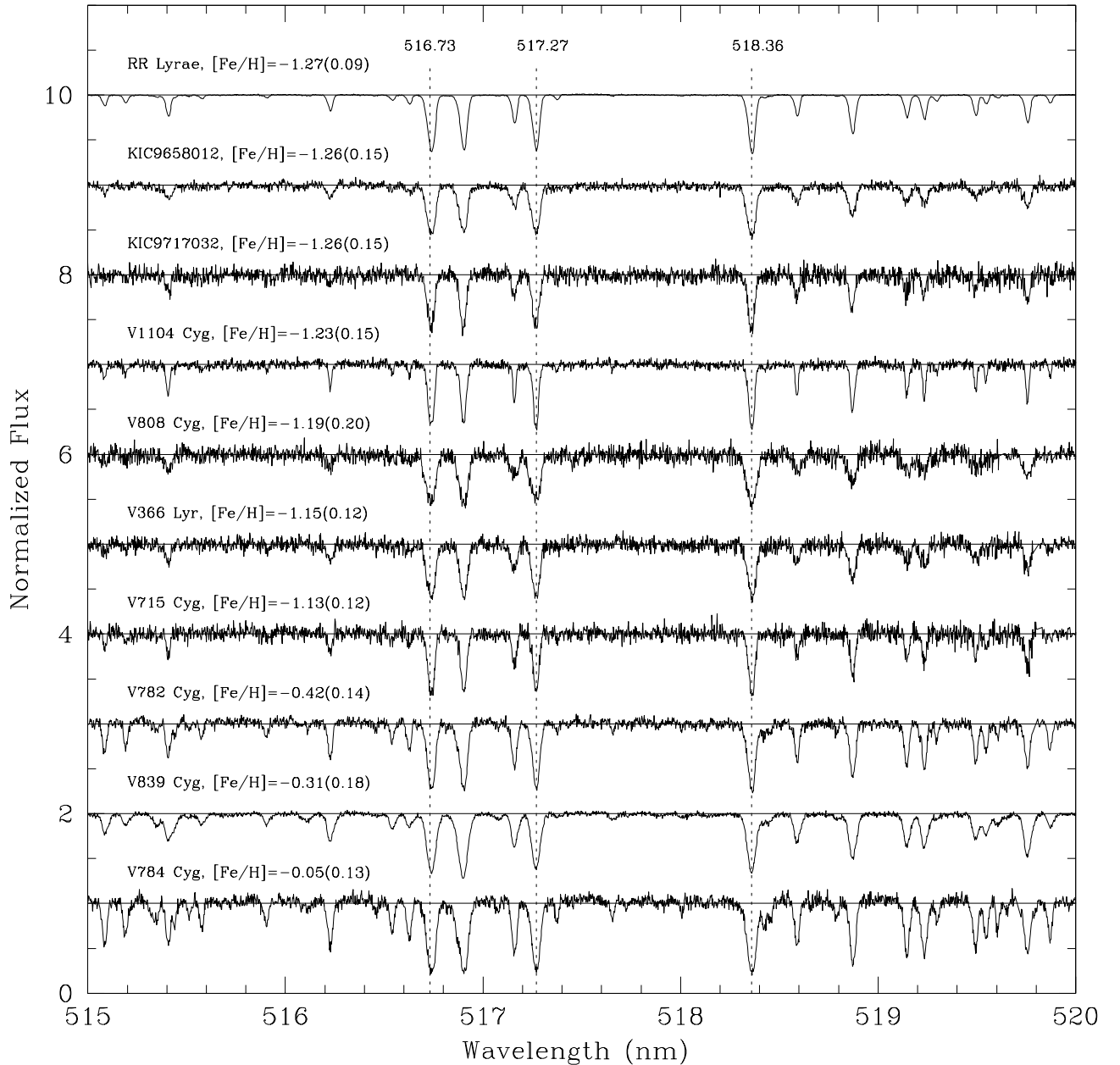


FIG. 7B.— Continuation of mosaic, in this case for nine *Kepler*-field RR Lyr stars more metal rich than RR Lyrae itself (shown at top). The three metal-rich RR Lyrae stars (bottom) are clearly distinguishable from the more metal-poor stars.

radius. This effect is illustrated in the lower panel of Fig.5, where the FWHM for the three FeII lines near 450nm and for the TiII line at 450.1 nm are plotted as a function of the pulsation phase for the nine bright RR Lyr standard stars. The narrowest lines are seen to occur at the earliest phases ( $\sim 0.3$ - $0.4$ ), and at all phases the FeII lines (solid symbols) are significantly narrower than the TiII line (crosses). The same pattern for these four lines is also seen for the *Kepler* stars (where phase range and scatter are larger), for RR Lyrae (Fig. 4 of K10), and for XZ Apr (Fig. 18 of For *et al.* 2011).

#### 4.3. Radial Velocities

It is well known that the *RVs* derived from spectra of RR Lyr stars are phase dependent and are not necessarily the same as the velocities that the stars would have if they were not pulsating (Oke 1966, Liu & Janes 1989, 1990a,b). Furthermore, the derived *RVs* depend on the spectral lines used for their measurement: *RV* curves calculated with metal lines tend to have smaller amplitudes than those calculated using Balmer-series lines ( $H\alpha$ ,  $H\beta$ ,  $H\gamma$ ) – a difference that has recently been quantified by Sesar (2012). A nice illustration of both effects is given in

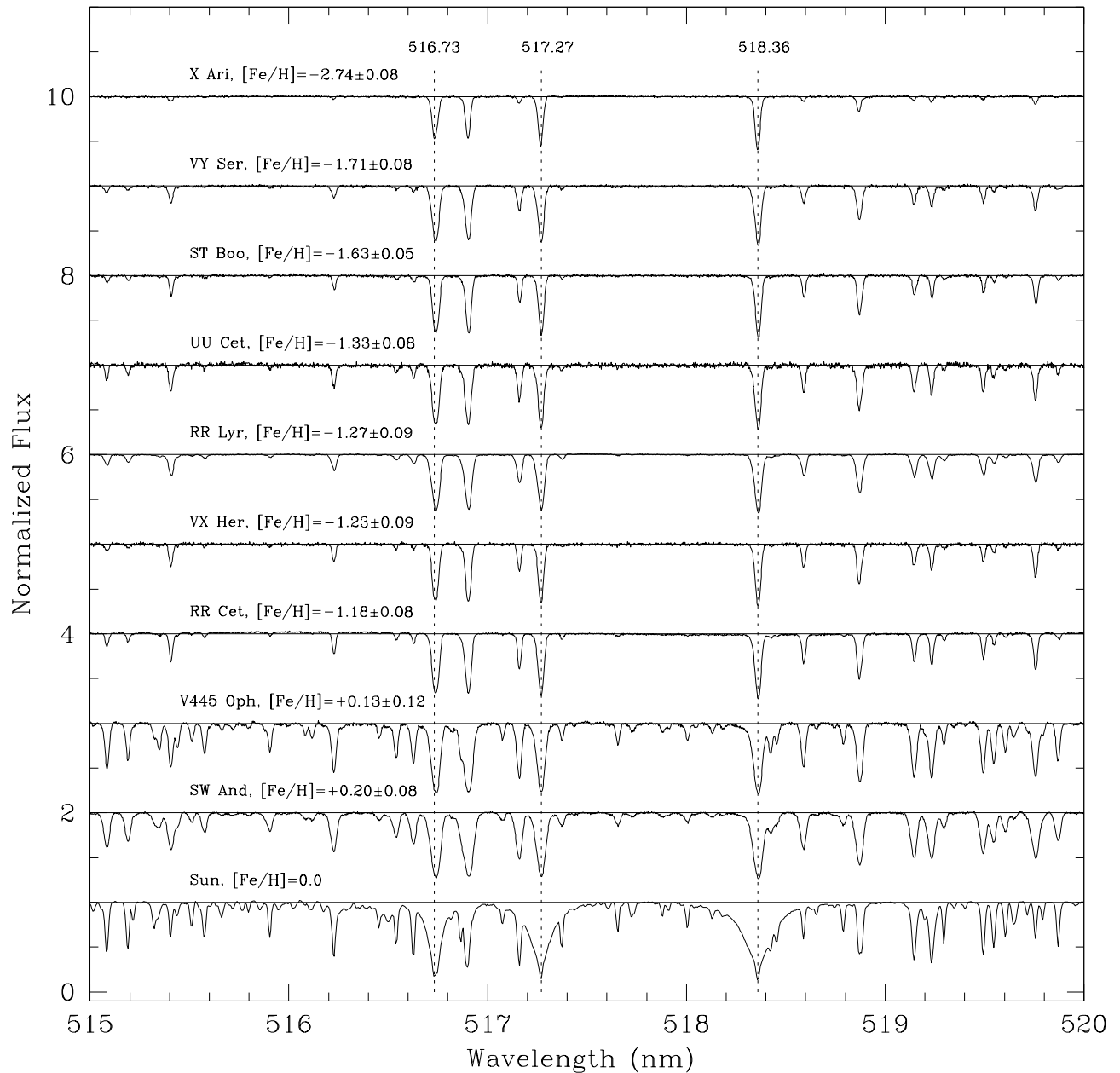


FIG. 7C.— Continuation of mosaic, in this case for the nine bright RR Lyr standard stars (including RR Lyrae), sorted in order of increasing metal abundance, and for the Sun. The broad Mg I lines in the solar spectrum readily show the greater pressure broadening in the Sun than in the RR Lyr stars.

Fig.2 of Preston (2011), which shows multiple  $RV$  curves for the southern RRab stars Z Mic and RV Oct.

In general, the  $RV$ s of RR Lyr stars are most negative near maximum light (*i.e.*, at  $\phi_{\text{puls}} \sim 0$ ) and most positive near minimum light (which, depending on the risetime, occurs for RRab stars around  $\phi_{\text{puls}} \sim 0.80 - 0.95$  and at earlier phases for RRC stars). Fundamental-mode pulsators also tend to show larger  $RV$  variations than first-overtone pulsators (as is also the case for the light variations), with double-mode (RRd) and other multi-mode pulsators showing the most complex variations. If a star

exhibits the Blazhko effect then the  $RV$  curve will reflect the amplitude and phase variations of such stars, and if pulsational velocities are required (e.g., Baade-Wesselink studies) then the observed  $RV$  must be corrected for projection effects (see Nardetto *et al.* 2004, 2009).

For our spectra the heliocentric  $RV$ s given in Tables 4-5 were derived using metal lines and the IRAF ‘fxcor’ routine. The heliocentric corrections were made during standard pipeline reductions, by *Upena* for the CFHT data and by MAKEE for the Keck data. For the ES-PaDOnS spectra only the limited wavelength range 511-

TABLE 6  
 $\gamma$ -VELOCITIES FOR THE RR LYR STANDARD STARS

Star	$\phi_{\text{puls}}$	$\gamma$ -velocity [km/s]		
		Layden	This paper	diff.
(1)	(2)	(3)	(4)	5
ST Boo	0.359	+13 $\pm$ 4	+1.7 $\pm$ 3	11 $\pm$ 5
V445 Oph	0.436	-22 $\pm$ 5	-22.6 $\pm$ 4	1 $\pm$ 6
RR Lyr	0.535	-63 $\pm$ 8	-72.0 $\pm$ 2	9 $\pm$ 8
SW And	0.557	-21 $\pm$ 2	-14.1 $\pm$ 3	7 $\pm$ 4
X Ari	0.310	-35 $\pm$ 3	-41.6 $\pm$ 3	-7 $\pm$ 4
VX Her	0.318	-375 $\pm$ 40	-361.5 $\pm$ 5	-14 $\pm$ 40
VY Ser	0.449	-145 $\pm$ 1	-142.8 $\pm$ 3	-2 $\pm$ 3
UU Cet	0.379	-116 $\pm$ 20	-110.3 $\pm$ 5	-6 $\pm$ 21
RR Cet	0.365	-75 $\pm$ 1	-74.4 $\pm$ 3	-1 $\pm$ 3

NOTE. — The columns contain: (1) star name; (2) pulsation phase at the mid-time of the spectrum; (3) the  $\gamma$ -velocity from L94; (4) the  $\gamma$ -velocity from the present paper; and (5) the  $\gamma$ -velocity difference, in the sense Layden minus this paper. Note also that RR Lyr, SW And and ST Boo are Blazhko variables with modulation periods of 39.6 d (see K11), 36.8 d (Szeidl 1988; see also Le Borgne *et al.* 2012), and 284 d (see Le Borgne *et al.* 2012), respectively.

518 nm was used for the cross-correlations and a typical  $RV$  uncertainty is  $\sim \pm 0.2$  km/s. The HIRES flux spectra were normalized using MAKEE and very accurate pixel shifts were calculated by cross-correlating all pairs of spectra that were taken over the three night run. The results were used to derive very precise and accurate relative velocities that were then shifted to the mean of the  $RV$ s computed relative to the known wavelengths.

The derived heliocentric  $RV$ s for the three M92 red giant standard stars (see Table 5) are all close to the cluster mean of  $-120$  km/s, suggesting that all are cluster members (see Roederer & Sneden 2011, Cohen 2011). Comparison with the  $RV$ s derived by Drukier *et al.* (2007) gives a median difference of  $\sim 0.5$  km/s and an RMS difference of 0.2 km/s.

The  $\gamma$ -velocities for the nine bright RR Lyrae standard stars were computed using Liu’s  $RV$  template and are given in Table 6. The last column contains the differences between our estimates and those of Layden (1994), where the mean difference is 1.3 km/s.

#### 4.4. [Fe/H] and Atmospheric Parameters

Estimation of metal abundances and other atmospheric parameters from high dispersion spectra depends on numerous assumptions regarding the stellar atmosphere where the spectral lines were formed. In our analyses, which were performed using the VWA, MOOG and SME packages, the lines were assumed to form in a one-dimensional plane-parallel atmosphere under local thermodynamic equilibrium (LTE) conditions. For RR Lyr stars (absolute magnitudes  $\sim 0.5$ ) the atmospheric extensions are sufficiently small (less than 1% according to Fig. 1 of Heiter & Eriksson 2006) that the plane-parallel assumption was judged to be adequate for the derivation of iron-to-hydrogen ratios.

The observed Kepler-field RR Lyr stars are a mixture of halo and old-disk stars, with distances ranging from  $265 \pm 11$  pc for RR Lyrae (Benedict *et al.* 2011) to  $\sim 25$  kpc for the faintest stars (N11); therefore they are expected to be old and to have a wide range of chemical and kinematic characteristics. In the H-R diagram they are horizontal branch stars at various stages of evolution away from the zero-age horizontal branch (ZAHB), and

over a pulsation cycle  $L$  and  $T_{\text{eff}}$  trace out a loop in the instability strip. The masses are expected to be in the range  $0.5\text{-}0.8 M_{\odot}$ , and most of the stars are expected to be near the ZAHB-level appropriate for the mass and metal abundance of the star (see Fig. 13 of N11).

The Blazhko and non-Blazhko RR Lyr stars in the Kepler field occur in approximately equal proportions. The pulsations of the non-Blazhko stars are mainly fundamental or first-overtone radial modes. To date no ‘classical’ double-mode RR Lyrae stars (*i.e.*, RRd stars) pulsating simultaneously in both modes have been identified; however, Molnar *et al.* (2012) recently detected a very weak first-overtone pulsation in RR Lyrae. When averaged over a pulsation cycle the mean values of  $T_{\text{eff}}$  are expected to range from 6000-7500 K, with the ab-type stars having cooler mean surface temperatures than the c-type stars. The ranges of the mean values of  $\log g$  and  $L$  are expected to be 2-3 and 40-60  $L_{\odot}$ . The instantaneous values for these quantities, which are phase dependent, span much wider ranges – see, for example, Jurcsik *et al.* (2009a,b,c), who suggested that the  $T_{\text{eff}}$  range might be as large as 3500 K (5500-9000 K), the range of  $\log g \sim 1.5$  to 4, and the range of  $L \sim 30\text{-}90 L_{\odot}$ . For all three physical characteristics the maxima occur slightly before  $\phi_{\text{puls}}=1$ . Because the CFHT and Keck spectra were taken at pulsation phases away from maximum light the RRab stars were expected to have ‘instantaneous’  $T_{\text{eff}}$  values in the considerably smaller range 6000-6500 K (see figs.7-10, 36-37 of For *et al.* 2011), with  $\log g$  between 2 and 3. An exception is V839 Cyg, which was observed just after maximum light, at  $\phi_{\text{puls}} = 0.12$ , and therefore expected to have a rather higher temperature. Unlike solar-like stars which typically have a microturbulent parameter  $\xi_t \sim 1$  km/s, the  $\xi_t$  for RR Lyr stars generally range from 2.5 to 4.0 km/s, with instantaneous values at maximum radius tending to occur at the lower end of this range (*i.e.*,  $\xi_t \sim 2.5\text{-}3.0$  km/s for phases between 0.2 and 0.6 – see Figs. 13-14 and 17 of For *et al.* 2011). Other information is available for some of the brighter stars. For example, for RR Lyrae at  $\phi_{\text{puls}} = 0.54$  the  $\log g$  and  $T_{\text{eff}}$  are expected to be  $\sim 2.75$  and  $6250 \pm 100$  K (see Table 5.2 of Kolenberg 2002), both of which vary from one Blazhko cycle to the next.

For the solar photosphere the abundance of iron relative to the number of hydrogen atoms per unit volume was assumed to be  $\log \epsilon(\text{Fe}) = 7.50$ , where  $\log \epsilon(\text{Fe}) \equiv \log(N_{\text{Fe}}/N_{\text{H}}) + 12.0$  and  $\log N_{\text{H}} = 12.0$ . This value is consistent with the iron abundance  $7.45 \pm 0.08$  recommended by Holweger (2001), the value 7.52 adopted by MOOG (Sneden 2002), and with the most recent value  $7.50 \pm 0.04$  given in the review by Asplund *et al.* (2009). For iron abundances relative to hydrogen and relative to the Sun we use  $[\text{Fe}/\text{H}]_* = \log(N_{\text{Fe}}/N_{\text{H}})_* - \log(N_{\text{Fe}}/N_{\text{H}})_{\text{solar}}$ . When abundances are expressed relative to the *total* number of atoms per unit volume (e.g., the values output from VWA and Kurucz’s ATLAS9 program), the photospheric ‘abundance’ of Fe is denoted  $A_{\text{Fe}} \equiv \log(N_{\text{Fe}}/N_{\text{total}})$ , where  $N_{\text{Fe}}$  is the number of Fe atoms per unit volume and  $N_{\text{Fe}}/N_{\text{total}}$  is the corresponding fraction of Fe relative to the total number density of atoms. If the number densities for hydrogen and helium are assumed to be  $\log N_{\text{H}} = 12.0$  and  $\log N_{\text{He}} = 10.99$  then these two elements are the only significant contributors to  $N_{\text{total}}$  and we have  $\log N_{\text{total}} = 12.04$ . Thus,

TABLE 7  
SPECTROSCOPIC IRON-TO-HYDROGEN ABUNDANCES (VWA) FOR THE *Kepler*-FIELD RR LYRAE STARS

Star	Obs.	$\phi_{\text{puls}}$	S/N	FWHM	$T_{\text{eff}} / \log g / \xi_t$	$[\text{Fe}/\text{H}]_{\text{spec}}$		
						Fe I lines	Fe II lines	adopted
(1)	(2)	(3)	(4)	(5)	(6)	(7)	(8)	(9)
(a) 17 Non-Blazhko RRab-type stars								
NR Lyr	CFHT	0.29	37	0.163 (02)	6500/ 2.6/ 2.5	$-2.54 \pm 0.13$ (6)	$-2.53 \pm 0.17$ (5)	$-2.54 \pm 0.11$
FN Lyr	CFHT	0.28	32	0.209 (19)	6300/ 2.44/ 2.5	$-2.00 \pm 0.13$ (10)	$-1.97 \pm 0.12$ (12)	$-1.98 \pm 0.09$
NQ Lyr	CFHT	0.32	30	0.197 (15)	6000/ 1.80/ 2.5	$-1.88 \pm 0.19$ (11)	$-1.90 \pm 0.10$ (3)	$-1.89 \pm 0.10$
V350 Lyr	Keck	0.53	34	0.293 (11)	6180/ 2.9/ 2.6	$-1.84 \pm 0.15$ (12)	$-1.81 \pm 0.14$ (10)	$-1.83 \pm 0.12$
V894 Cyg	CFHT	0.39	28	0.193 (08)	6200/ 2.46/ 2.0	$-1.65 \pm 0.18$ (11)	$-1.66 \pm 0.16$ (9)	$-1.66 \pm 0.12$
AW Dra	CFHT	0.30	38	0.202 (05)	6540/ 2.40/ 2.5	$-1.33 \pm 0.13$ (9)	$-1.33 \pm 0.12$ (6)	$-1.33 \pm 0.09$
KIC 7030715	CFHT	0.26	19	0.26 (04)	6500/ 2.64/ 2.5	$-1.32 \pm 0.07$ (6)	$-1.34 \pm 0.15$ (3)	$-1.33 \pm 0.08$
V1107 Cyg	Keck	0.48	21	0.220 (17)	6300/ 2.8/ 3.0	$-1.23 \pm 0.42$ (33)	$-1.31 \pm 0.18$ (11)	$-1.29 \pm 0.23$
V368 Lyr	Keck	0.43	20	0.183 (02)	6300/ 2.8/ 3.0	$-1.33 \pm 0.31$ (22)	$-1.25 \pm 0.24$ (10)	$-1.28 \pm 0.20$
KIC 9658012	Keck	0.84	37	0.413 (16)	6500/ 2.8/ 3.0	$-1.22 \pm 0.26$ (26)	$-1.31 \pm 0.12$ (11)	$-1.28 \pm 0.14$
KIC 9717032	Keck	0.23	19	0.262 (06)	6620/ 2.8/ 3.5	$-1.27 \pm 0.17$ (14)	$-1.26 \pm 0.17$ (13)	$-1.27 \pm 0.15$
V715 Cyg	Keck	0.51	21	0.241 (13)	6400/ 3.0/ 3.0	$-1.13 \pm 0.12$ (25)	$-1.14 \pm 0.14$ (12)	$-1.13 \pm 0.09$
V2470 Cyg	CFHT	0.32	26	0.262 (11)	6400/ 2.44/ 2.6	$-0.59 \pm 0.14$ (45)	$-0.59 \pm 0.21$ (14)	$-0.59 \pm 0.13$
V782 Cyg	Keck	0.42	34	0.290 (12)	6525/ 3.2/ 2.9	$-0.40 \pm 0.15$ (102)	$-0.43 \pm 0.14$ (19)	$-0.42 \pm 0.10$
KIC 6100702	CFHT	0.26	23	0.281 (10)	6500/ 2.50/ 2.5	$-0.19 \pm 0.14$ (36)	$-0.13 \pm 0.12$ (6)	$-0.16 \pm 0.09$
V839 Cyg	Keck	0.12	70	0.375 (03)	7200/ 3.1/ 4.0	$+0.07 \pm 0.18$ (137)	$-0.09 \pm 0.14$ (16)	$-0.05 \pm 0.14$
V784 Cyg	Keck	0.47	27	0.323 (12)	6400/ 3.3/ 4.3	$-0.05 \pm 0.15$ (107)	$-0.06 \pm 0.13$ (10)	$-0.05 \pm 0.10$
(b) 12 Blazhko RRab-type stars (excluding RR Lyrae)								
V2178 Cyg	Keck	0.43	41	0.211 (09)	6450/ 2.8/ 3.0	$-1.63 \pm 0.24$ (17)	$-1.67 \pm 0.09$ (11)	$-1.66 \pm 0.13$
V450 Lyr	Keck	0.57	21	0.236 (17)	6450/ 3.0/ 3.0	$-1.52 \pm 0.13$ (13)	$-1.50 \pm 0.21$ (9)	$-1.51 \pm 0.12$
V353 Lyr	Keck	0.32	20	0.205 (17)	6300/ 2.8/ 3.0	$-1.48 \pm 0.20$ (15)	$-1.50 \pm 0.35$ (4)	$-1.50 \pm 0.20$
V360 Lyr	Keck	0.52	29	0.378 (20)	6400/ 2.8/ 10:	$-1.46 \pm 0.37$ (72)	$-1.54 \pm 0.44$ (26)	$-1.50 \pm 0.29$
V354 Lyr	Keck	0.26	30	0.298 (14)	6400/ 2.8/ 3.0	$-1.44 \pm 0.24$ (20)	$-1.44 \pm 0.20$ (13)	$-1.44 \pm 0.16$
V1104 Cyg	Keck	0.42	33	0.174 (03)	6300/ 2.8/ 3.0	$-1.25 \pm 0.25$ (51)	$-1.21 \pm 0.15$ (17)	$-1.23 \pm 0.15$
V808 Cyg	Keck	0.70	19	0.473 (16)	6300/ 2.8/ 3.0	$-1.20 \pm 0.27$ (15)	$-1.18 \pm 0.25$ (7)	$-1.19 \pm 0.18$
V783 Cyg	CFHT	0.58	16	0.23 (01)	6400/ 2.1/ 2.6	$-1.19 \pm 0.18$ (13)	$-1.13 \pm 0.14$ (2)	$-1.16 \pm 0.11$
V366 Lyr	Keck	0.69	21	0.332 (24)	6430/ 3.0/ 3.0	$-1.13 \pm 0.13$ (16)	$-1.19 \pm 0.10$ (10)	$-1.16 \pm 0.09$
V355 Lyr	CFHT	0.19	17	0.247 (16)	6900/ 3.28/ 2.5	$-1.13 \pm 0.14$ (10)	$-1.17 \pm 0.30$ (1)	$-1.14 \pm 0.17$
KIC 11125706	CFHT	0.33	69	0.232 (04)	6200/ 2.35/ 2.25	$-1.09 \pm 0.13$ (57)	$-1.09 \pm 0.10$ (17)	$-1.09 \pm 0.08$
V838 Cyg	CFHT	0.36	13	0.236 (28)	6850/ 2.12/ 2.4	$-1.02 \pm 0.19$ (4)	$-1.00 \pm 0.10$ (3)	$-1.01 \pm 0.10$
(c) Five RRc-type stars (including the RRc/HADS? star KIC 3868420)								
KIC 9453114	CFHT	0.28	29	0.278 (27)	6500/ 2.5/ 2.5	...	$-2.13 \pm 0.12$ (4)	$-2.13 \pm 0.12$
KIC 4064484	Keck	0.59	33	0.288 (11)	6500/ 2.8/ 3.0	$-1.65 \pm 0.22$ (9)	$-1.54 \pm 0.12$ (6)	$-1.58 \pm 0.13$
KIC 3868420	CFHT	0.47	96	0.359 (09)	7480/ 3.9/ 2.0	$-0.35 \pm 0.14$ (13)	$-0.29 \pm 0.08$ (6)	$-0.31 \pm 0.08$
KIC 8832417	CFHT	0.29	30	0.349 (16)	7000/ 3.30/ 2.5	$-0.22 \pm 0.19$ (27)	$-0.29 \pm 0.09$ (7)	$-0.27 \pm 0.11$
KIC 5520878	Keck	0.39	40	0.319 (02)	7250/ 3.9/ 2.4	$-0.18 \pm 0.18$ (76)	$-0.19 \pm 0.12$ (18)	$-0.18 \pm 0.10$
(d) Nine bright RR Lyrae metal abundance standards (including RR Lyrae)								
X Ari	Keck	0.31	223	0.188 (05)	6075/ 2.4/ 2.0	$-2.75 \pm 0.08$ (9)	$-2.74 \pm 0.17$ (11)	$-2.74 \pm 0.09$
VY Ser	Keck	0.45	120	0.232 (03)	6170/ 2.8/ 2.5	$-1.73 \pm 0.12$ (29)	$-1.69 \pm 0.08$ (16)	$-1.71 \pm 0.07$
ST Boo	Keck	0.36	135	0.198 (02)	6313/ 2.6/ 1.8	$-1.66 \pm 0.12$ (39)	$-1.60 \pm 0.04$ (15)	$-1.62 \pm 0.06$
UU Cet	Keck	0.38	66	0.226 (03)	6150/ 2.6/ 1.6	$-1.34 \pm 0.14$ (68)	$-1.32 \pm 0.07$ (19)	$-1.33 \pm 0.08$
RR Lyr	Keck	0.54	252	0.276 (06)	6400/ 2.8/ 3.0	$-1.27 \pm 0.22$ (95)	$-1.27 \pm 0.09$ (15)	$-1.27 \pm 0.12$
VX Her	Keck	0.32	97	0.202 (02)	6690/ 2.9/ 2.2	$-1.22 \pm 0.17$ (51)	$-1.23 \pm 0.17$ (17)	$-1.23 \pm 0.12$
RR Cet	Keck	0.37	184	0.212 (03)	6420/ 2.9/ 1.9	$-1.17 \pm 0.15$ (65)	$-1.19 \pm 0.08$ (17)	$-1.18 \pm 0.09$
V445 Oph	Keck	0.44	106	0.315 (05)	6200/ 2.8/ 1.8	$+0.15 \pm 0.14$ (218)	$+0.11 \pm 0.13$ (16)	$+0.13 \pm 0.10$
SW And	Keck	0.56	151	0.367 (06)	6660/ 3.6/ 2.2	$+0.19 \pm 0.14$ (225)	$+0.21 \pm 0.09$ (19)	$+0.20 \pm 0.08$

NOTE. — The columns contain: (1) Star name; (2) Source of the spectra, either ‘Keck I 10m + HIRES’ or ‘CFHT 3.6-m + ESPaDOnS’; (3) Pulsation phase at mid-exposure; (4) Signal-to-noise ratio per pixel for the co-added spectra, measured at  $\sim 570$  nm and calculated using the VWA ‘rainbow’ widget; (5) Average full-width at half-minimum value [Å] for the three Fe II lines at 4508, 4515 and 4520 Å, derived from the spectrum (either single or co-added exposures) analyzed by VWA – the uncertainty (given in parentheses) is approximated by the standard deviation of the mean FWHM for the three lines; (6) The assumed values for the model effective temperature  $T_{\text{eff}}$  [K], surface gravity  $\log g$  [ $\text{cm s}^{-2}$ ] and microturbulent velocity  $\xi_t$  [km/s] – in general the  $T_{\text{eff}}$  have uncertainties  $\sim \pm 150$  K, the  $\log g$  are  $\pm 0.10$  to  $0.20$ , and the  $\xi_t$  are  $\pm 0.3$  to  $0.5$  km/s; (7) [Fe/H] abundance based on the Fe I lines (number of lines given in parentheses); (8) [Fe/H] abundance based on the Fe II lines (number of lines given in parentheses); (9) Adopted VWA spectroscopic metal abundance, equal to the weighted (in inverse proportion to uncertainty) average of the abundances in columns (7) and (8).

the solar number fractions of H, He and Fe are, respectively,  $N_{\text{H}}/N_{\text{total}} = 91.1\%$ ,  $N_{\text{He}}/N_{\text{total}} = 8.9\%$ , and  $N_{\text{Fe}}/N_{\text{total}} = 0.0029\%$  (*i.e.*, the log of the Fe abundance relative to the *total* number density is  $\log(N_{\text{Fe}}/N_{\text{tot}}) = -4.54$ , which follows from  $A_{\text{Fe}} = \log \epsilon(\text{Fe}) - \log N_{\text{total}} = 7.50 - 12.04$ ).

#### 4.4.1. Parameter Estimation with VWA and MOOG

The bulk of the spectroscopic data analyses of both the CFHT and Keck data was carried out with the spectral synthesis program VWA<sup>19</sup> (Bruntt *et al.* 2002, 2008, 2010a,b). This all-purpose program has the capability of normalizing and co-adding spectra, computing synthetic spectra, selecting suitable lines for abundance determination, measuring EWs, calculating expected EWs for the assumed model parameters, and calculating abundances for a wide range of elements/ions. The abundances follow from iteratively varying the model parameters, calculating synthetic spectra, and then comparing the EWs calculated from the spectra with the measured EWs.

For each RR Lyrae star the following photospheric parameters were derived: the effective temperature,  $T_{\text{eff}}$  [K]; the surface gravity,  $\log g$  [ $\text{cm/s}^2$ ]; the microturbulent velocity,  $\xi_t$  [km/s]; the macroturbulent velocity,  $v_{\text{mac}}$ ; the projected rotational velocity,  $v \sin i$ ; and the spectroscopic iron-to-hydrogen ratio,  $[\text{Fe}/\text{H}]_{\text{spec}}$ . Because the RR Lyr stars are undergoing (mainly) radial pulsations, these parameters are ‘instantaneous’ quantities, specific for the times (phases) at which the spectroscopic observations were made. The metal abundances, while depending on the assumed atmospheric conditions, should be independent of the observed pulsation phases (see Figs.13-14 of For *et al.* 2011, which show the variation with pulsation phase of their derived  $T_{\text{eff}}$ ,  $\log g$ ,  $[\text{Fe}/\text{H}]$  and  $\xi_t$  values).

The synthetic spectra were calculated within VWA using the SYNTH code (Piskunov 1992; Valenti & Piskunov 1996), with atomic parameters (*eg.*,  $\log gf$  values) and line-broadening coefficients retrieved from the Vienna atomic line database, VALD (Kupka *et al.* 1999)<sup>20</sup>. Two sets of model stellar atmospheres were used. For all the stars the model atmosphere grid of ATLAS9 models provided by Heiter *et al.* (2002) was used. For this grid the step-increments in effective temperature, surface gravity and metal abundance are  $\Delta T_{\text{eff}} = 250$  K,  $\Delta \log g = 0.5$ , and  $\Delta [\text{Fe}/\text{H}] = 0.25$  dex. For the bright RR Lyrae stars both ATLAS9 and MARCS models were used.

The derivation of  $[\text{Fe}/\text{H}]_{\text{spec}}$  values followed from analysis of the normalized flux spectra. For each star an initial set of values for the atmospheric parameters was assumed, and a synthetic spectrum was calculated. The usual starting values were:  $T_{\text{eff}} = 6500$  K,  $\log g = 2.50$ ,  $\xi_t = 2.50$  km/s and  $v_{\text{mac}} = 2$  km/s. After adjusting the projected rotational velocity,  $v \sin i$  and the resolving power ( $R = 65000$  for the CFHT spectra and 36000 for the Keck spectra) for each analyzed spectrum, the spectrum was Doppler shifted according to the  $RV$  (see Tables 4-5) and aligned with the synthetic template spec-

trum.

The final set of fitted lines was inspected and poor fits rejected. The microturbulent velocity,  $\xi_t$  was determined by requiring that the correlation between the derived Fe abundances and the reduced EWs (*i.e.*,  $\text{EW}/\lambda$ ) was near zero;  $T_{\text{eff}}$  was estimated by requiring that the correlation of Fe abundance and the lower excitation potential (EP) was near zero; and the surface gravities were calculated by requiring good agreement between the iron abundances determined from lines of the Fe I and Fe II ionization stages (which depended on the assumed  $T_{\text{eff}}$  and  $\log g$  values). Although LTE conditions are assumed by VWA, the effect of departures from LTE on the  $[\text{Fe}/\text{H}]$  values derived using the Fe I lines were considered, and where appropriate the corrections calculated by Rentzsch-Holm (1996) were applied; these were usually smaller than  $\sim 0.10$  dex. The Fe II lines were assumed to be unaffected by deviations from LTE.

**Table 7** summarizes the basic spectroscopic information derived from the VWA analyses of the CFHT and Keck spectra, where the stars are sorted by type (non-Blazhko, Blazhko, RRc, etc.), and within a given type by spectroscopic metal abundance. The pulsation phases (column 3) are mid-exposure values (*i.e.*, average values of the mid-times when multiple spectra were taken), and the S/N per pixel (column 4) are for the co-added normalized spectra<sup>21</sup>. The FWHM values (column 5) are for the co-added spectra and the  $T_{\text{eff}}$ ,  $\log g$  and  $\xi_t$  values (column 6) are either those assumed for the adopted VWA runs, or are interpolated values for two similar atmosphere models. The value  $v_{\text{mac}}$  was arbitrarily set to either 2 or 3 for all the stars, while the projected rotational velocity,  $v \sin i$ , was set to 2 km/s for the Keck spectra and 7-10 km/s for the CFHT spectra; the impact on these choices on the derived abundances seems to have been minimal. The iron-to-hydrogen abundances (columns 7-8) are for the neutral and singly-ionized ions, the weighted average of which,  $[\text{Fe}/\text{H}]$ , is given in column 9. The derived metallicities range from a low of  $-2.54 \pm 0.11$  dex (for NR Lyr) to a high of  $-0.05 \pm 0.10$  dex (for V784 Cyg). The same two stars were the extremes identified by N11 in their analysis of the Q1-Q5 *Kepler* photometry of non-Blazhko variables, and the four non-Blazhko stars that were suspected (from their locations in Fig.9 of N11) of being metal rich (V782 Cyg, V784 Cyg, KIC 6100702 and V2470 Cyg) are confirmed as such. Not included in Table 7 are four stars for which the VWA analysis of the co-added spectrum proved inconclusive or impossible: (1) V1510 Cyg, a non-Blazhko star ( $Kp=14.5$  mag); (2) the faint non-Blazhko star V346 Lyr ( $Kp=16.4$  mag); (3) the faint Blazhko star KIC 9973633 ( $Kp=17.0$  mag), for which the S/N of the co-added Keck spectrum (not plotted in Fig.7) was insufficient for estimating  $[\text{Fe}/\text{H}]$ ; and (4) the faint ( $Kp=17.4$  mag) extreme-Blazhko star V445 Lyr (see Guggenberger *et al.* 2012). In all cases except KIC 9973633 we were able to derive  $[\text{M}/\text{H}]$  values using SME (see Table 9).

The EWs derived using VWA are in good agreement with the values measured by hand using the IRAF ‘splot’ routine, with values calculated with ARES, and with the

<sup>19</sup> The VWA software was written by Hans Bruntt (University of Aarhus, Denmark), in IDL, and is publicly available at <https://sites.google.com/site/vikingpowersoftware/>.

<sup>20</sup> See <http://www.astro.uu.se/vald>.

<sup>21</sup> A comparison of the MAKEE and ‘rainbow’ S/N values for the seven stars with only single exposures shows the MAKEE values to be systematically larger (by  $\sim 16\%$ ) than the ‘rainbow’ values.

TABLE 8  
 SPECTROSCOPIC IRON-TO-HYDROGEN ABUNDANCES (MOOG)

Star (1)	$T_{\text{eff}} / \log g / \xi_t / [\text{Fe}/\text{H}]$ (2)	$\log \epsilon(\text{FeI})$ (3)	$\log \epsilon(\text{FeII})$ (4)	$\log \epsilon(\text{Fe})$ (5)	$[\text{Fe}/\text{H}]_{\text{spec}}$ (6)
X Ari	6000/ 3.0/ 2.0/ -2.5	$4.73 \pm 0.12$ (105)	$5.19 \pm 0.18$ (24)	$4.91 \pm 0.07$	$-2.59 \pm 0.12$
VY Ser	6250/ 3.0/ 2.0/ -1.5	$5.83 \pm 0.12$ (147)	$6.01 \pm 0.12$ (26)	$5.92 \pm 0.06$	$-1.58 \pm 0.11$
ST Boo	6250/ 3.0/ 2.0/ -1.5	$5.78 \pm 0.12$ (177)	$6.09 \pm 0.12$ (29)	$5.94 \pm 0.06$	$-1.57 \pm 0.11$
RR Lyr	6000/ 3.0/ 2.0/ -1.5	$5.96 \pm 0.14$ (145)	$6.25 \pm 0.09$ (19)	$6.14 \pm 0.05$	$-1.36 \pm 0.10$
VX Her	6750/ 3.0/ 2.0/ -1.5	$6.24 \pm 0.12$ (169)	$6.35 \pm 0.13$ (24)	$6.29 \pm 0.06$	$-1.21 \pm 0.11$
SW And	6250/ 3.0/ 2.0/ +0.0	$7.35 \pm 0.15$ (177)	$7.42 \pm 0.15$ (11)	$7.39 \pm 0.08$	$-0.12 \pm 0.13$
V782 Cyg	6250/ 3.0/ 2.0/ +0.0	$7.41 \pm 0.30$ (162)	$7.45 \pm 0.28$ (11)	$7.43 \pm 0.14$	$-0.07 \pm 0.19$
V445 Oph	6250/ 3.0/ 2.0/ +0.0	$7.45 \pm 0.11$ (188)	$7.61 \pm 0.13$ (11)	$7.52 \pm 0.06$	$+0.02 \pm 0.11$
V784 Cyg	6250/ 3.0/ 2.0/ +0.0	$7.86 \pm 0.35$ (142)	$7.92 \pm 0.34$ (7)	$7.89 \pm 0.17$	$+0.39 \pm 0.22$

NOTE. — The columns contain: (1) the star name; (2) the assumed values for the (WebMARCS) model effective temperature,  $T_{\text{eff}}$  [K], surface gravity,  $\log g$  [ $\text{cm s}^{-2}$ ], microturbulent velocity,  $\xi_t$  [km/s], and metal abundance, [Fe/H]; (3) the [FeI/H] abundance (based on the number of Fe I lines given in parentheses); (4) the [FeII/H] abundance (based on the number of Fe II lines given in parentheses); (5) the weighted average of the [FeI/H] and [FeII/H] abundances; (6) the adopted MOOG spectroscopic iron abundance.

values calculated from the synthetic spectra. The EWs of the standard stars also agree (to within the uncertainties arising from the observations being made at different phases) with the values listed in Table 3(b) of C95<sup>22</sup>. To minimize the effects of line saturation only Fe I and Fe II lines with  $\text{EW} < 90 \text{ m}\text{\AA}$  were used in our analysis. A table of measured and calculated EWs ( $\text{m}\text{\AA}$ ) for the Fe I and Fe II lines (program and standard stars), including the assumed lower excitation potentials and  $\log gf$  values (from the VALD database), is available from the first author.

As a check on the VWA results [Fe/H] abundances for several of the stars were also derived using the LTE Stellar Line Analysis program MOOG (Snedden 1973, 2002; Sneden *et al.* 2011)<sup>23</sup>. In this case EWs were calculated using the highly-automated program ARES (Sousa *et al.* 2007, 2008). A comparison of the EWs derived by ARES, by VWA, and by the IRAF ‘splot’ routine, showed excellent agreement for EWs between 5 and 100  $\text{m}\text{\AA}$ . The WEBMARCS grid of model atmospheres (Gustafsson *et al.* 1975, 2008)<sup>24</sup> was used for the MOOG calculations. These models used the Grevesse *et al.* (2007) compositions for the solar photosphere, and the available grid had  $T_{\text{eff}}$  values up to 7000 K with a step size of 250 K. Unfortunately the smallest surface gravities available were for  $\log g=3$ , which is larger than the value appropriate for most RR Lyrae stars.

The MOOG results are summarized in **Table 8**. The assumed model atmospheric parameters are given in column 2, where the uncertainties are  $\sim \pm 150 \text{ K}$  for  $T_{\text{eff}}$ ,  $\pm 0.2 \text{ cm/s}^2$  for  $\log g$ , and  $\pm 0.5 \text{ km/s}$  for  $\xi_t$ . Columns 3-4 give  $\log \epsilon$  values (relative to hydrogen) for the Fe I and Fe II ions (standard output from the ‘ABFIND’ routine in MOOG). Also given are the number of lines used to derive the abundance. Column 5 contains the average iron abundance,  $\log \epsilon(\text{Fe})$ , weighted inversely by the Fe I and Fe II uncertainties, and the last column gives [Fe/H] values, derived by adding  $12.50 \pm 0.05$  to the column 5

abundances. Since only a limited number of MOOG runs were made the uncertainties are larger than for the VWA results, the largest discrepancies occurring for V782 Cyg and SW And.

#### 4.4.2. Parameter Estimation with SME

Atmospheric parameters for the program and standard RR Lyr stars were also derived using the ‘Spectroscopy Made Easy’ (SME) program of Valenti & Piskunov (1996)<sup>25</sup>. SME compares observed spectra with synthetic spectra, where the latter are computed by solving the radiative transfer equations. Parameter estimates are calculated by minimizing (using Levenberg-Marquart) a  $\chi^2$  statistic that measures the lack of agreement between the observed and fitted intensities. Unlike VWA and MOOG, which are based on comparing calculated and measured EWs, SME matches sections of spectra. SME does not actually calculate Fe I and Fe II abundances, but rather, the abundances assumed for the Sun are scaled and used to calculate a mean metal abundance, [M/H], which we assume to be comparable to [Fe/H].

The spectra that were analyzed with SME were the co-added normalized Keck and CFHT spectra and the Kurucz-Hinckle solar spectrum. The derived photospheric quantities were  $T_{\text{eff}}$ ,  $\log g$  (cgs units),  $\xi_t$ ,  $v_{\text{mac}}$ ,  $v \sin i$  and [M/H]. For most of the SME analyses the synthetic spectra were calculated for the  $\lambda$ -interval 500-520 nm, for which VALD returned atomic parameters for 476 lines. This interval is free of Balmer lines, around which the continua were usually poorly defined. The interval 480-520 nm was tried, but spurious results were found, presumably owing to the presence of  $\text{H}\gamma$ . For several stars the interval 440-460 nm was also analyzed, using 952 lines identified by VALD, and the results were averaged with those from 500-520 nm.

Our estimates of the atmospheric parameters were obtained iteratively by varying the initial values supplied to SME until the ‘best’ overall estimates were found. The usual reduction procedure was to take as starting values the parameter set calculated by VWA (see Table 7) and then to solve simultaneously for two parameters at a time. First  $\xi_t$  and  $v_{\text{mac}}$  were calculated, then  $v \sin i$  and  $R (= \lambda/\Delta\lambda)$ , then  $T_{\text{eff}}$  and  $\log g$ . After each run the

<sup>22</sup> For RR Lyrae itself the Clementini *et al.* EWs are larger than the ARES EWs for lines with  $\text{EWs} \geq 100$ ; however, such lines are not used here.

<sup>23</sup> MOOG is publicly available at [www.as.utexas.edu/~chris/moog.html](http://www.as.utexas.edu/~chris/moog.html) (2010 version).

<sup>24</sup> The WEBMARCS models, also known as ‘MARCS 2008’, or ‘MARCS 35’, or ‘new MARCS’ models, are available on-line at <http://marcs.astro.uu.se>

<sup>25</sup> SME was written in IDL and is freely available at <http://www.stsci.edu/~valenti/sme/>.

TABLE 9  
PHYSICAL CHARACTERISTICS DERIVED USING SME

Star (1)	$T_{\text{eff}}$ (2)	$\log g$ (3)	$\xi_t$ (4)	$v_{\text{mac}}$ (5)	$v \sin i$ (6)	[M/H] (7)
<b>X Ari</b> †	6200	1.85	4.8	9.5	2.7	-2.71
NR Lyr†	6363	2.56	4.4	7.9	4.8	-2.51
KIC 9453414	6204	2.04	6.4	29.3	4.3	-2.15
V1510 Cyg	5706	1.76	4.9	10.8	4.9	-2.00
FN Lyr	6203	2.21	4.7	8.0	4.6	-1.91
NQ Lyr	5980	1.56	4.4	8.4	4.5	-1.87
V350 Lyr	6131	2.29	5.1	16.7	3.0	-1.82
V445 Lyr	6227	1.70	5.3	12.4	5.4	-1.78
<b>VY Ser</b>	6167	2.10	4.4	11.3	3.2	-1.71
V2178 Cyg	6301	2.35	4.2	9.2	4.3	-1.66
V894 Cyg	6220	1.92	3.8	7.2	4.4	-1.65
<b>ST Boo</b> †	6327	1.91	3.8	10.5	2.1	-1.61
V353 Lyr	6093	1.84	4.8	4.8	4.1	-1.57
V450 Lyr	6280	2.34	3.6	12.7	5.0	-1.51
KIC 4064484	6473	2.39	4.0	18.4	4.9	-1.51
V360 Lyr	6202	2.42	5.3	18.9	5.0	-1.48
V346 Lyr	6108	2.34	4.2	9.6	5.0	-1.48
V354 Lyr	6391	2.05	4.6	15.0	4.2	-1.43
V1107 Cyg	6087	2.23	5.1	11.4	3.0	-1.40
<b>VX Her</b>	6533	2.46	3.8	9.0	2.2	-1.38
KIC 7030715	6221	1.99	4.2	13.5	10.0	-1.37
AW Dra	6461	2.02	4.4	5.9	3.6	-1.34
<b>UU Cet</b>	6269	2.31	4.2	9.1	2.4	-1.33
<b>RR Lyr</b> †	6445	3.13	5.1	11.7	5.6	-1.33
V368 Lyr	6231	1.93	3.3	9.5	3.0	-1.29
KIC 9658012	6314	2.15	4.3	15.0	12.9	-1.27
KIC 9717032	6461	2.14	5.0	14.8	9.8	-1.24
<b>RR Cet</b>	6459	2.40	4.0	8.8	3.8	-1.22
V1104 Cyg	6352	2.08	2.0	0.4	2.0	-1.19
V355 Lyr	6869	2.29	5.8	18.3	5.0	-1.15
V715 Cyg	6265	2.19	3.7	11.1	4.6	-1.14
V808 Cyg	6169	2.19	6.4	25.2	4.3	-1.14
V366 Lyr	6263	2.26	5.1	19.8	5.3	-1.13
V783 Cyg	6122	1.59	3.9	14.3	5.0	-1.10
KIC 11125706	6145	1.67	2.3	14.7	6.6	-1.09
V838 Cyg	6600	1.81	4.3	14.0	5.0	-1.01
V2470 Cyg	6220	2.13	2.6	9.7	6.5	-0.59
V782 Cyg	6446	3.17	3.7	12.0	4.6	-0.42
V839 Cyg†	6982	2.46	3.5	18.4	5.4	-0.31
KIC 3868420†	7612	3.71	2.3	23.0	5.7	-0.28
KIC 8832417	6999	3.30	3.5	15.3	4.8	-0.25
KIC 5520878	7266	3.66	3.0	15.2	5.1	-0.18
KIC 6100702	6471	2.83	3.1	10.2	4.7	-0.18
<b>Sun</b>	5770	4.44	0.8	8.7	2.1	+0.00
V784 Cyg	6305	2.84	3.6	13.4	5.7	+0.00
<b>V445 Oph</b>	6496	3.15	2.9	12.0	2.5	+0.14
<b>SW And</b>	6996	3.70	4.2	16.2	2.9	+0.19

NOTE. — Most of the entries in this table are based on analysis of 476 lines in the wavelength interval 500-520 nm. The stars with a † following the name include additional measurements made using 952 lines in the interval 440-460 nm. The names of the nine Keck standard stars (and the Sun) are printed in ‘boldface’. The V1104 Cyg results are based on analysis of the Keck spectrum (the CFHT spectra for this star were too noisy to measure).

prior input values were replaced with the revised values. Lastly, with the newer set of SME parameters, we solved for [M/H].

**Table 9** contains the final results of the SME analyses, sorted in order of increasing metal abundance. A total of 47 stars were analyzed. The co-added spectrum of KIC 9973633 was not measured owing to its very low S/N.

#### 4.4.3. Comparison of Atmospheric Parameters

In **Table 10** the VWA, MOOG and SME iron abundances are compared. Also included for comparison with our values are the [Fe/H] values derived by L94, Suntzeff, Kraft & Kinman (1994), C95, Lambert *et al.* (1996, here-

after L96), Feast *et al.* (2008), and Wallerstein & Huang (2010). Because C95 assumed  $\log \epsilon(\text{Fe})=7.56$ , whereas we adopted the value  $\log \epsilon(\text{Fe})=7.50$ , the C95 metallicity values (from their Table 12) have been increased by 0.06 dex. L96 report  $\log \epsilon(\text{FeII})$  values, to which we have added 7.50 to give the abundances in column 5. The L94 metallicities are based on measurements of the Ca II K-line.

X Ari, with [Fe/H]  $\sim -2.65$  dex, is probably more metal deficient than NR Lyr, the most metal-poor RR Lyr star in the *Kepler* field, which we estimated to have [Fe/H]  $= -2.54 \pm 0.11$  dex (Table 7). Recently Haschke *et al.* (2012) derived a spectroscopic [Fe/H]  $= -2.61$  dex for X Ari, a value consistent with our estimate and with the value derived by Wallerstein & Huang (2010). It is unclear whether the metal-rich end is defined by the standard star V445 Oph or by SW And. Our VWA and SME analyses suggest that the [Fe/H] values for both stars are greater than that of the Sun, while the MOOG analyses suggest that SW And may be more metal-poor and V445 Oph more metal rich than the Sun. Most previous analyses lean toward V445 Oph being the more metal rich, as does our photometric [Fe/H] (see Figs. 4 and 12). In any case, both have metallicities similar to that of the most metal-rich star in the *Kepler* field, V784 Cyg.

For VY Ser a metal abundance [Fe/H]  $= -1.77 \pm 0.10$  dex was derived by Carney & Jones (1983). The good agreement between this value and our VWA, MOOG and SME estimates is undoubtedly due to their spectra and ours having been taken at similar phases (0.61 versus our 0.48). Furthermore, their  $\log g = 2.3 \pm 0.3$  and  $\xi_t = 4.2 \pm 0.5$  km/s agree with our SME values of 2.1 (cgs units) and 4.4 km/s; and their  $T_{\text{eff}} = 6000 \pm 150$  K is in accord with our SME estimate of 6167 K.

In **Fig. 8** the SME estimates of the atmospheric parameters  $T_{\text{eff}}$ ,  $\log g$ ,  $\xi_t$  and [M/H] are compared (solid squares) with the values derived using VWA. While the results are similar, the temperatures from SME tend to be smaller than the VWA values (upper left panel), the mean difference being  $\sim 100$  K, with an RMS scatter  $\sim 100$  K. The surface gravities from SME are also smaller on average than the VWA values (lower left panel) – mean  $\Delta \log g \sim -0.5$  with an RMS scatter of 0.3. The trend seen in  $\xi_t$  (upper right panel) implies that the SME-derived values are systematically larger than the VWA values in most cases, where the difference increases as  $\xi_t$  increases (not shown in the diagram is the extreme outlier V360 Lyr, where  $\Delta \xi_t = -4.7$  km/s is due primarily to the large  $\xi_t$  ( $=10$  km/s) adopted for the VWA analysis). Despite these differences the lower right panel shows that there is reasonably good agreement of the [M/H] abundances derived with SME and the [Fe/H] values derived using VWA (and MOOG) – the outliers at the bottom of the panel are V1107 Cyg, V839 Cyg, and VX Her (a standard star). For the VWA analyses, the  $v_{\text{mac}}$  values were generally set to 2-3 km/s and  $v \sin i$  values of 2 km/s and 7-10 km/s were adopted for the Keck and CFHT spectra, respectively. These values differ considerably from the  $v_{\text{mac}}$  values derived by SME, which have a mean of 13.0 km/s (standard deviation  $\sigma = 5.4$  km/s, N=43 stars), and from the  $v \sin i$  values (see bottom panel of Fig.9) derived by SME, which have a mean of 4.3 km/s ( $\sigma = 1.2$  km/s, N=40, excluding the three stars with  $v \sin i > 9$  km/s).

Also plotted in Fig. 8 (as crosses) are the differences

TABLE 10  
 SPECTROSCOPIC IRON-TO-HYDROGEN ABUNDANCES FOR THE KECK STANDARD STARS

Star	[Fe/H] - previous papers						[Fe/H] - this paper		
	L94	SKK94	C95	L96	Fer98	Wal10	VWA	MOOG	SME
(1)	(2)	(3)	(4)	(5)	(6)	(7)	(8)	(9)	(10)
X Ari	-2.40	-2.16	-2.44	-2.53	-2.43	-2.68	$-2.74 \pm 0.09$	$-2.59 \pm 0.12$	$-2.71 \pm 0.10$
VY Ser	-1.82	-1.83	-1.65	-1.75	-1.79	...	$-1.71 \pm 0.07$	$-1.58 \pm 0.11$	$-1.71 \pm 0.10$
ST Boo	-1.86	...	-1.62	...	-1.76	-1.77	$-1.62 \pm 0.06$	$-1.57 \pm 0.11$	$-1.61 \pm 0.10$
RR Cet	-1.52	-1.55	-1.32	...	-1.45	...	$-1.27 \pm 0.12$	...	$-1.22 \pm 0.10$
UU Cet	...	-1.88	-1.32	...	-1.28	...	$-1.33 \pm 0.08$	...	$-1.33 \pm 0.10$
RR Lyr	-1.37	-1.37	-1.32	-1.47	-1.39	...	$-1.27 \pm 0.12$	$-1.36 \pm 0.10$	$-1.33 \pm 0.10$
VX Her	...	-1.37	-1.52	...	-1.58	-1.48	$-1.23 \pm 0.12$	$-1.21 \pm 0.11$	$-1.38 \pm 0.10$
SW And	-0.38	-0.41	-0.00	-0.23	-0.24	-0.16	$+0.20 \pm 0.08$	$-0.12 \pm 0.13$	$+0.19 \pm 0.10$
V445 Oph	-0.23	-0.30	+0.23	...	-0.19	+0.24	$+0.13 \pm 0.10$	$+0.02 \pm 0.11$	$+0.14 \pm 0.10$

NOTE. — The columns contain: (1) the star name; (2) [Fe/H] from Table 9 of L94, where [Fe/H] is based on the Ca II K-line; (3) [Fe/H] from Table 3 of Suntzeff, Kraft & Kinman (1994), based on  $\Delta S$  measurements; (4) [Fe/H] from Table 12 of C95, made more metal rich by 0.06 since Clementini *et al.* (1995) assumed for the Sun  $\log \epsilon(\text{Fe})=7.56$ , whereas we are assuming 7.50; (5) [Fe/H] from Table 5 of Lambert *et al.* (1996) - the  $\log \epsilon$  given, which are the Fe II values, have had the assumed solar Fe abundance (7.50) subtracted; (6) [Fe/H] from Table 1 of Fernley *et al.* (1998) - these same values were adopted by Feast *et al.* (2008); (7) [Fe/H] from Table 2 of Wallerstein & Huang (2010), based on analysis of Apache Point Observatory spectra; (8-10) spectroscopic [Fe/H] values derived here using VWA, MOOG and SME.

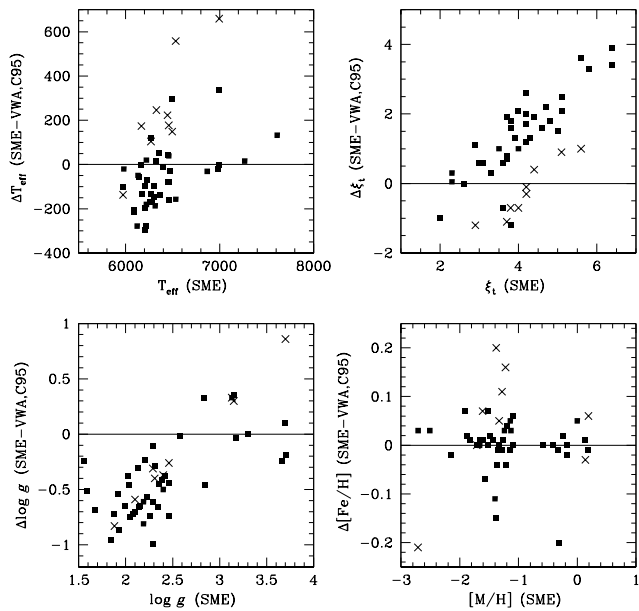


FIG. 8.— Comparison of physical parameters derived using SME with those derived using VWA (or assumed for the VWA analyses). Also shown (as crosses) are the parameter differences for the nine Keck standards, as derived using SME compared with the values derived independently by C95.

between our SME-derived parameters for the nine Keck RR Lyrae standard stars and the corresponding values derived by C95. Since the pulsation phases for our Keck spectra differ from those of the Palomar 1.5-m spectra analyzed by C95 the effective temperatures are expected to differ. On the other hand, because the RRab stars lie on the red side of the instability strip and both studies used spectra taken away from maximum light the  $T_{\text{eff}}$  should be similar; in fact,  $\Delta T_{\text{eff}}(\text{SME}-\text{C95})$  (upper left panel) does not exceed 700 K and is typically  $\sim 200$  K. The largest differences occur for VX Her (558 K) and for SW And (659 K). The difference for VX Her is readily explained by the different  $\phi_{\text{puls}}$  values: the average pulsation phase for the five C95 spectra is  $\phi_{\text{puls}}=0.61$  and therefore they measured  $T_{\text{eff}}=5978$  K; on the other hand

the Keck spectrum was taken at  $\phi_{\text{puls}}=0.32$  and the average  $T_{\text{eff}} = 6660 \pm 70$  K from the VWA, MOOG and SME analyses is hotter. The large temperature difference for SW And is problematic. The average  $\phi_{\text{puls}}$  for the three C95 spectra is 0.82, which is to be compared with  $\phi_{\text{puls}}=0.56$  for our Keck spectrum. According to For, Sneden & Preston (2011, Figs.8-10) both phases are near minimum temperature and therefore  $T_{\text{eff}} \sim 6200$  K is expected in both cases. The  $T_{\text{eff}} = 6337$  K derived by C95 is consistent with this prediction, as is the  $T_{\text{eff}}$  from our MOOG analysis; however, both the VWA and SME analyses suggest a higher temperature, and as a consequence a slightly higher [Fe/H] value.

The comparison of surface gravities (Fig. 8, lower left panel) is intriguing, with the differences for the nine standard stars lying along the line  $\Delta \log g = 0.89 \log g(\text{SME}) - 2.46$ , *i.e.*, the gravities derived by SME tend to be smaller than the C95 values when  $\log g$  is less than 2.76 and larger when  $\log g$  is greater than 2.76. A linear trend is also seen when our VWA  $\xi_t$  estimates for the standard stars (crosses in the upper right panel) are compared with the C95 microturbulent parameter, where the former values are offset by  $\sim 2$  km/s. Despite these atmospheric parameter differences, the metallicities derived here and by C95 are all within  $\sim 0.2$  dex of each other (bottom right panel), with a difference  $< 0.1$  dex in most cases.

#### 4.4.4. Correlations of Atmospheric Parameters

Fig. 9 shows the SME-derived atmospheric parameters  $v_{\text{mac}}$ ,  $\xi_t$ , and  $v \sin i$ , plotted as a function of  $T_{\text{eff}}$ . Each panel includes the values derived for the program RR Lyr stars, for the Sun, for the candidate HADS star KIC 3868420, and for the bright Keck RR Lyrae standard stars. As expected, the RRc stars, KIC 5520878 and KIC 8832417 (both of which are metal-rich) are the hottest among the RR Lyr stars. The candidate HADS star KIC 3868420 (also metal-rich) is even hotter. Differences between KIC 3868420 and the *bona fide* hot RRc stars appear to be comparatively small. While this observation lends support to the possibility that it may be an unusual metal-rich short-period RRc star, possibly an RRe (second overtone?) pulsator (Walker & Nemec 1996; Kovács 1998), identification as a hot HADS star of 1.6 to

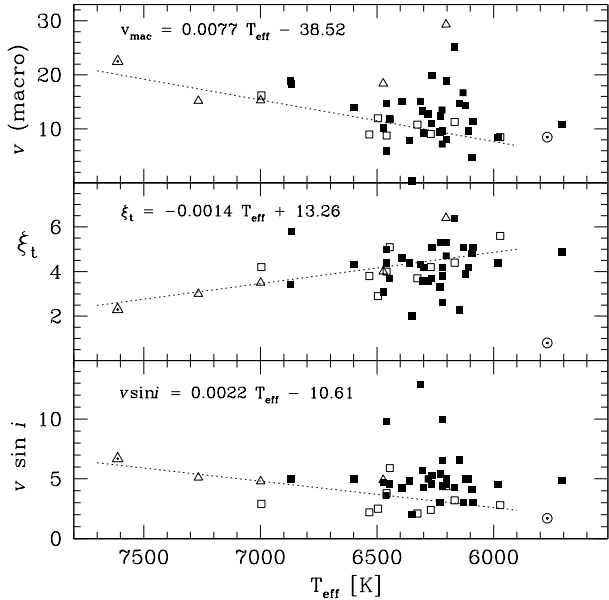


FIG. 9.— Macroturbulent velocity (top panel), microturbulent velocity (middle panel), and projected rotation velocity (bottom panel) for the program and standard stars, all derived with SME, and all with units of [km/s]. The equations of the fitted lines (based on the high-S/N standard star data only) are as indicated on the graphs. Included in the diagrams are the program star RRab stars (solid black squares), the RRc stars (open triangles), the bright Keck RRab standard stars (open squares), the Sun (circled dot) and the candidate HADS star KIC 3868420 (dotted triangle).

2 solar masses seems more likely. Balona & Nemeč (2012) found that  $\delta$  Sct stars hotter than  $\log T_{\text{eff}} = 3.88$  are quite common and suggested that KIC 3868420, based on its photometric and kinematic properties, is not an SX Phe star (*i.e.*, a halo population  $\delta$  Sct star such as are found among the blue stragglers in globular clusters). The metal-poor RRc star KIC 9453414 has the highest derived macro-turbulent velocity of all the program stars, *i.e.*,  $v_{\text{mac}} = 29$  km/s. The three stars with the greatest projected rotation velocities are the non-Blazhko RRab stars KIC 9658012, KIC 9717032 and KIC K7030715 – all the other stars have  $v \sin i$  values smaller than 7 km/s. The RRab star with the coolest  $T_{\text{eff}}$  is V1510 Cyg, a non-Blazhko star for which we were unable to perform a successful VWA analysis of the CFHT spectra. V808 Cyg (a Blazhko star) also has a high  $v_{\text{mac}}$  and V1104 Cyg (another Blazhko star) has the extremely low value of  $v_{\text{mac}} = 0.4$  km/s (see top panel of Fig. 9) For the standard stars (all with high S/N spectra) and the RRc stars, in Fig. 9 three linear trends are apparent: the hottest stars tend to have higher  $v_{\text{mac}}$ , lower  $\xi_t$ , and higher  $v \sin i$  velocities than the cooler stars. Equations of the fitted trend lines are given on the graphs. It is interesting to note that the  $v_{\text{mac}}$  and  $v \sin i$  trends are similar to those for the 23 bright solar-type stars studied by Bruntt *et al.* (2010b) and summarized in their Fig. 11, although at a given  $T_{\text{eff}}$  the RR Lyr stars appear to have higher  $v_{\text{mac}}$  values than the solar-type stars.

In **Fig. 10** the atmospheric parameters derived with SME for the RR Lyr stars are compared with the same quantities (also derived using SME) for the 253 halo metal-poor red giants and red horizontal branch (RHB) stars investigated by Barklem *et al.* (2005) as part of the

HERES survey. In all four panels KIC 3868420 (dotted triangle) appears to be similar to the two metal-rich RRc stars KIC 5520878 and KIC 8832417, suggesting again that it might be a short period RRc star and not a HADS star. The  $\xi_t$  vs.  $\log g$  diagram (upper left panel) shows that the RR Lyrae stars have systematically higher micro-turbulent velocities than the HERES metal-poor red giants and RHB stars with the same  $\log g$ . The  $\log g$  vs.  $T_{\text{eff}}$  diagram (upper right panel), where the  $\log g$  scale is reversed, closely resembles an H-R diagram. At a given surface gravity the RR Lyrae stars are hotter than the RHB stars, which in turn are hotter than the metal-poor red giants. As before the hottest stars are the RRc stars (and KIC 3868420), and the two metal-rich RRc stars are seen to have higher surface gravities and temperatures than the two metal-poor RRc stars. The  $v_{\text{mac}}$  versus projected rotational velocity diagram (lower left panel) identifies those stars with the most extreme values of  $v_{\text{mac}}$  and  $v \sin i$  (see earlier discussion). The mean  $v_{\text{mac}}$ , excluding the three outliers with  $v_{\text{mac}}$  greater than 20 km/s, equals 12.1 km/s ( $\sigma=4.2$  km/s, 40 RR Lyr stars), and the corresponding mean  $v \sin i$  (after eliminating the three  $v \sin i$  outliers) is 4.3 km/s ( $\sigma=1.2$  km/s, 40 RR Lyr stars). The surface gravity versus metallicity diagram (lower right panel) reveals a clear trend between  $\log g$  and [M/H]: the metal-rich RR Lyrae stars have larger surface gravities (hence smaller luminosities) than the more metal-poor RR Lyrae stars, which was explained by Sandage’s (1958) ‘stacked horizontal-branch luminosity levels’ model (see Bono *et al.* 1997, and discussion in N11). No significant differences between the Blazhko and non-Blazhko stars are evident in any of the diagrams of Fig. 10.

## 5. PHOTOMETRIC METAL ABUNDANCES FROM $P$ - $\phi_{31}$ -[Fe/H] RELATIONSHIPS

Derivation of metal abundances from correlations relating pulsation period, spectroscopic [Fe/H], and one or more parameters that characterize the shape of the photometric light curve (e.g.,  $\phi_{31}^s$ ,  $A_{\text{tot}}$ , risetime, etc.) was discussed in §3. In this section we use the accurate pulsation periods and Fourier light curve parameters presented in §3, and the spectroscopic metal abundances derived in §4, to derive new  $P$ - $\phi_{31}$ -[Fe/H] regressions for the *Kepler*-field RRab and RRc stars. Using our fitted models we estimate  $[\text{Fe}/\text{H}]_{\text{phot}}$  for the program stars and investigate the applicability of the models to Blazhko and non-Blazhko stars. Because the spectroscopic [Fe/H] values are derived from high dispersion spectra analyzed using standard reduction procedures, the derived metallicities are on the scale of the high dispersion spectroscopy (*i.e.*, the Carretta *et al.* 2009, hereafter C9 scale).

### 5.1. RRab Stars

Several models were evaluated for the *Kepler*-field RRab stars and the optimum fit was achieved with the following nonlinear model:

$$[\text{Fe}/\text{H}] = b_0 + b_1 P + b_2 \phi_{31}^s + b_3 \phi_{31}^s P + b_4 (\phi_{31}^s)^2, \quad (2)$$

where  $\phi_{31}^s$  is the mean  $\phi_{31}^s$  (Kp) value and [Fe/H] is the VWA spectroscopic value (see Table 7). Excluded from the final calibration were five Blazhko stars with large residuals: V445 Lyr and V2178 Cyg, both of which

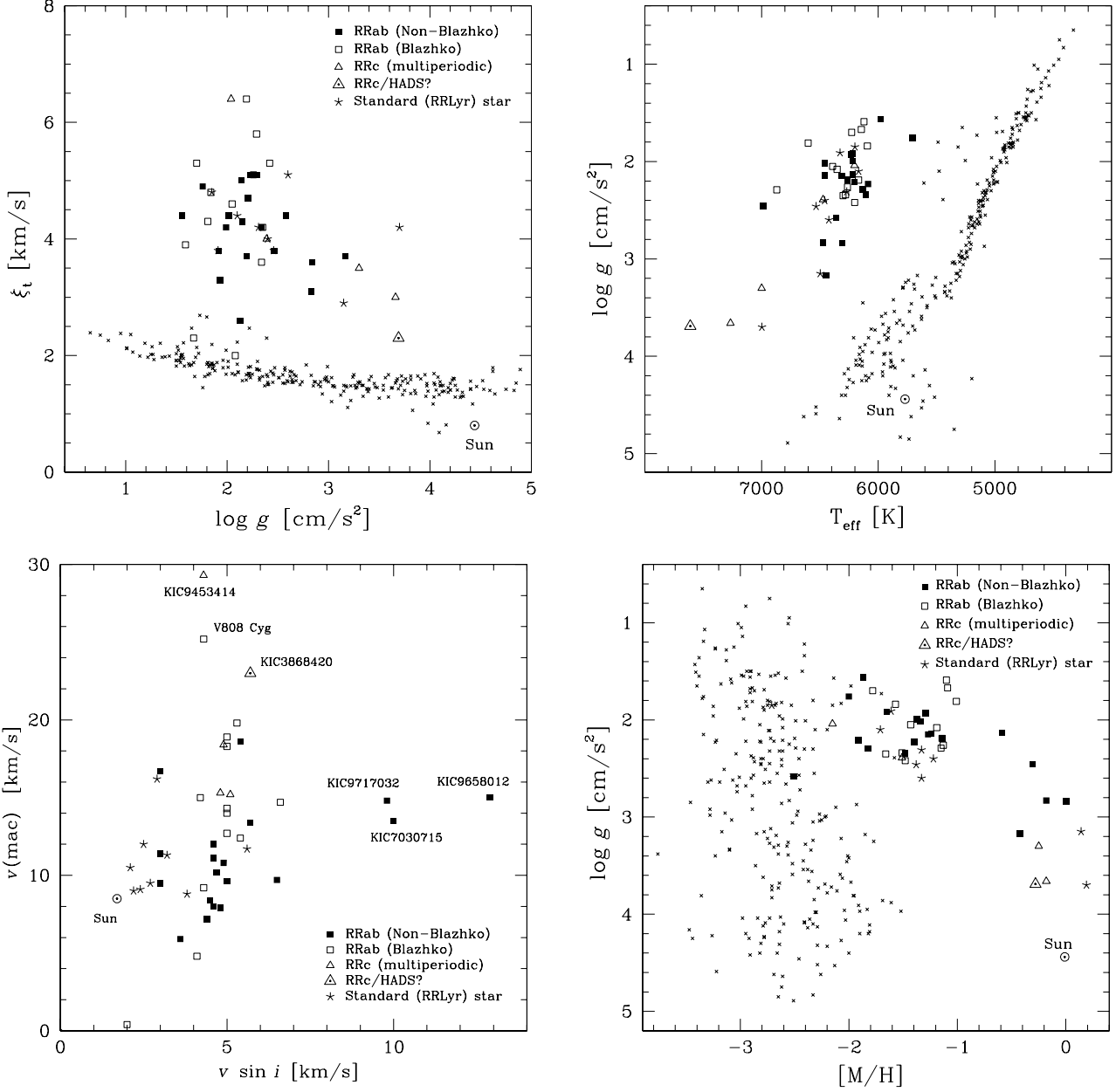


FIG. 10.— Four diagrams comparing the atmospheric parameters for the *Kepler*-field RR Lyrae stars, the nine RR Lyrae standards, and the Sun (all derived with SME), with the same parameters (also derived with SME) for the HERES metal-poor halo red giants and red horizontal branch stars (from Barklem *et al.* 2005). [**Upper Left**] Microturbulent velocity,  $\xi_t$  [km/s], versus surface gravity,  $\log g$  [cm/s<sup>2</sup>] - the HERES stars are plotted as small crosses; [**Upper Right**] Surface gravity,  $\log g$  [cm/s<sup>2</sup>], versus effective temperature,  $T_{\text{eff}}$  [K] - here the HERES stars clearly are seen to be mainly red giants, subgiants and  $\sim 10$  red horizontal branch stars; [**Lower Left**] Macro-turbulent velocity,  $v_{\text{mac}}$ , versus projected rotation velocity,  $v \sin i$  [km/s], with labels identifying the most extreme stars ( $v_{\text{mac}}$  and  $v \sin i$  were not given for the HERES stars); [**Lower Right**] Surface gravity,  $\log g$  [cm/s<sup>2</sup>], versus metal abundance,  $[M/H]$ .

exhibit extremely large amplitude and frequency modulations (see Table 2, and right side of Fig. 3), and KIC 11125706, V838 Cyg and V1104 Cyg, which have small amplitude and frequency modulations (see Table 2, Figs. 2-3 and §3.2.1). Also excluded from the calibration were two non-Blazhko stars with unreliable metallicities, V346 Lyr and V1510 Cyg. The resulting estimated coefficients and their standard errors are:  $b_0 = -8.65 \pm 4.64$ ,  $b_1 = -40.12 \pm 5.18$ ,  $b_2 = 5.96 \pm 1.72$ ,  $b_3 = 6.27 \pm 0.96$  and  $b_4 = -0.72 \pm 0.17$ . The RMS error of the fit was 0.084 dex, with adjusted  $R^2=0.98$ . Seventeen of the 26

calibration stars were non-Blazhko variables and nine were Blazhko stars. The photometric  $[\text{Fe}/H]$  values derived from the fitted model are given in column 9 of Table 1, where the estimated standard errors were calculated using the usual Gaussian theory formula for non-linear least squares regression (analogous to Eqns. 4-5 of JK96, except that we have ignored the errors in  $\phi_{31}^s$  and  $P$  owing to the high accuracy of the *Kepler* photometry).

In Fig. 11 the fitted photometric metallicities are plotted against the spectroscopic metallicities (top panel). Also shown (bottom panel) are the differences,  $\Delta[\text{Fe}/H]$

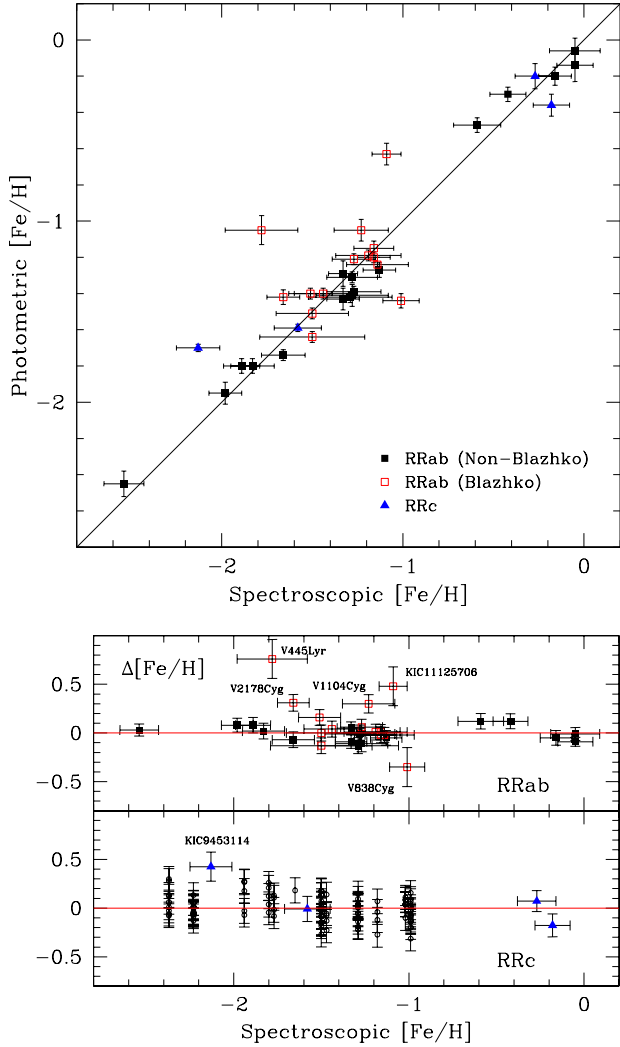


FIG. 11.— Comparison of the spectroscopic and photometric metallicities for the *Kepler*-field RR Lyrae stars. The diagonal line in the top panel is the 1:1 relation. The bottom panel contains the  $[\text{Fe}/\text{H}]$  differences (photometric minus spectroscopic) for the RRAb (upper) and RRC (lower) stars, where the vertical error bars are the standard errors of the differences. Included in the lowest graph are the residuals for the M07 globular cluster RRC calibration data set (small open circles). A color version of this figure is given in the on-line version of the paper.

$= [\text{Fe}/\text{H}]_{\text{phot}} - [\text{Fe}/\text{H}]_{\text{spec}}$ , plotted against  $[\text{Fe}/\text{H}]_{\text{spec}}$ . Included in the graphs are the five Blazhko stars that were excluded from the final calibration (labelled in the bottom panel). All of the calibrating stars lie close to the 1:1 line, with  $|\Delta[\text{Fe}/\text{H}]| < 0.13$  dex for all 17 non-Blazhko stars.

The largest metallicity differences correspond to the five Blazhko stars excluded from the calibration. It is perhaps not surprising that the two most extreme Blazhko stars (V445 Lyr, V2178 Cyg) showed the greatest disagreement. Since both stars exhibit considerable variation in  $\phi_{31}^s$  over a Blazhko cycle, and since the calibration model (Eqn. 2) is nonlinear, it is questionable (Jensen’s inequality) whether substitution of mean  $\phi_{31}$  rather than averaging the ‘instantaneous’  $[\text{Fe}/\text{H}]$  values is the appropriate way of calculating  $[\text{Fe}/\text{H}]_{\text{phot}}$ . The  $[\text{Fe}/\text{H}]_{\text{phot}}$  given in Table 1 were calculated using the first

(*i.e.*, substitution of mean- $\phi_{31}^s$ ) method. To investigate the second method we computed  $[\text{Fe}/\text{H}]_{\text{phot}}$  for the five Blazhko stars by averaging (over complete Blazhko cycles) the metal abundances evaluated (Eqn. 2) at each ‘instant’ along the  $\phi_{31}^s$  time series. As expected, the two methods gave similar results for the three low amplitude/frequency modulators. However, for V445 Lyr and V2178 Cyg averaging over the instantaneous abundances gave  $[\text{Fe}/\text{H}]_{\text{phot}} = -1.69$  and  $-1.65$  dex, respectively, both of which are much closer to the spectroscopic abundances:  $-1.78$  dex for V445 Lyr (which is from the SME analysis since the VWA analysis was inconclusive), and  $-1.66 \pm 0.13$  dex for V2178 Cyg.

Of course the spectroscopic metallicities are also uncertain and contribute to the differences. Four of the five Blazhko stars seem to have reliable (and consistent) metal abundances from the VWA and SME analyses. The largest difference, that for V445 Lyr (Fig. 11), was calculated assuming the SME abundance,  $-1.78$  dex (which appears to be consistent with the partial spectrum shown in Fig. 7a). Consideration of the pulsation phases at the times of the spectroscopic observations, and of the Blazhko properties of the stars, reveal no obvious patterns: the pulsation phases range from 0.31 to 0.43; four of the five stars have Blazhko periods  $\sim 50$  days, while V2178 Cyg has a considerably longer  $P_{\text{BL}} = 234 \pm 10$  d; and the Blazhko phases range from 0.32 to 0.82.

We conclude that since the large metallicity differences found for extreme Blazhko stars are reduced when ‘instantaneous’  $[\text{Fe}/\text{H}]_{\text{phot}}$  values are averaged instead of calculated using the mean- $\phi_{31}$  method, and that the two methods give the same result for the non-Blazhko and less extreme Blazhko stars, that this method might be preferable for future  $[\text{Fe}/\text{H}]_{\text{phot}}$  calculations.

In Fig. 12 two sets of isometallicity curves have been added to the  $P$ - $\phi_{31}$  diagram (see Fig. 4). The solid curves (black) were calculated by solving our nonlinear relation (equation 2) for five  $[\text{Fe}/\text{H}]$  values (ranging from  $-2.0$  to  $-0.1$  dex), and the dashed lines (blue) were calculated using the well-known JK96 formula (their equation 3) and solving for  $[\text{Fe}/\text{H}] = -2.0, -1.0$  and  $0.0$  dex. Since our photometry is on the *Kp* system it was necessary to transform the JK96 formula to the *Kp* system, which was done using equation 2 of N11, *i.e.*,  $\phi_{31}^s(V) = \phi_{31}^s(Kp) - 0.151 (\pm 0.026)$ , resulting in

$$[\text{Fe}/\text{H}] = -5.241 - 5.394P + 1.345 \phi_{31}^s(Kp). \quad (3)$$

The original version of this relation was established using a calibration data set consisting of 81 galactic-field RR Lyr stars with reliable *V* light curves and high dispersion spectroscopic (HDS) abundances. It was considered optimal after various linear and nonlinear models were investigated, and gives photometric abundances on the HDS metallicity scale established by Jurcsik (1995). It is applicable for stars meeting the *compatibility condition*,  $D_m < 3$ , a criterion that fails to hold for stars with peculiar light curves, such as certain Blazhko variables and RR Lyr stars in advanced evolutionary stages.

In general our nonlinear model and the JK96 model agree for  $[\text{Fe}/\text{H}] < -1.0$  dex, with progressively larger discrepancies occurring as  $[\text{Fe}/\text{H}]$  decreases. It is well-known that for the lowest  $[\text{Fe}/\text{H}]$  stars the JK96 formula gives metallicities too metal-rich by  $\sim 0.3$  dex, the

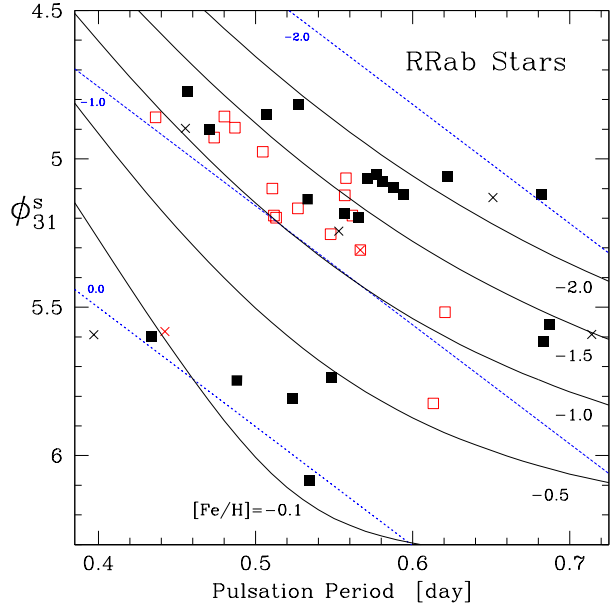


FIG. 12.— Period- $\phi_{31}$  diagram for the *Kepler*-field RRab stars. Also show are five isometallicity curves (black solid curves) derived from our nonlinear  $P-\phi_{31}^s$ -[Fe/H] relation (eqn. 2), and three isometallicity curves (blue dotted lines) derived from the JK96 linear relation. The *Kepler*-field non-Blazhko RRab stars (black filled squares) and Blazhko RRab stars (red open squares) are also plotted, along with six Keck spectroscopic standard stars (crosses). The  $\phi_{31}^s$  values were derived from sine-series Fourier decomposition of the  $Kp$ -passband observations. A color version of this figure is given in the on-line version of the paper.

problem having been identified by JK96 themselves and discussed further by Nemec (2004) and Smolec (2005). Our model appears to correct this problem (compare the [Fe/H] =  $-2.0$  dex curves in Fig.12), in part due to the wider inclusion in our sample of stars more metal-poor than  $-2.0$  dex, as well as our use of a nonlinear rather than linear model. It should also be noted that JK96 adopted a spectroscopic [Fe/H] of  $-2.10$  dex for X Ari, whereas the spectroscopic metallicities in Table 10 suggest a much lower value, [Fe/H]  $\sim -2.65$  dex.

The *Kepler*-field RR Lyr stars divide into two groups, those with  $\phi_{31}^s(Kp) \sim 5$  having low metallicities, [Fe/H]  $< -1$  dex, and a high metallicity group with  $\phi_{31}^s(Kp) \sim 5.7$ . Four of the five *Kepler* stars comprising the latter group were identified as metal-rich by N11 (V782 Cyg, V784 Cyg, KIC 6100702 and V2470 Cyg); to this group we can now add V839 Cyg (and the Keck standard stars V445 Oph and SW And).

### 5.2. RRc stars

The  $P-\phi_{31}$ -[Fe/H] relation for RRc stars was investigated previously by M07. Two nonlinear formulas were derived, one for metallicities on the ZW84 scale (Zinn & West 1984) and the other for the CG97 scale (Carretta & Gratton 1997). For calibration purposes 106 stars in 12 galactic globular clusters were used, with cluster mean metallicities ranging from  $-2.2$  to  $-1.0$  dex.

With only four RRc stars in our sample it was not possible to derive independently a similar relation for the *Kepler*-field RRc stars. We therefore added the *Kepler* stars to the M07 calibration data set (kindly sent to us by Dr. Morgan) and derived a new relation. The inclusion of

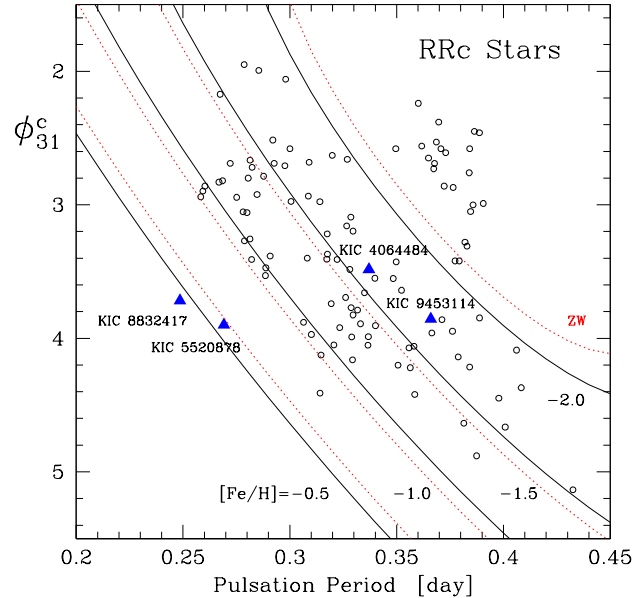


FIG. 13.— Period- $\phi_{31}$  diagram for RRc stars. The *Kepler*-field RRc stars (blue triangles) have been labelled with KIC number. Also plotted are the 106 Galactic globular cluster RRc stars that were used by M07 in the derivation of their  $P-\phi_{31}^c$ -[Fe/H] relations (small open circles), and two sets of isometallicity curves (the black curves are for the C9 scale, and the red dotted curve for the ZW84 scale). The  $\phi_{31}^c$  values were derived from cosine Fourier decomposition of  $V$ -passband observations. A color version of this figure is given in the on-line version of the paper.

the *Kepler* stars extends the [Fe/H] range to considerably higher metallicities.

Since most of the data were from the M07 sample we chose to work with  $\phi_{31}^c(V)$  Fourier phase parameters. The  $\phi_{31}^s(Kp)$  values for the *Kepler* stars were transformed to  $\phi_{31}^c(V)$  values using equation 2 of N11, which, while probably not optimal for the hotter RRc stars (since it was derived for non-Blazhko RRab stars) is all that is presently available; the sine-to-cosine transformation was made using  $\phi_{31}^c = \phi_{31}^s - \pi$ .

The metallicities assumed for the *Kepler* stars were those given in Table 7, and the [Fe/H] values assumed for the globular cluster stars were the cluster means given in Table A.1 of C9. The latter are very similar to the metal abundances adopted by W. Harris in the latest edition (2010) of his on-line catalog of globular cluster parameters (Harris 1996).

Using the revised data set and the  $\phi_{31}^c(V)$  phase parameters we refit the M07 model,

$$[\text{Fe}/\text{H}] = b_0 + b_1 P + b_2 \phi_{31}^c + b_3 \phi_{31}^c P + b_4 P^2 + b_5 (\phi_{31}^c)^2, \quad (4)$$

where the metallicities are now on the C9 scale. After removing nine outliers (V17 in M9; V26 in NGC 6934; V27 and V19 in M2; V50 in M15; V3, V11 and V14 in NGC 4147; and KIC 9453114) the estimated model coefficients and their standard errors were found to be:  $b_0 = 1.70 \pm 0.82$ ,  $b_1 = -15.67 \pm 5.38$ ,  $b_2 = 0.20 \pm 0.21$ ,  $b_3 = -2.41 \pm 0.62$ ,  $b_4 = 18.00 \pm 8.70$ , and  $b_5 = 0.17 \pm 0.04$ . The root MSE of the fit was 0.13 dex, the adjusted  $R^2 = 0.94$ , and the calibration sample size  $N=101$  stars. The fitted [Fe/H]<sub>phot</sub> (and their standard errors) for the *Kepler*-field RRc stars are given in column (9) of Table 1.

The metallicity differences for the four *Kepler*-field

RR Lyr stars (blue triangles) and for the globular cluster stars (small open circles) are plotted in the bottom panel of Fig. 11. For the three *Kepler* stars that were included in the calibration the differences are small, all under 0.18 dex; for KIC 9453114 the derived  $[\text{Fe}/\text{H}]_{\text{phot}}$  is 0.43 dex more metal rich than the  $[\text{Fe}/\text{H}]_{\text{spec}}$ ,  $-2.13 \pm 0.12$  dex. For the cluster stars the groups correspond to the individual clusters, with the vertical variation reflecting the range of the  $P$  and  $\phi_{31}$  values within each cluster (for clarity the uncertainties in the  $[\text{Fe}/\text{H}]_{\text{spec}}$  have been omitted).

In **Fig. 13** the  $P$ - $\phi_{31}^c$  diagram is plotted for the RRc stars in the *Kepler*-field and in the M07 globular clusters (the symbols are the same as in Fig. 11). Also shown are two sets of isometallicity curves for  $[\text{Fe}/\text{H}]$  ranging from  $-2.0$  dex to  $-0.5$  dex. The solid curves (black) were calculated using the new  $P$ - $\phi_{31}^c(V)$ - $[\text{Fe}/\text{H}]$  relation (equation 4) and solving for the four different  $[\text{Fe}/\text{H}]$  values; and the dotted curves (red) are the same curves transformed (using the transformation equation given in C9) to the ZW84 scale.

## 6. SUMMARY

Metal abundances, RVs and atmospheric properties have been derived for 41 RR Lyr stars located in the field of view of the *Kepler* space telescope. The spectroscopic  $[\text{Fe}/\text{H}]$  values range from  $-2.54 \pm 0.13$  (NR Lyr) to  $-0.05 \pm 0.13$  dex (V784 Cyg). Four stars that were suspected by N11 from Q0-Q5 *Kepler* photometry of being metal-rich (KIC 6100702, V2470 Cyg, V782 Cyg and V784 Cyg) are here confirmed as such, and three more metal-rich RR Lyr stars are identified: V839 Cyg, KIC 5520878 and KIC 8832417 (the last two being RRc stars).

For all but five Blazhko RRab stars and one RRc star the  $[\text{Fe}/\text{H}]_{\text{spec}}$  are in good agreement with newly calculated  $[\text{Fe}/\text{H}]_{\text{phot}}$  values derived from detailed analyses of  $\sim 970$  days of quasi-continuous high-precision Q0-Q11 long- and short-cadence *Kepler* photometry. Revised pulsation periods and times of maximum light are given for all the stars (these were needed for calculating the pulsation phases at the times of the spectroscopic observations and the  $[\text{Fe}/\text{H}]_{\text{phot}}$  values), and updated Blazhko periods and times of maximum amplitude are given for the amplitude modulated variables (needed for calculating Blazhko phases).

We conclude that empirical Fourier-based  $P$ - $\phi_{31}$ - $[\text{Fe}/\text{H}]$  relations *can* be used to derive  $[\text{Fe}/\text{H}]_{\text{phot}}$  for non-Blazhko and most Blazhko RRab stars (provided that the modulation is not too extreme and that sufficient Blazhko cycles are used when calculating the average  $\phi_{31}$ ); similar conclusions previously were reached by Smolec (2005) for Blazhko and non-Blazhko stars in the LMC and Galactic bulge (OGLE survey), and by Jurcsik *et al.* (2012) for Galactic field stars observed by the Konkoly Blazhko Survey. For three of the four RRc stars the  $[\text{Fe}/\text{H}]_{\text{phot}}$  calculated from empirical Fourier relations are in good agreement with the measured  $[\text{Fe}/\text{H}]_{\text{spec}}$  values. We also suggest that the use of ‘instantaneous’  $[\text{Fe}/\text{H}]_{\text{phot}}$  values might be preferable to the usual method of calculating  $[\text{Fe}/\text{H}]_{\text{phot}}$  using mean- $\phi_{31}$  values.

All the Blazhko stars are found to exhibit both amplitude and frequency modulations, and five of the 21 non-

Blazhko RRab stars are more metal-rich than  $[\text{Fe}/\text{H}] \sim -1.0$  dex while none of the 16 Blazhko stars is more metal-rich than this. Several stars are found to have special photometric characteristics:

(1) V838 Cyg, classified originally as a non-Blazhko star (B10, N11), has been discovered here to be a Blazhko star with a complex power spectrum and the smallest amplitude modulation yet detected in such a star,  $\Delta A_1 = 0.0024$  mag – it joins KIC 11125706 as the current record holders;

(2) V2178 Cyg is an extreme Blazhko star with a unique up-down pattern seen in the time variation of its Fourier  $\phi_{31}$  parameter (Fig. 4);

(3) V354 Lyr has a Blazhko period of just under two years, the longest  $P_{\text{BL}}$  of any *Kepler* Blazhko star;

(4) the candidate RRc star KIC 3868420 is shown to have a high metallicity, a high surface gravity, a high  $v_{\text{mac}}$  and a low  $RV$ ; while its atmospheric characteristics are not unlike those of the two metal-rich RRc stars in the *Kepler* field, we conclude based on the shape of its light curve and its rather short period that it more probably is a HADS star than an RRc star;

(5) V349 Lyr (KIC 7176080) has been classified previously as a Blazhko star with an amplitude modulation period greater than 127 days, and as a non-Blazhko star; analysis of the currently available data (Q1-Q13) supports the latter classification.

Finally, atmospheric parameters are derived for the stars, from which we conclude that the RR Lyrae stars have higher microturbulent velocities (and are hotter) than the red horizontal branch and metal-poor red giants of the same surface gravity. The observations also directly confirm that the more metal-rich RR Lyrae stars have higher surface gravities than the more metal poor RR Lyrae stars.

The CFHT and Keck spectra contain much more chemical information than the  $[\text{Fe}/\text{H}]$  values and atmospheric parameters presented here. Of particular interest are relative abundance ratios  $[\text{X}/\text{Fe}]$ , especially  $[\alpha/\text{Fe}]$  ratios which are related to the supernovae history of the Galaxy. The expectation is that the  $\alpha$ -elements (O, Ne, Mg, Si, S, Ca, Ti) produced mainly by Type II supernovae, will be enhanced with respect to Fe (produced mainly by Type Ia supernovae) by  $\sim 0.4$  for the stars more metal poor than  $[\text{Fe}/\text{H}] = -0.8$  dex (see C95). Such measurements will be presented elsewhere.

## 7. ACKNOWLEDGMENTS

Funding for the *Kepler* Discovery mission is provided by NASA’s Science Mission Directorate. The authors thank the entire *Kepler* team without whom these results would not be possible. We thank Nadine Mansett and her team of service observers at the Canada-France-Hawaii 3.6-m telescope for successfully acquiring the CFHT spectra. JN would like to thank Jozsef Benkő, Johanna Jurcsik, László Molnár and Róbert Szabó for discussions on Blazhko stars and for their hospitality at KASC5 and in Budapest. He also greatly appreciates discussions with Katrien Kolenberg regarding her RR Lyrae work, with Robert Stellingwerf concerning his PDM2 program, with BiQing For concerning the results of her Ph.D. thesis, with Andrzej Pigulski for discussions about the ASAS-North survey. John Feldmeier sent information on the two BOKS survey RR Lyr stars, Géza Kovács

kindly provided JN with his Fourier decomposition software, and Siobahn Morgan sent her file of Fourier parameters for RRc stars in galactic globular clusters. Finally, special thanks go to Amanda Linnell Nemec, Young-Beom Jeon and Robert Szabó for their helpful comments on the manuscript, and to George Preston for his useful referee report. JN acknowledges support from the Camosun College Faculty Association; JC and BS acknowledge NSF grant AST-0908139; and PM is supported by Polish NCN grant DEC-2012/05/B/ST9/03932. This project has been supported by the Hungarian OTKA Grants

K76816, K83790 an MB08C 81013 and the "Lendület-2009" Young Researchers Program of the Hungarian Academy of Sciences. AD was supported by the Hungarian Eötvös fellowship and by the János Bolyai Research Scholarship of the Hungarian Academy of Sciences. Finally, all the authors wish to recognize and acknowledge the very significant cultural role and reverence that the summit of Mauna Kea has always had within the indigenous Hawaiian community; we are most fortunate to have had the opportunity to conduct observations from this mountain.

## REFERENCES

- Alcock, C., Allsman, R., Alves, D.R. *et al.* 1998, ApJ, 492, 190  
 Alcock, C., Allsman, R., Alves, D.R. *et al.* 2000, ApJ, 542, 257  
 Alcock, C., Alves, D.R., Becker, A. *et al.* 2003, ApJ, 598, 597  
 Alcock, C., Alves, D.R., Axelrod, T.S. *et al.* 2004, AJ, 127, 334  
 Arp, H.C. 1955, AJ, 60, 317  
 Asplund, M., Grevesse, N. *et al.* 2009, ARA&A, 2009, 47, 481  
 Balona, L.A. & Nemec, J.M. 2012, MNRAS, 426, 2413  
 Barklem, P.S., Christlieb, N. *et al.* 2005, A&A, 439, 129  
 Benedict, G.F., McArthur, B.E. *et al.* 2011, AJ, 142:187  
 Benkó, J.M., Kolenberg, K. *et al.* 2010, MNRAS, 409, 1585 (B10)  
 Blazhko, S. 1907, Astron. Nachr., 175, 325  
 Bono, G., Caputo, F., Cassisi, S. *et al.* 1997, ApJ, 483, 811  
 Bono, G., Caputo, F. & DiCriscienco, M. 2007, A&A, 476, 779  
 Brown, T.M., Latham, D.W. *et al.* 2011, AJ, 142, 112  
 Bruntt, H., Catala, C. *et al.* 2002, A&A, 389, 345  
 Bruntt, H., De Cat, P. & Aerts, C. 2008, A&A, 478, 487  
 Bruntt, H., Deleuil, M. *et al.* 2010a, A&A, 519, A51  
 Bruntt, H., Bedding, T. *et al.* 2010b, MNRAS, 405, 1907  
 Buchler, J.R. & Moskalik, P. 1992, ApJ, 391, 736  
 Buchler, J.R. & Kolláth, Z. 2011, ApJ, 731:24  
 Cacciari, C., Corwin, T.M. & Carney, B. 2005, AJ, 129, 267  
 Caputo, F., Castellani, V. *et al.* 2000, MNRAS, 316, 819  
 Carney, B.W. & Jones, R. 1983, PASP, 95, 246  
 Carretta, E. & Gratton, R.G. 1997, A&AS, 121 95 (CG97)  
 Carretta, E., Bragaglia, A. *et al.* 2009, A&A, 508, 695 (C9)  
 Cassisi, S., Castellani, V. *et al.* 1999, A&AS, 134, 103  
 Clement, C., Muzzin, A. *et al.* 2001, AJ, 122, 2587  
 Clementini, G., Carretta, E. *et al.* 1995, AJ, 110, 2319 (C95)  
 Cohen, J.G. 2011, ApJ, 7430, L38  
 Cohen, J.G. & Melendez, J. 2005a, AJ, 129, 303  
 Cohen, J.G. & Melendez, J. 2005b, AJ, 129, 1607  
 Cohen, J.G. & Huang, W. 2009, ApJ, 701, 1053  
 Collinge, M.J., Sumi, T. & Fabrycky, E. 2006, ApJ, 651, 197  
 Donati, J.-F. *et al.* 1997, MNRAS, 291, 658  
 Drukier, G.A. *et al.* 2007, AJ, 133, 1041  
 Feast, M.W., Laney, C.D. *et al.* 2008 MNRAS, 386, 2115  
 Feldmeier, J. *et al.* 2011, AJ, 142:2  
 Fernley, J., Barnes, T.G. *et al.* 1998, A&A, 330, 515  
 For, B.-Q., Sneden, C. & Preston, G.W. 2011, ApJS, 197, 29  
 Garofalo, A., Cusano, F., Clementini, G. *et al.* 2013, ApJ, 767, 62  
 Gilliland, R.L., Jenkins, J.M. *et al.* 2010, ApJ, 713, L160  
 Gratton, R., Bragaglia, A. *et al.* 2004, A&A, 421, 937  
 Grevesse, N., Asplund, M. *et al.* 2007, Space Sci. Rev. 130, 105  
 Guggenberger, E. *et al.* 2012, MNRAS, 424, 649 (G12)  
 Gustafsson, B., Bell, R.A. *et al.* 1975, A&A, 42, 407  
 Gustafsson, B., Edvardsson, B. *et al.* 2008, A&A, 486, 951  
 Harris, W.E. 1996, AJ, 112, 1487  
 Haschke, R., Grebel, E.K. *et al.* 2012, AJ, 144:88  
 Heiter, U. *et al.* 2002, A&A, 392, 619  
 Heiter, U. & Eriksson, K. 2006, A&A, 452, 1039  
 Hinkle, K. *et al.* 2000, Visible and Near-IR Atlas of the Arcturus Spectrum 3727-9300 Å (San Francisco: ASP)  
 Holweger, H. 2001, AIP Conf. Proc. 598, 23  
 Jenkins, J.M., *et al.* 2010, ApJ, 713, L87  
 Jurcsik, J. 1995, Acta Astron., 45, 653  
 Jurcsik, J. & Kovács, G. 1996, A&A, 312, 133 (JK96)  
 Jurcsik, J. *et al.* 2005, A&A, 430, 1049  
 Jurcsik, J. *et al.* 2006, AJ, 132, 61  
 Jurcsik, J. *et al.* 2009a, MNRAS, 393, 1553  
 Jurcsik, J. *et al.* 2009b, MNRAS, 397, 350  
 Jurcsik, J. *et al.* 2009c, MNRAS, 400, 1006  
 Jurcsik, J. *et al.* 2012, MNRAS, 423, 993  
 Koch, D.G., Borucki, W.J., Basri, G., *et al.* 2010, ApJ, 713, L79  
 Kolenberg, K. 2002, Ph.D. thesis, Katholieke Universiteit Leuven.  
 Kolenberg, K., Fossati, L. *et al.* 2010, ApJ, 713, L198 (K10)  
 Kolenberg, K., Bryson, S. *et al.* 2011, MNRAS, 411, 878 (K11)  
 Kolláth, Z., Molnár, L. & Szabó, R. 2011, MNRAS, 414, 1111  
 Kovács, G. 1998, ASP Conf. Ser., 135, 52  
 Kovács, G. 2005, A&A, 438, 227  
 Kovács, G. 2009, AIP Conf.Proc.1170, *Stellar Pulsation: Challenges for Theory and Observation*, eds. J.A.Guzik & P.A.Bradley, p.261  
 Kovács, G. & Jurcsik, J. 1996, ApJ, 466, L17  
 Kovács, G. & Walker, A.R. 2001, A&A, 371, 579  
 Kovács, G. & Zsoldos, E. 1995, A&A, 293, L57  
 Kunder, A. & Chaboyer, B. 2008, AJ, 136, 2441  
 Kunder, A. & Chaboyer, B. 2009, AJ, 138, 1284  
 Kupka, F., Piskunov, N.E. *et al.* 1999, A&AS, 138, 119  
 Kurucz R. L., Furenlid I., Brault J., Testerman L., 1984, Solar Flux Atlas from 296 to 1300 nm. National Solar Observatory, Sunspot, New Mexico , USA  
 Lambert, D.L., Heath, J.E. *et al.* 1996, ApJS, 103, 183 (L96)  
 Layden, A.C. 1994, AJ, 108, 1016 (L94)  
 Le Borgne, J.-F., Klotz, A., Poretti, E., *et al.* 2012, AJ, 144:39  
 Lenz, P. & Breger, M. 2005, CoAst, 146, 53  
 Liu, T. & Janes, K.A. 1989, ApJS, 69, 593  
 Liu, T. & Janes, K.A. 1990a, ApJ, 354, 273  
 Liu, T. & Janes, K.A. 1990b, ApJ, 360, 561  
 Molnár, L., Kolláth, Z., Szabó, R. *et al.* 2012, ApJ, 757, L13  
 Morgan, S.M., Wahl, J.N. *et al.* 2007, MNRAS, 374, 1421 (M07)  
 Moskalik, P. & Buchler, J.R. 1991, ApJ, 366, 300  
 Moskalik, P., Smolec, R. *et al.* 2012, arXiv:1208.4251v1  
 Moskalik, P. & Kołaczowski, Z. 2009, MNRAS, 394, 1649  
 Moskalik, P. & Poretti, E. 2003, A&A, 398, 213  
 Nardetto, N. *et al.* 2004, A&A, 428, 131  
 Nardetto, N. *et al.* 2009, A&A, 502, 951  
 Nemec, J.M. 2004, AJ, 127, 2185  
 Nemec, J.M., Walker, A. & Jeon, Y.-B. 2009, AJ, 138, 1310  
 Nemec, J.M., Smolec, R. *et al.* 2011, MNRAS, 417, 1022 (N11)  
 Oke, J.B. 1966, ApJ, 145, 468  
 Oosterhoff, P. Th. 1939, The Observatory, 62, 104  
 Oosterhoff, P.Th. 1944, Bull. of the Astron. Inst. Neth., 10, 55  
 Pietrukowicz, P., Udalski, A. *et al.* 2012, ApJ, 750:169  
 Piskunov, N.E. 1992, in 'Stellar Magnetism', eds., Yu.V. Glagolevskij & I.I. Romanyuk (St. Petersburg, Nauka), p.92  
 Preston, G.W. 1959, ApJ, 130, 507  
 Preston, G.W. 2009, "RR Lyrae Atmospherics: Wrinkles Old and New". Henry Norris Russell Lecture, <ftp://ftp.obs.carnegiescience.edu/pub/gwp/HNRlecture>  
 Preston, G.W. 2011, AJ, 141:6  
 Rentsch-Holm, I. 1996, A&A, 312, 966  
 Rey, S.-C., Lee, Y.-W. *et al.* 2000, AJ, 119, 1824  
 Roederer, I.U. & Sneden, C. 2011, AJ, 142:22  
 Sandage, A.R. 1958, in *Stellar Populations*, ed. D.O'Connell (*Ricerche Astr. Specola Vaticana*, Vol.5), p.41  
 Sandage, A.R. 1981, ApJ, 248, 161  
 Sandage, A.R. 1990, ApJ, 350, 603  
 Sandage, A.R. 2004, AJ, 128, 858  
 Sandage, A.R. 2010, ApJ, 722, 79  
 Schörck, T., Christlief, N., Cohen, J. *et al.* 2009, A&A, 507, 817

- Sesar, B. 2012, *AJ*, 144, 114  
Sesar, B., Ivezić, Z. *et al.* 2010, *ApJ*, 708, 717  
Simon, N.R. 1985, *ApJ*, 299, 723  
Simon, N.R. 1988, *ApJ*, 328, 747  
Simon, N.R. & Lee, A.S. 1981, *ApJ*, 248, 291  
Simon, N.R. & Teays, T.J. 1982, *ApJ*, 261, 586  
Simon, N.R. & Clement, C. 1993, *ApJ*, 410, 526  
Smolec, R. 2005, *Acta Astron.* 55, 59  
Smolec, Soszynski, Moskalik *et al.* 2012, *MNRAS*, 419, 2407  
Snedden, C. 1973, Ph.D. thesis, Univ. Texas  
Snedden, C. 2002, Manual (MOOG: An LTE Stellar Line Analysis Program)  
Snedden, C., For, B.-Q. and Preston, G.W. 2011, *Carnegie Obs. Astrophys. Ser.*, Vol.5: RR Lyrae Stars, Metal-Poor Stars, and the Galaxy, ed. A.McWilliam (Pasadena: Carnegie Observatories)  
Soszynski, I., Udalski, A. *et al.* 2009, *Acta Astron.* 59, 1  
Soszynski, I., Udalski, A. *et al.* 2010, *Acta Astron.* 60, 165-178  
Soszynski, I., Dziembowski, W.A. *et al.* 2011, *Acta Astron.* 61, 1  
Sousa, S.G., Santos, N.C. *et al.* 2007, *A&A*, 469, 783  
Sousa, S.G., Santos, N.C., Mayor, M. *et al.* 2008, *A&A*, 487, 373  
Stellingwerf, R. 1978, *ApJ*, 224, 953  
Suntzeff, N.B., Kraft, R.P & Kinman, T.D. 1994, *ApJS*, 93, 271  
Szabó, R., Kolláth, Z., *et al.* 2010, *MNRAS*, 409, 1244  
Szeidl, B. 1988, in *Multimode Stellar Pulsations*, eds. Kovács, Szabados & Szeidl (Budapest, Kultura), 45  
Szeidl, B., Jurcsik, J. *et al.* 2012, *MNRAS*, 424, 3094  
Udalski, A., Olech, A. & Szymanski, M. 1997, *Acta Astron.* 47, 1  
Valenti, J.A. & Piskunov, N. 1996, *A&AS*, 118, 595  
Vogt, S.S. *et al.*, 1994, *Proc. SPIE*, 2198, 362  
Walker, A.R. & Nemeč, J.M. 1996. *AJ*, 112, 2026  
Wallerstein, G. & Huang, W. 2010, *Mem.S.A.It.*, 81, 952  
Wils, P., Lloyd, C. & Bernhard, K. 2006, *MNRAS*, 368, 1757  
Zinn, R. & West, R.J. 1984, *ApJS*, 55, 45 (ZW84)